Design, Synthesis and Testing of Metal-Organic Frameworks as Porous Materials for Carbon Dioxide Capture

By

Junaid Khan

Reg# 00000118424

Session 2015-17

Supervised by

Prof. Dr. Naseem Iqbal

A Thesis Submitted to the US-Pakistan Center for Advanced Studies in Energy in partial fulfillment of the requirements for the degree of

MASTERS of SCIENCE in

ENERGY SYSTEMS ENGINEERING

US-Pakistan Center for Advanced Studies in Energy (USPCAS-E)

National University of Sciences and Technology (NUST)

H-12, Islamabad 44000, Pakistan

March 2019

Design, Synthesis and Testing of Metal-Organic Frameworks as Porous Materials for Carbon Dioxide Capture

By

Junaid Khan

Reg# 00000118424

Session 2015-17

Supervised by

Prof. Dr. Naseem Iqbal

A Thesis Submitted to the US-Pakistan Center for Advanced Studies in Energy in partial fulfillment of the requirements for the degree of

MASTERS of SCIENCE in

ENERGY SYSTEMS ENGINEERING

US-Pakistan Center for Advanced Studies in Energy (USPCAS-E)

National University of Sciences and Technology (NUST)

H-12, Islamabad 44000, Pakistan

March 2019

THESIS ACCEPTANCE CERTIFICATE

Certified that final copy of MS/MPhil thesis written by Mr/Ms Junaid Khan, (Registration No. 00000118424), of USPCASE (School/College/Institute) has been vetted by undersigned, found complete in all respects as per NUST Statues/Regulations, is within the similarity indices limit and is accepted as partial fulfillment for the award of MS/MPhil degree. It is further certified that necessary amendments as pointed out by GEC members of the scholar have also been incorporated in the said thesis.

Signature: _____

Name of Supervisor _____

Date: _____

Signature (HoD): _____

Date: _____

Signature (Dean/Principal): _____

Date: _____

Certificate

This is to certify that work in this thesis has been carried out by **Mr. Junaid Khan** and completed under my supervision in Energy Storage and Conservation Laboratory, US-Pakistan Center for Advanced Studies in Energy (USPCAS-E), National University of Sciences and Technology, H-12, Islamabad, Pakistan.

Supervisor: _____

Dr. Naseem Iqbal
USPCAS-E
NUST, Islamabad

GEC member # 1: _____

Dr. Majid Ali
USPCAS-E
NUST, Islamabad

GEC member # 2: _____

Dr. Nadia Shahzad
USPCAS-E
NUST, Islamabad

GEC member # 3: _____

Dr. Rabia Liaquat
USPCAS-E
NUST, Islamabad

HoD- (ESE) _____

Dr. Naseem Iqbal
USPCAS-E
NUST, Islamabad

Principal/ Dean _____

Dr. Zuhair S. Khan
USPCAS-E
NUST, Islamabad

Dedication

I dedicate this work to my parents, family and teachers for their love, motivation and inspiration.

Table of Contents

Abstract

The CO_2 concentration in the atmosphere is constantly rising mainly through industrial and power plant discharges this has led to urgent calls for strategies to reduce CO_2. Metal organic frameworks (MOFs), also known as coordination polymers, represent an interesting type of solid crystalline materials that can be straight forwardly self-assembled through the coordination of metal ions/clusters with organic linkers. These unique advantages enable MOFs to be used as a highly versatile and tunable platform for exploring multifunctional MOF materials. Amine groups being basic in nature have excellent affinity towards acidic CO_2 group. Amine functionalized metal organic framework materials have promising tendencies as dry adsorbents for post-combustion CO_2 capture, owing to their enhanced CO_2 capture capacity. This research work is focused on the synthesis of a new amino functionalized Cu based MOF using 2-aminoterephthalic as a linker. Another aspect of this research work is also to compare the the physical properties of the amine functionalized MOF with that of a MOF which does not have any amine in its structure. The adsorption capacities of these both MOFs are compared in this study to show whether amine plays a role in increasing the adsorption capacity of a MOF. The structure was confirmed by Single Crystal XRD studies. The Single Crystal XRD studies reveal that an amine functionalized MOF is prepared which has free $–NH_2$ group aiding in the CO_2 adsorption. Both the MOFs were also characterized using techniques of XRD, SEM, EDS and TGA. The N_2 adsorption studies of the amine functionalized MOF was carried out to know its surface area and pore size. The CO_2 adsorption study of both the MOFs tells us that the amine functionalized MOF exhibits a better CO_2 capture tendency of 5.85 $mmolg^{-1}$ at 25°C and 20 bar pressure as compared to the Cu-BDC MOF which has a capacity of 0.922 $mmolg^{-1}$ at 10°C and 15 bar pressure.

Keywords: *metal organic framework; organometallic framework structure; Cu based MOFs; CO_2 adsorbent; Amine functionalized MOF; carbon capture; gas storage*

List of Figures

List of Tables

List of Journals/Conference Papers

I. Junaid Khan, Naseem Iqbal, "*Synthesis and application of Cu based MOF as a CO_2 adsorbent*", Second International Conference on Energy Systems for Sustainable Development (ESSD-2018), 21-23 February 2018, COMSATS Lahore, Pakistan. (Presented and published in proceedings).

II. Aisha Asghar, Naseem Iqbal, Tayyaba Noor, Junaid Khan "*Ethylene Diamine (EDA) modification of MOF-5 for enhanced CO_2 capture applications"*, 9th International Conference for Environmental Science & Engineering (ICESE-2019), 20-22 March 2019, Belgium. (Accepted and to be published in Journal of Environmental Science & Development after presenting)

III. Junaid Khan, Naseem Iqbal, Aisha Asghar, Tayyaba Noor *"Effect of Amino Functionalization on Cu-BDC MOF for CO_2 Capture Capacity"*, Microporous & Mesoporous Materials, Elsevier. (Paper under review)

* Annex I

* Annex II

* Annex III

List of Abbreviations

ABDC	Amino-Benzenedicarboxylate
BDC	Benzenedicarboxylate
BET	Brunauer-Emmett-Teller
BTC	1, 2, 3-benzenetricaboxylate
CPM-5	Crystalline Porous Materials
DMF	N, N-dimethylformamide
EDS	Energy Dispersive X-ray Spectroscopy
EIA	Energy Information Administration
GHG	Greenhouse Gas
IPCC	Intergovernmental Panel on Climate Change
LBS	Lewis Base Site
MOFs	Metal Organic Frameworks
OMS	Open Metal Site
SCXRD	Single Crystal X-ray Diffraction
SEM	Scanning Electron Microscope
TGA	Thermal Gravimetrical Analysis
XRD	X-ray Diffraction

Chapter 1: Introduction

1.1 Introduction:

The main work presented in this thesis is related to the investigation of CO_2 adsorption by metal organic frameworks (MOF).

1.2 Climate Change and CO_2 Emission:

Environmental issues and global warming have motivated many researchers and scientists working for the welfare of the environment to work for the betterment of the world. As the population is increasing rapidly, so is the global energy consumption. The Energy Information Administration (EIA) has predicted that if the energy consumption increases at this rate, there will be a 57% increase in the global energy consumption by 2030 [1]. Many scientists are of the view that the most common cause of environmental issues is the emission of the greenhouse gases. Among the anthropogenic GHGs, the one which is the most significant is Carbon dioxide (CO_2). Out of the total global warming effect, CO_2 emission is responsible for approximately 60 % [2].

The potential sources of CO_2 emission are mainly four which are; transportation, power plants utilizing fossil fuels, industrial processes and de-carbonization (hydrogen production from feed stock which is carbon rich). [3]. Out of these four sources, the one which is the main contributor is the power plants powered by fossil fuels. Fossil fuels provide 81 percent of the world's commercial energy supply [3]. 30 Pg (petagram) of CO_2 is produced annually just by consuming fossil fuels. The burning of fossil fuels attribute to about three-fourth of the rise in atmospheric CO_2. [4] (see Table 1-1).

Previously, the atmospheric sink was thought to be so large that it could accommodate the excess CO_2 hence the CO_2 concentration would not exceed and remained relatively maintained. This was the case until the world saw industrial revolution. Due to industrial revolution, the balance of the earth was disturbed and after that, the CO_2 concentration has increased by more than one third by volume to 368 ppm in the year 2000 [3] and 388 ppm in 2010 [3] from 280ppm. The annual rise in the amount of CO_2 at present is about 2 ppm per annum which means that of the total CO_2 emissions, more than one third of it does not leave the atmosphere and remains trapped. [3]. IPCC

[4] predicts that by 2100, the atmosphere may retain up to 570 ppm of CO_2 which can cause a rise in about 1.9℃ of the average global temperature and hence a 3.8 m rise in the mean sea level[5].

To reduce the total CO_2 emissions into the atmosphere, several approaches can be adopted which includes the efficient use of energy in order to decrease the intensity of carbon, use of other fuels like renewable energy and hydrogen which can replace fossil fuels and development of new technologies to capture carbon which may enhance the CO_2 sequestration [6]. Out of these approaches, the one which is the most favorable is the capture of carbon from the source such as power plants. The use of biomass, nuclear energy, hydrogen and solar energy as an alternative to the widely used fossil fuels is not yet viable commercially since these technologies are yet at the development stage and another reason being that the energy demand is so high that these sources become obsolete.

Table 1-1: Fossil fuel emission levels (Pounds/Billion BTU of energy input)[4]

Pollutant	Natural Gas	Coal	Oil
Carbon Dioxide	117000	208000	164000
Carbon Monoxide	40	208	33
Nitrogen Oxides	92	457	448
Sulphur Dioxide	1	2591	1122
Particulates	7	2744	84
Mercury	0	0.016	0.007
Total	117140	214000	165687

1.3 Research Motivation and Objective:

In the carbon capture and storage strategy, several reports have shown that it is vital to achieve high CO_2 adsorption capacity with the least cost which is associated with CO_2 separation. Many other traditional approaches associated with CO_2 adsorption, such as aqueous ammonia-based absorption, amine-based absorption and other adsorption materials like activated carbons and zeolites have various limitations. These limitations have prompted researchers to search for methods and technologies which can act as an alternative to remove CO_2 from flue gas.

The main objective of this research work was an attempt to develop a new MOF which can have an enhanced CO_2 adsorption capacity than the one with similar metal. The pathway selected was by choosing a metal and linker which would act as a basis for the work being carried out. Several tasks addressed for the research were:

1. Selection of amine based linker for MOF synthesis
2. Synthesis of an amine functionalized MOF
3. Synthesis of a non-amine MOF
4. Characterization of the MOFs
5. CO_2 adsorption studies of the MOFs
6. Comparing the results of the MOF

1.4 Thesis Outline and Organization:

In chapter 2 of this thesis, literature relevant to the CO_2 capture technologies is explored and explained. In the literature review, previous capture technologies for CO_2 are investigated and a detailed information is also provided for the emerging technologies in the field of CO_2 adsorption.

The chapter 3 of the thesis is focused on the characterization techniques which are generally applied to characterize a material. The main techniques used for characterization include SEM, EDS, BET, XRD, TGA and SCXRD. The basic theory of these techniques is provided in this chapter.

Chapter 4 of the thesis is dedicated to the methods and materials used for the synthesis of the MOFs. In this chapter the conditions used for the characterization of the MOFs is also discussed in detail.

Chapter 5 explains the results of the tests conducted. Here in this chapter the results of the MOFs were compared with each other and the achievements acquired are explained.

The work carried out during this research is shown below as a figurative flow chart which helps is easily understanding the path of the research.

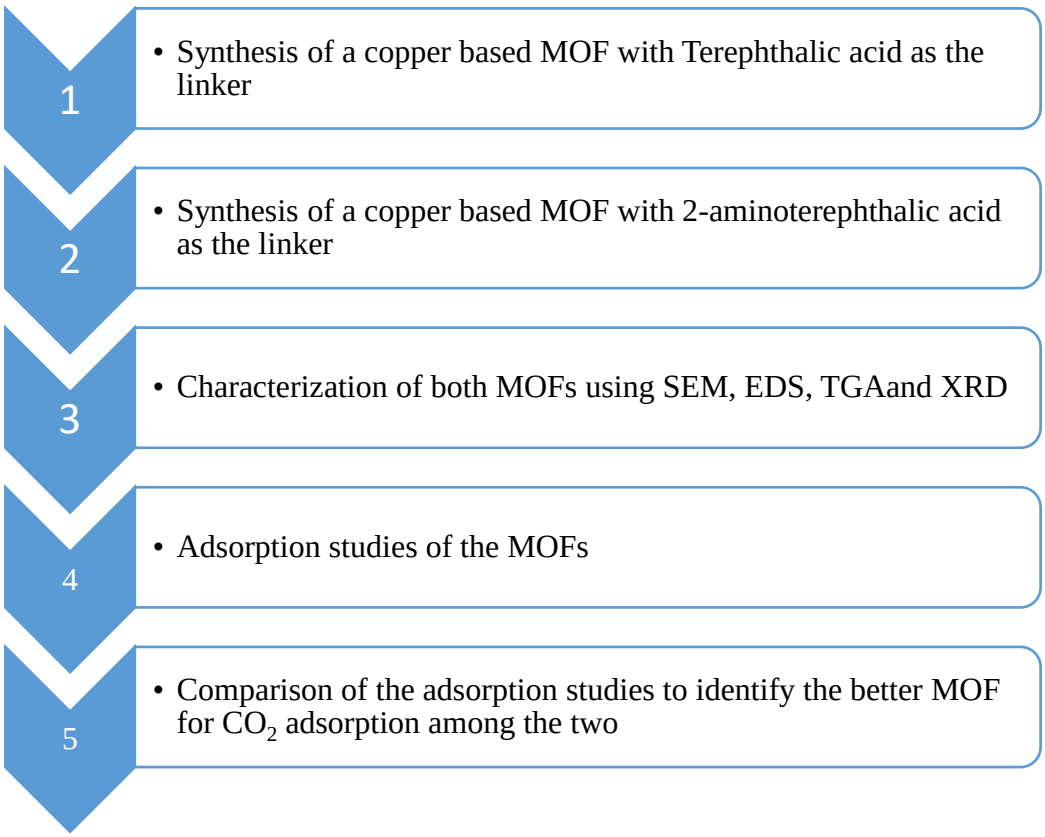

References

[1] EIA, 2010. International Energy Outlook 2010. Us DOE. http://www.eia.doe.gov/oiaf/ieo/index.html.

[2] Yamasaki A. An overview of CO_2 mitigation options for global warming emphasizing CO_2 sequestration options. J Chem Eng Jpn 2003; 36(4):361-75.

[3] S.A. Rackley, Carbon Capture and Storage, Elsevier, 2010.

[4] Thornes, J.E. IPCC, 2001. Climate change 2001: Impacts, adaptation and vulnerability. Contribution of Working Group II to the Third Assessment Report of the Intergovernmental Panel on Climate Change. Int. J. Climatol. 2002, 10, 1285–1286.

[5] Stewart C, Hessami M. A study of methods of carbon dioxide capture and sequestration - the sustainability of a photosynthetic bioreactor approach. Energ Convers Manage. 2005; 46(3): 403-20.

[6] Yang H, Xu Z, Fan M, Gupta R, Slimane R, Bland A, et al. Progress in carbon dioxide separation and capture: A review. J Environ Sci. 2008; 20(1): 14-27.

Chapter 2: Literature Review

2.1 Introduction:

One of the main challenge in the CO_2 capture technologies is that the material which is used for capturing CO_2 should be such that it can be regenerated. If this is not the case, then the chemical materials used to produce the CO_2 capture material will deplete the global suppliers as the material will be used just once. Another challenge for the material is its ability to separate CO_2 from the mixture of gases. Table 2-1 shows the gases (by weight) which are present in the pre-combustion and post-combustion processes [1]. The relatively small difference in the gas properties in Table 2-1 is a disadvantage in separation of gas [2].

Table 2-1 Composition of gases (by weight) in post-combustion and pre-combustion processes [2]

Composition	**Post Combustion**	**Pre Combustion**	**Kinetic Diameter (Å)**	**Quadrupole moment (10^{-27} esu^{-1} cm^{-1})**	**Polarizability (cm^{-25} cm^{-3})**
CO_2	15-16%	35.50%	3.30	43.0	29.1
H_2O	5-7%	0.20%	2.65		14.5
O_2	3-4%		3.46	3.9	15.8
H_2		61.50%	2.89	6.62	8.04
CO	20 ppm	1.10%	3.76	25.0	19.5
SO_x	<800 ppm				
NO_x	500 ppm	3.49		17.0	
N_2	70-75%	0.25%			
Conditions					
Temp.	50-75℃	40℃			
Pressure	1 bar	30 bar			

There are three main approaches which are used to reduce the CO_2 emissions from power plants:

1. Post-combustion capture [3]
2. Pre-combustion capture [3]
3. Oxy-fuel combustion [3]

Figure 2-1 shows these three approaches. In the following paragraphs, the advantages and disadvantages are described for each process.

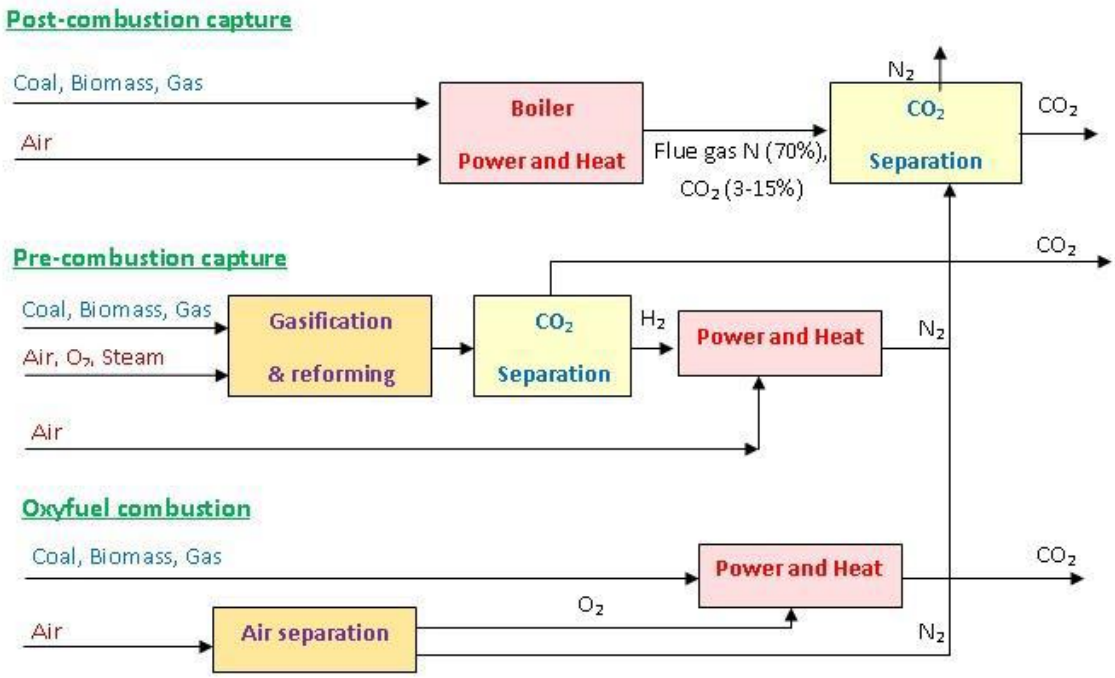

Figure 2-1: CO_2 capture from power generation [4]

2.2 Pre-Combustion Capture:

In the Pre-combustion capture, the fuel is de-carbonized prior to the use of it for the generation of energy or any other use. This happens by the gasification of the biomass, coal or primary fuel. In this method, oxygen or air reacts with the fuel giving of mainly hydrogen and carbon monoxide. The hydrogen produced is then used for running the power plant producing energy. The advantage of pre-combustion capture is that the CO_2 capture equipment used is smaller. Another advantage is that such solvents which have

lower regeneration energy can be used in this process [4]. The disadvantage of this process is the high capital cost of installing the facility.

2.3 Oxy-fuel Combustion Capture:

In Oxy-fuel combustion, the combustion of the fuel is carried out in an oxygen rich environment rather than air. This produces a combustion product which is mainly composed of CO_2. An advantage of this process is that it only requires CO_2 separation and purification since the concentration of CO_2 in the flue gas is over 80% [5]. This reduces the operation cost of the process as no solvents and reagents are used. Due to this there are also less problems to the environment. The disadvantage of this process is that it consumes a large quantity of oxygen hence increasing the capital cost and consumption of energy.

2.4 Post-Combustion Capture:

In the post-combustion capture of CO_2, the main technique is the removal of CO_2 from the flue gases before releasing it to the atmosphere. This is a process which is more challenging than the other processes because it has a higher quantity (generally 5-15% v/v, depending upon the fuel) [3], high temperature of the flue gas and partial pressure of CO_2 being low in the flue gas [4]. In addition, low carbon dioxide concentration creates additional disadvantages due to the high energy required and powerful chemical solvent used to release the carbon dioxide. Despite these challenges, post-combustion carbon capture is a promising technique because it can be retrofitted to existing units [5]. There are several technologies for post-combustion carbon dioxide capture which can be categorized as conventional or new emerging technologies. The following paragraphs will focus on post-combustion capture technologies from fossil fuel power plants including conventional, technologies such as amine-based absorption as conventional carbon dioxide capture technology, aqueous ammonia based absorption, membranes, and new emerging technologies such as adsorption materials like zeolites, activated carbons, and metal organic frameworks.

2.4.1 Amine-based Chemical Absorption

The chemical absorption of carbon dioxide capture is based on the exothermic reaction of a sorbent with the carbon dioxide present in the gas stream usually at room

temperature [3]. Then the reaction is reversed in a stripping or regeneration process at a higher temperature. The most extensively studied and used solvents are amine or carbonate solutions which are suitable for carbon dioxide capture at low partial pressures.

Amine absorbers (scrubbers) are commercially available as large scale technologies for post-combustion separation of carbon dioxide from flue gases. Amines are available in three forms primary, secondary, and tertiary. Each of them possesses advantages and disadvantages. For example, to enhance the reaction rate, primary amines are most preferable followed by secondary then tertiary. For regeneration energy and loading capacity the most preferred type would be tertiary, followed by secondary, and then primary [5].

Monoethanolamine (MEA) is an industrially important primary alkanolamine, which has been used in the natural gas industry to absorb carbon dioxide from nature gas for more than 60 years and is considered the most mature technology. Figure 2-2 illustrates the amine-based carbon dioxide capture process from the flue gas. The flue gas entering the process at close to atmospheric pressure and required operating temperature typically 50°C is bubbled through a packed absorber column (amine scrubber) containing 25-30% aqueous monoethanolamine (MEA) solution at high pressure (60-70 atm) [6]. Amine absorbs carbon dioxide to form a carbamate species. Flue gas exiting the top of the absorber is washed with water to reduce the entrained solvent droplets and then vented to the atmosphere. Following the absorption process, the rich solvent (high content of carbon dioxide reaction product) passes through a desorber column (stripping column) that operates at 100-140°C and marginally at a higher pressure than the absorber in order to release the carbon dioxide with high purity (over 99%) which may be later compressed for commercial utilization or storage [2,3]. Despite the improvements to the amine-based system for post-combustion carbon dioxide chemical absorption, amine scrubbing technologies still have number of challenges and disadvantages. Some of these disadvantages include that the process in general requires large equipment size and intensive energy input, there is a low carbon dioxide loading capacity, high equipment corrosion rate, and amines are subject to degradation in the presence of oxygen, SO_2, NO_2

and HCl, which makes for additional requirements for solvent recovery and waste stream disposal [3].

2.4.2 Aqueous Ammonia-based Absorption

The aqueous ammonia-based absorption process is terms of operation to the amine

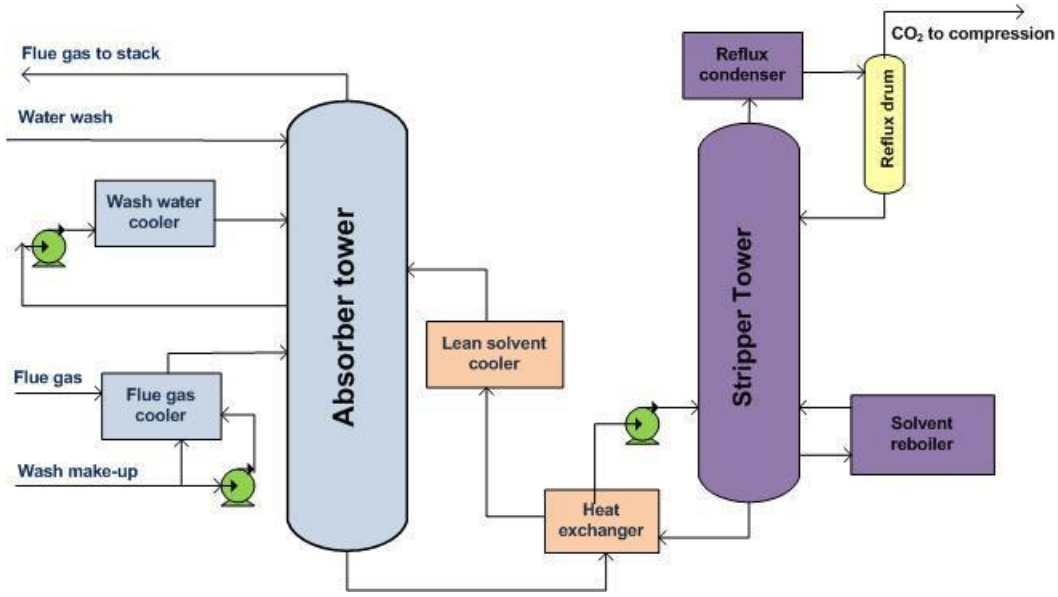

Figure 2-2: Process flow diagram for amine-based CO_2 capture from flue gas

systems. However, the reaction of ammonia and its derivatives with CO_2 has the advantage of having a lower heat of reaction than the equivalent amine based reactions (reaction of ammonium carbonate (AC), CO_2, and water to form ammonium bicarbonate (ABC)). This results in significant energy improvements and cost reductions compared to an amine based absorption system [5]. In addition, the aqueous ammonia process can capture all three major acidic gases (SO_2, NO_2, and CO_2) in a single process which is expected to reduce the total cost and complexity of the emission control systems. Furthermore, absorbent degradation is expected to be eliminated for the aqueous ammonia based absorption Process. One more advantage of ammonia-based absorption is the possibility of utilizing the major by-products including ammonium nitrate and ammonium sulfate to produces fertilizer.

There are several drawbacks and concerns regarding aqueous ammonia chemical absorption process such as the high volatility of ammonia, cooling the flue gas to the 0-

10°C range, and loss of ammonia during the regeneration process because of the elevated temperature [7].

2.4.3 Membranes

The first implementation of membranes for gas separation technology was in the 1980s and since then membranes have been widely used in many industrial separation processes. Membranes are similar to filters, by separating specific component from a mixture of gases in a feed stream. There are various separation mechanisms: 1) solution/diffusion, 2) adsorption/diffusion, 3) molecular sieve and ionic transport [4]. In general, a flue gas stream will be passed through the membrane and the separation of CO_2 will be achieved due to one of the following concepts: a partial pressure difference of CO_2 across the membrane, a reversible chemical reaction with carriers like carbonates, amines molten salt hydrates dissolved in the membrane liquid, or porous inorganic materials including zeolites, palladium alloy tubes and ceramics [8]. Despite the promising high CO_2 separation efficiency, membranes technologies have some drawbacks including a lack of stability under the reforming environment and they are still in the research development phase.

2.4.4 Adsorption Materials

As discussed in the previous paragraphs there are several challenges and shortcomings in terms of the recent carbon capture technologies, where no single technology is able to meet the requirements set by the DOE/NETL: (90% CO_2 capture at less than a 35% increase in the cost of electricity) [9,10]. Therefore, there is a crucial need for developing an alternative capture technology that can both lower the operation cost and have a significant advantages for energy efficiency. Adsorption processes using solid physical adsorbents such as pressure, vacuum, or temperature swing adsorption cycles, possess potential advantages compared to the other capture technologies (i.e. chemical and physical absorption processes) including less regeneration energy required, greater capacity, and selectivity and ease of handling.

There are many physical adsorbent materials that have been considered for CO_2 capture such as, activated carbon, zeolites and zeolite-like materials, and metal organic frameworks (MOF). However, suitable adsorbent for CO_2 capture from flue gas should

satisfy several important criteria to compete with the present technologies, including: 1) high adsorption capacity: the CO_2 equilibrium adsorption capacity represented by its adsorption isotherm is very important criteria in order to evaluate new adsorbents in terms of the capital cost of the capture system. With the knowledge of the adsorption equilibrium capacity the amount of the adsorbent required can be obtained, and consequently the volume of the absorber vessels. The suitable adsorbent for CO_2 capture from flue gas should at least exhibit a CO_2 adsorption capacity of 2 - 4 mmol/g [11]; 2) high selectivity for CO_2: the adsorption selectivity of the adsorbent is defined as the ratio of the CO_2 capacity to other bulk gas components (i.e. N_2 and O_2). This is one of the main properties of adsorbent material, because it has a direct impact on the purity of the CO_2 captured, and consequently on the economics of the separation process [11]; 3) adequate adsorption/desorption kinetics is required a good adsorbent should exhibit fast adsorption/desorption kinetics under the operating conditions and a high rate of adsorption. In addition, adsorption kinetics primarily affect the cycle time of a fixed bed adsorption column; 4) the stability during repeated adsorption/desorption cycling it is also important it is crucial property of an adsorbent because it determines the life time of the adsorbents and the frequency of their replacement. Therefore, the stability of the adsorbents has direct impact on the economics the adsorption process; 5) it is also crucial to consider the mechanical strength of the adsrobent: suitable adsorbents should demonstrate a stable microstructure and morphology under several operating conditions, such as high volumetric flow rate of the flue gas, vibration, and temperature. Also, a good adsorbent should tolerate the presence of moisture and other impurities in the feed (i.e. water vapor, O_2 and SO_2). Otherwise, the CO_2 adsorption process will require a large sorbent recovery rate and a special strategy to accomplish this. As a result, the mechanical strength of adsorbents also has a direct impact on the overall economics of the CO_2 separation process; 6) low operating cost: although the cost of the adsorbent is the most important characteristic to evaluate a new adsorbent, there is limited information on adsorbent costs and other economic considerations in literature. According to a study performed by Tarka et al. [12] on the sensitivity analysis of adsorbents for economic performance, a cost of \$5/kg of adsorbent results is ideal, and \$15/kg of adsorbent is deemed uneconomical. Bu, \$ 10/kg of adsorbent is considered economical for a CO_2 capture process.

Possible gas adsorptive separation is usually achieved by one or more several of the following mechanisms using adsorbent materials [13]: 1) size and/or shape exclusion of certain component of a gas mixture, which is called the molecular sieving effect; 2) the kinetic effect due to the different diffusion rates where certain components are adsorbed faster than others; 3) the thermodynamic effect, based on the surface and/or adsorbate packing interactions; 4) the quantum effect, due to the differences in the diffusion rates in the narrow micropores of some light molecules.

2.4.4.1 Activated Carbon

There is wide varity of carbon based adsorbent materials such as activated carbons, graphenes, and carbon nanotubes. However, activated carbons are the most commonly investigated materials in literature, and widely used as adsorbents in various industrial applications such as gas purification, water treatment, and monitoring air pollution [14,15]. Activated carbons are compossed of carbon-containing biological materials such as coal (e.g. bituminous coal, lignite), industrial by-products (e.g. scraps of polymeric materials, petroleum, coke pitch), and wood or other biomass materials (e.g. cocoanut shells, saw dust olive stones) [16]. Therefore, activated carbons have a huge advantage over other adsorbents in terms of the low cost of raw materials. In addition, the wide variety of resources for activated carbons leads to variations in the pore size distribution, pore structures, and active surface area of the activated carbons [17]. The production of activated carbons from raw materials usually consists of two steps: carbonization, and activation [18]. The former step includes heating and thermal decomposition of the starting material at a temperature of 500-1200℃ in an inert atmosphere to make carbonaceous materials (Char) which have poor surface properties. Therefore, it is essential to follow the carbonization process with an activation step, during which the carbonaceous materials are modified to produce a suitable porosity, and active sites. The activation of the carbonaceous materials can be achieved by either physical or chemical activation. Physical activation can be carried out by the treatment of the material with water vapor and/or CO_2 at 700-100℃ [19]. On the other hand, chemical activation can be achieved by the carbonization of the starting material in the presence of dehydration agents such as KOH, $ZnCl_2$, or H_3PO_4 [20][17].

In literature it was found that activated carbons exhibit lower adsorption capacities than those of zeolites or molecular sieves under low pressure, and ambient temperature [21,22]. In addition, the adsorption capacity of activated carbons decreases significantly with increasing temperature [23]. For example, Na et. al. [24] measured the CO_2 adsorption isotherms on activated carbons at a partial pressure of 0.1 bar and two different temperatures 298 K and 328 K. They found that, activated carbons exhibits a drop in the adsorption capacity from 1.1 to 0.25 mmol/g as the temperature increases from 298 to 328 K. In addition, they found that the CO_2 adsorption capacity decreased from ca. 3.2 to 1.6 mmol/g, when the temperature increased from 288 to 328 K at 1 bar. In another study performed by Do et.al [23], the CO_2 adsorption isotherm on Ajax activated carbon was investigated at a pressure of up to 0.2 bar at three different temperatures. The results showed that the CO_2 adsorption capacity dropped from ca. 0.75 to 0.1 mmol/g as the temperature increased from 298 to 373 K. Chue et.al [21] investigated the heat of adsorption of activated carbon and zeolites revealing that the heat of adsorption (ΔHad) of activated carbon (ΔHad = -30 kJ/mol) is lower than that of zeolites (ΔHad = -36 kJ/mol). The CO_2 adsorption capacity of anthracite coal with a 2 h activation period at 890°C was ca. 1.49 mmol /g measured using thermogravimetric analysis (TGA) [25]. Moreover, the CO_2 adsorption equilibrium isotherms of BPL activated carbon were performed using TGA by Kikkinides et. al [26]. Their results showed that BPL activated carbon exhibits a CO_2 adsorption capacity of ca. 2.1 mmol/g at 298 K and a pressure of 1 bar. Finally, activated carbons are thermally stable.

In summary, activated carbons are advantageous in that they are inexpensive and are less affected by the presence of moisture in the feed gas relative to other solid adsorbents such as zeolites, they require mild adsorption regeneration [27], and are thermally stable [28]. However, activated carbons have some limitations such as, limited CO_2 removal at high pressure and low temperature [29], decreased CO_2 adsorption capacity as the temperature increases [23], low adsorption capacity and selectivity at low partial pressures of CO_2, and in general, contaminates in the flue gas have detrimental effecs on the CO_2 adsorption capacity.

2.4.4.2 Zeolites

Zeolites are highly microporous crystalline framework materials that can be found naturally or fabircated synthetically. Zeolites are one of the most investigated adsorbent materials in literature for adsorption and separation processes [17], due to their unique properties such as pore size, ability of molecular sieving, and varied chemical compositions that affect their adsorption performance. Zeolites consists of a periodic array of TO_4 tetrahedrals (T=Si or Al) [30, 31]. The presence of the alumina atom in the convectional zeolites based on silicate frameworks lead to a negative charge on the framework, with exchangeable cations within the pore structure (usually Na or other alkali or alkaline earth metals). This unique structure of zeolite enables the alkali cations to generate strong electrostatic interactions with acidic molecules such as CO_2 [17,29]. Therefore, varying the Si/Al ratio and nature of the extra-framework cations can play a significant role in controlling the CO_2 adsorptive properties. Several studies in literature addressed the effect of Si/Al ratio, nature of the cations and type of zeolite on the CO_2 adsorption capacity.

Literature shows that zeolites with low Si/Al ratios are one of the promising adsorbents for CO_2 adsorption and separation applications [32,33,34,35,36,37]. However, CO_2 adsorption on zeolites still has some limitations since they are strongly affected by temperature pressure and the presence of water. Zeolites CO_2 adsorption capacities decreases as the temperature increases and increase as the gas-phase partial pressure of CO_2 increases. In addition, zeolites are strongly sensitive to the water content in the flue gas, and because of their highly hydrophilic character extensive drying of the flue gas is needed prior to CO_2 capture or a very highly regeneration temperatures is required (often in excess of 300°C) [21,39]. This additional drying and high regeneration temperature poses an extra cost which significantly affects the adsorption applications of zeolites.

2.4.4.3 Metal Organic Frameworks (MOFs)

2.4.4.3.1 Material Characteristics and Synthesis

Metal organic frameworks are newly emerged class of crystalline porous materials that have attracted recent attention in the past two decades owing to their enormous structural and chemical diversity including: robustness, high surface area (up to 5000 cm^2/g) high thermal and chemical stabilities, high void volume (55-90%), low densities

(from 0.21 to 1 g/cm^3) [41], and their potential applications in gas storage, ion exchange, molecular separation, drug delivery, and heterogeneous catalysis [13,42-44].

MOF materials generally consist of three dimensional organic-inorganic hybrid networks formed by metal based nodes (e.g. Al^{3+}, Cr^{3+}, Cu^{2+}, or Zn^{2+}) bridged by organic linking groups (e.g. carboxylate, pyridyl) principally through coordination bonds. Due to the strong coordination bonds, MOFs are geometrically and crystallographically well-defined framework structures. MOFs can be tuned and designed systematically based on changing the nature of organic linker and/or changing the connectivity of the inorganic moiety and how the building blocks come together to form a net. This remarkable and easy tunability of MOFs is a key feature that distinguishes these materials from traditional porous materials, such as zeolites and activated carbon. In addition, it allows the optimization of the pore dimension and surface chemistry within metal-organic frameworks that was previously absent in zeolite materials [13].

A large number of new MOFs have emerged in the last few years; however, their methods of preparation and synthesis are quite similar. Most are synthesized by employing a so called "modular synthesis", wherein a mixture of metal precursors and appropriate ligands are combined under mild conditions to afford a crystalline porous network. In most of the resulting materials the solvent used during synthesis is removed by applying vacuum, heat, or exchange with volatile molecules, resulting in large pore volume and large surface area accessible to guest molecules. Synthesis approaches such as solvothermal synthesis (conventional approach), microwave synthesis [46], sonication synthesis [47], mechanochemical synthesis [48], and solid start synthesis [49] have been developed for MOFs synthesis. Despite the simplicity of the synthesis of MOFs, there are several challenges in the preparation of new materials related to the optimization of the reaction conditions that lead to the desired MOF, in high yield and crystallinity. The following parameters can play a key role in MOFs' optimization and synthesis: temperature, solvent compositions, reaction times, reagent ratios, reagent concentrations, and pH of the co-solvent solution [45]. Accordingly, slight change in any of these parameters can result in large number of network connectivities, many of which are nonporous and have adverse effect on the gas storage and separation applications. Therefore, large number of reactions trails are required to discover the new desired MOFs in which the reaction parameters are

systematically varied. As a result high throughput technologies have been employed for the synthesis of new MOFs in the recent years [50,51].

2.4.4.3.2 Structural Features

Arbitrarily, MOFs can be categorized into four following sub-sets: rigid frameworks, flexible/dynamic frameworks, surface functionalized frameworks and open metal sites. Rigid MOFs usually have stable and robust porous frameworks with permanent porosity, whereas flexible MOFs show extreme changes of shape when the guest molecules are inserted or removed, and are affected by external stimuli, such as pressure, and temperature, which is absent in the traditional adsorbent such as zeolites and activated carbons. In addition, rigid frameworks retain their porosity upon adsorption and desorption; however, flexible and dynamic frameworks exhibit framework transformation upon removal of guest solvent but restore their porous structure by adsorption of gas molecule at high pressures [52]. Such properties of flexible frameworks promote beneficial capture and release performance of gaseous molecules. Selective adsorption in rigid MOFs may occur as a result of molecular sieving, and/or preferential adsorption based on the different strengths of the adsorbent adsorbate and adsorbate-adsorbate interactions. However, selective adsorption in flexible dynamic MOFs occurs due to the flexibility and the breathing effects of the framework porous structure. Therefore, flexible MOFs are more complicated the evaluation of their performance is more complex and the selective adsorption is more difficult to study and compare to rigid frameworks. Moreover, usually rigid MOFs present a normal type-I shape adsorption isotherm. On the other hand flexible MOFs exhibit stepwise adsorption and/or show hysteretic desorption isotherms for CO_2 and other gases. Novel MOFs, such as MIL- 53 series [53,54], MIL- 88 [55] and SNU-M10 [56] provide a typical examples of breathing frameworks during adsorption and desorption of CO_2.

Open metal sites enhance MOFs performance by providing a mechanism for the separation of (quadru) polar/non polar gas pairs such as CO_2/CH_4. The selective adsorption mechanism may occur due to the coordination of CO_2 to the metal center in an end-on fashion, i.e., O==C==O...Cu^{2+} [57]. The most attractive enhancement of open metal site MOFs is that the presence of water in such frameworks possesses outstanding enhancements in their CO_2 capture ability. One of the most studied materials featuring open

metal sites structure is $Cu_3(btc)_2$ (HKUST-1), which consists of paddlewheel $Cu_2(COO^-)$ units connected through btc^{3-} ligands. Recent studies showed that HKUST-1 framework containing 4 wt.% water exhibited a significant increase in CO_2 adsorption capacity about four times that of the benchmark material zeolite 13X [58] and enhanced CO_2/CH_4 and CO_2/N_2 selectivities [59]. In this case, the mechanism of adsorption was due to the interaction of quadrupole moment of CO_2 with the electric field created by the water molecules which coordinated the open Cu^{2+} sites [58].

The fourth set of MOFs is surface functionalized frameworks. The surface functionalized frameworks enhanced the capacity and selectivity of MOFs for CO_2 adsorption by grafting a functional group with a high affinity for CO_2 (e.g. arylamine [66], alkylamine [67], and hydroxyl [68] groups) onto the surface of porous materials though ligand modification or coordination to unsaturated metal centers. These functional groups enhance the selective interaction between CO_2 and the functionalized molecule as well as the constriction in the pore space of functionalized framework compared to the parent nonfunctionalized material [68]. For example, amino-MIL-53 (Al) exhibited superior separation factor of 60 in the CO_2 uptake relative to CH_4 at low coverage compared with approximately 5 for the parent non-functionalized framework, in addition to increased magnitude of zero-coverage adsorption enthalpy increased from -20.1 to -38.4 kJ/mol upon functionalization [69]. Similar enhancements have been observed in the aminefunctionalized frameworks USO-2-Ni and USO-3-In-A relative to their parent nonfunctionalized frameworks [70].

One of the most studied MOFs in literature to date is $Zn_4O(BDC)_3$ (MOF-5) which consist of tetrahedral $[Zn_4O]^{6+}$ clusters connected by ditopic BDC^{2-} ligands to form a cubic three dimensional network. Yaghi et al. [71] reported the synthesis of sixteen MOF-5 functionalized derivatives they were noted as IRMOF-1 through IRMOF-16, and they were characterized by stable porosity upon substitution with linear dicarboxylate ligands [71]. The IRMOFs family features offer tunable pore spaces and pore functionality relative to the length of the functional group. IRMOF-16 represents the largest of the IRMOF of the IRMOFs series with crystal density of 0.21 g/mL, which was the smallest reported crystal density up to that time for any crystalline material. Following the same concept several new

MOFs have been developed such as, the $Zr_6O_4(OH)_4(BDC)_6$(UiO-66) [72] Al(OH)(BDC) (MIL-53) [73] and Cu_2(BPTC) (NOTT-100) [74].

2.4.4.3.3 CO_2 Adsorption Capacity

The evaluation of new adsorbent materials for CO_2 capture applications depends on many factors, such as the adsorption capacity, selectivity and enthalpy of adsorption. However, most of MOF literature has paid initial attention to CO_2 adsorption capacity by measuring the adsorption equilibrium rather than measuring the adsorption dynamic under fixed bed configuration. The adsorption equilibrium can be measured either gravimetrically or volumetrically. The gravimetric CO_2 uptake, which refers to the quantity of CO_2 adsorbed within a unit of mass of the material, can provide the mass of the MOF required to form the adsorbent bed. On the other hand, the volumetric CO_2 uptake measures how densely the CO_2 can be stored within the material providing information on the volume of the adsorbent bed. In general both measuring techniques are important to determine the heat efficiency of the MOF, in terms of the energy required for regeneration and desorption of the captured CO_2.

Lots of MOFs have been investigated experimentally for CO_2 adsorption and related gas separation. The results of these experiments have been summarized in Table 2-2 which represents the adsorption capacity for MOFs collected at ambient temperatures, with pressures ranging from low pressure (<1.2 bar) to atmospheric pressure in most of the cases. The adsorption isotherms measured at ambient temperature and low pressure are mainly controlled by chemical feature of the pore surface, and most of the high capacity materials are those of highly functionalized surfaces. In addition, at these conditions the adsorption isotherms are most resembled to post combustion CO_2 capture application whereas, the post combustion flue gas pressure is at (~ 1 bar) and partial pressure of CO_2 is low (P_{CO2} ~ 0.15 bar). However, the high pressure adsorption isotherms are more relevant to the pre-combustion application (see Table 2-3). The Adsorption isotherms at high pressure are mostly influenced by the surface area of MOFs, where the greatest adsorption isotherm capacities are dictated for high surface area MOFs. The focus of this review will be on adsorptions at ambient temperature and low pressure simulating post combustion applications.

Most of the MOFs adsorption isotherms present a Langmuir shape, where at low CO_2 partial pressure small changes in pressure result in large changes in capacity with a linear slope; however few MOFs exhibit other types of isotherms including: stepwise isotherms, sigmoidal isotherms, and hysteretic isotherms. There is a disagreement on the cause of the deviation of adsorption isotherms from Langmuir isotherm behavior. Some authors attributed the stepwise isotherms to the structural features of the MOFs such as MCF-19 that has abiporous structure of cages and channels [75]. Others attributed the sigmoidal isotherm to the electrostatic interactions between CO_2 molecules in the MOF pores such as, MOF-5, MOF-177, and MOF-210 [66,76]. Seo et al. [77] attributed the hysteretic isotherm behaviour of CO_2 adsorption on MOF Zn(2,7-ndc)(2,7-bdc=2,7-naphthalenedicarboxylater) to the unique arrangement of the pore channels and their narrow passages compared to the critical dimensions of the CO_2 molecule.

Table 2-2 Low pressure CO_2 adsorption capacities for different MOFs

Material	Common name	Surface Area (m^2/g)		Uptake Temperature (K)	Pressure (bar)	Capacity		Ref
		BET	Langmuir			wt%	mmol/g	
$Zn_4O(BTB)_2$	MOF-177	5400	4690	298	1	3.6		[75]
Zn/DOBDC		816		296	1	5.8		[65]
$Mg_2(dobc)$	Mg-MOF-74, CPO-27-Mg	1174	1733	298	1	27.5		[76]
				298	1	27.2		[77]
V(IV)O(BDC)	MIL-47	600	872	298	1	8.1		[77]
$Cu_3(BTC)_2(H_2O)_{1.5}$	HKUST-1, (4 wt % H_2O)			298	1	27		[59]
$Cu_3(BTC)_3(H_2O)_3$	HKUST-1, (8 wt % H_2O)			298	1	17.4		[59]

Material	Common name	Surface Area (m^2/g)		Uptake Temperature (K)	Pressure (bar)	Capacity		Ref
		BET	Langmuir			wt%	mmol/g	
Ni/(DOBDC)		1070		296	1	11.6		[65]
Ni_2(DOBDC)	Ni-MOF-74, CPO-27-Ni	936	1356	298	1	23.9		[77]
		1083	1312	303	1	22.6		[78]
Mg/DOBC		1495	1905	296	1	23.6		[65]
Ni_2(DHTP)		1083	1312	303	1	11		[64]
$Ni_3(pzdc)_2(7H\text{-}ade)_2(H_2O)_4$		165		298	1	9.8		[79]
Ni_3(pzde)(bptc)			505	195	1	24.3	5.5	[56]
Zn_2(dobdc)	Zn-MOF-74, CPO-27-Zn			296	1	19.8		[77]

Material	Common name	Surface Area (m^2/g)		Uptake Temperature (K)	Pressure (bar)	Capacity		Ref
		BET	Langmuir			wt%	mmol/g	
Co_2(dobdc)	Co-MOF-74, CPO-27-Co	957	1388	298	1	24.9		[77]
Cu_3(BTC)$_2$	HKUST-1	1400		293	1	19.8		[80]
				295	1	18.3		[77]
			1492	298	1	18.4		[59]
Al(OH)(bpydc)	MOF-253	2160	2490	298	1	6.2		[81]
Ni_2(2-amino-BDC)$_2$(DABCO)	USO-2-Ni-A	1530		298	1	14		[82]
Zn_3(NTB)$_2$	SNU-3		419	195	1		6.75	[83]
Cu_3(BPT(N2))$_2$	UMCM-150(N2)			298	1	10.8		[77]
Cr(OH)(BDC)	MIL-53(Cr)			304	1	8.5		[54]
Zn_4O(BDC)$_3$	MOF-5, IRMOF-1	2304	2517	296	1	8.5		[84]

Material	Common name	Surface Area (m^2/g)		Uptake Temperature (K)	Pressure (bar)	Capacity		Ref
		BET	Langmuir			wt%	mmol/g	
				295	1	9.24	2.1	[66]
$Co_2(adenine)_2(CO_2CH3)_2$	bio-MOF-11	1040		298	1	15.2		[85]
Zn(IDC)	IMOF-3	802		298	1	8.6		[86]
$Cu_3(TATB)_2$	CuTATB-60, PCN-6	3811	4436	298	1	15.9		[87]
$Zn(almeIm)_2$	ZIF-93	864		298	1	6.7		[88]
Mg(tcpbda)				298	1	6.5	1.49	[76]
$H_3[(Cu4Cl)_3(BTTri)_8]$	Cu-BTTri	1770	1900	298	1	14.3		[67]
$Zn_2(ox)(atz)_2$		782		293	1.2	14.2		[89]
$Zn_4O(PDC)_3$	IRMOF-11	2096		298	1.1	7.3		[66]
$Cu_3(TATB)_2$	Cu-TATB-30	2665	3065	298	1	13.4		[87]

Material	Common name	Surface Area (m^2/g)		Uptake Temperature (K)	Pressure (bar)	Capacity		Ref
		BET	Langmuir			wt%	mmol/g	
$Zn_4O(BDC\text{-}NH2)_3$	IRMOF-3	2160		298	1.1	5.1		[66]
$Cu_2(bdcppi)(DMF)_2$	SNU-50	2300	2450	298	1	13.7		[90]
$Cr_3O(H2O)2F(BDC)_3$	MIL-101(Cr)	2674		319	1	14.2		[91]
$Cu_2(bptc)(H2O)_2(DMF)_3$	MOF-505	1547		298	1.1	12.6		[66]
Al(OH)(2-amino-BDC)	NH2-MIL-53(Al), USO-1-Al-A	960		298	1	12		[70]
Al(OH)(bpydc) 3 $0.97Cu(BF4)_2$		705		298	1	11.8		[81]
Co(tImb) 3 DMF 3 H_2O		886	1170	298	1	11.7		[92]
Ni2(pbmp)	Ni-STA-12			304	1	9.9		[93]
$Zn_4O(BDC\text{-}C_2H_4)_3$	IRMOF-6	2516		298	1.2	4.6		[66]
Al(OH)(BDC)	MIL-53(Al), USO-1-Al	1300		298	1	10.6		[70]

Material	Common name	Surface Area (m^2/g)		Uptake Temperature (K)	Pressure (bar)	Capacity		Ref
		BET	Langmuir			wt%	mmol/g	
		1235	1627	303	1	9.2		[94]
In(OH)(BDC)				298	1	4		[70]
In(OH)(NH_2BDC)				298	1	8		[70]
$Ni_2(BDC)_2(DABCO)$	USO-2-Ni	1925		298	1	10		[70]
$Cu_3(BPT)_2$	UMCM-150			298	1	10.2		[77]

Table 2-3 High pressure CO_2 adsorption capacities for different MOFs

Material	Common name	Surface Area (m^2/g) BET	Langmuir	Uptake Temperature (K)	Capacity Pressure (bar)	wt%	mmol/g	Ref
$Zn_4O(BBC)_2(H2O)_3$	MOF-200	4530	10400	298	50	73.9		[95]
$Zn_4O(BDC)_3$	MOF-5, IRMOF-1	2296	3840	298	35		21.7	[66]
Mg_2(dobdc)	Mg-MOF-74	1542		278	36	68.9		[64]
V(BDC)(O)	MIL-47	1500		298	20		11	[96][97]
Al(BDC)(OH)	MIL-53(Al)	1100	1500	298	25		10	[96]
				304	25	30.6		[96]
Al(ABDC)(OH)	Amino-MIL-53(Al)			303	13	30	6.7	[69]
				303	5	10	2.3	[69][98]
$Zn_4O(BTB)_{4/3}$(NDC)	MOF-205	4460	6170	298	50	62.6		[95]
$Zn_4O(BTB)_2$	MOF-177	4500	5340	298	50	60.8		[95]

Material	Common name	Surface Area (m^2/g)		Capacity				
		BET	Langmuir	Uptake Temperature (K)	Pressure (bar)	wt%	mmol/g	Ref
$Zn_4O(BTB)_2$	MOF-177	4750	5640	298	42		33.5	[66]
		4690	5400	313	40	60.6		[99]
		4898	6210	298	30	56.8		[100]
Cr(OH)(BDC)	MIL-53(Cr)	1100	1500	304	25		10.1	[96]
Cr(OH)(BDC)(H_2O)	Hydrated MIL-53(Cr)			304	18		7.7	[54][101]
$Cr_3O(H_2O)2F(BDC)_3$	MIL-101(Cr)	4230	5900	304	50	56.9	40	[102]
		3360	4792	298	30	50.2		[103]
Ni_2(dobdc)	Ni-MOF-74, CPO-27-Ni	1218		278	22	54.2		[64]
$Zn_2O(ABDC)_3$	IRMOF-3	2160		298	35		18.7	[66]
[Cu(H_2O)]$_3$(ntei)	PCN-66	4000	4600	298	35	53.6		[104]

Material	Common name	Surface Area (m^2/g)		Uptake Temperature (K)	Capacity			Ref
		BET	Langmuir		Pressure (bar)	wt%	mmol/g	
$Zn_4O(BDC)(BTB)_{4/3}$	UMCM-1	4100	6500	298	24	52.7		[105]
$Al_4(OH)_8(BTEC)$	MIL-120	308	432	303	10		4.2	[106]
$Cu_4(TDCPTM)$	NOTT-140	2620		293	20	46.2		[107]
$Tb_{16}(TATB)_{16}(DMA)_{24}$		1783	3855	298	43	44.2		[108]
$Cr_3O(H_2O)_3F(BTC)_2$	MIL-100(Cr)	1900	3100	304	50	44.2	18	[109]
$Cu_3(BTC)_2$	HKUST-1	1270		313	30	42.8		[110]
		2211		303	40	40.1		[111]
		1571		298	15	35.9	12.7	[58]
		1781		298	35		10.7	[66]
$Cr_3O(H_2O)_2F(NTC)_{1.5}$	MIL-102(Cr)		42.1	304	30	13	3.1	[112]

Material	Common name	Surface Area (m^2/g) BET	Langmuir	Uptake Temperature (K)	Capacity Pressure (bar)	wt%	mmol/g	Ref
$H_3[(Cu_4Cl)_3(BTTri)_8]$	Cu-BTTri	1750	2050	313	40	42.8		[99]
Co(BDP)	Co-BDP	2030	2780	313	40	41.3		[99]
$Zn_2O(ABDC)_3$	IRMOF-11	2096		298	35	14.7		[66]
$[Cu(H_2O)]_3(btei)$	PCN-61	3000	3500	298	35	50.8		[104]
$Zn_2(BPnDC)_2(bpy)$	SNU-9		1030	298	30	29.9		[113]
$Zn_4O(DBDC)_3$	IRMOF-6	2296	3840	298	40		19.8	[66]
$Zn(BDC)(BPY)_{0.5}$	MOF-508b			303	5	26	6	[114]
$Zn_4O(BTE)_{4/3}(BPDC)$	MOF-210	6240	10400	298	50	74.2		[95]
$Al_{12}O(OH)_{18}(H_2O)_3(Al_2(OH)_4)(BTC)_6$	MIL-96(Al)			303	20	18.6		[77]

2.5 Summary

In summary, CO_2 capture is attracting the board attention of both science and technology, because of the large anthropogenic CO_2 emission in the last few decades as a potential way to reduce greenhouse gas emissions. Among the highlighted separation technologies in this review are amine-based absorption, aqueous ammonia-based absorption, and membrane Adsorption with metal organic frameworks seems to be the most promising CO_2 capture technologies. Metal organic frameworks represent a new class of crystalline porous material with advantages such as ease of design and synthesis high porosity and tunable pore properties. In addition, metal organic frameworks possess a great advantage over other capture technologies, due to the reduced heat capacity which reflects the quantity of energy required for heating of the sorbent material to the desorption (regeneration) temperature. MOFs hold several records between porous materials such as the highest surface area, the highest hydrogen uptake based on physical adsorption, and the highest methane, and CO_2 storage. Therefore, MOFs are promising candidates as separation materials for CO_2 capture; however, further investigation and research is needed in several aspects to make metal organic frameworks suitable for real-world applications. For example, controlling the structure of metal organic frameworks such as increasing the strength of the metal-ligand bonds through the incorporation of high-valent metal cations (e.g. Al^{3+} and Ti^{4+}) or more strongly binding ligands (e.g. pyrazolates and triazolate) that can improve the chemical and thermal stability of MOFs and make them more capable of withstanding the high level of water present in the flue gas steam in post-combustion CO_2 capture application.

References

[1] Stewart C, Hessami M. A study of methods of carbon dioxide capture and sequestration - The sustainability of a photosynthetic bioreactor approach. Energ Convers Manage 46 (2005) 403-20.

[2] D'Alessandro D, McDonald T. Toward carbon dioxide capture using nanoporous materials. Pure Appl Chem 83 (2011) 57-66.

[3] Rackley S. Carbon capture and storage. Burlington, MA: Butterworth-Heinemann/Elsevier, 2010.

[4] Olajire A. CO_2 capture and separation technologies for end-of-pipe applications – A review. Energy 35 (2010) 2610-28.

[5] Figueroa J, Fout T, Plasynski S, McIlvried H, Srivastava R. Advances in CO_2 capture technology-The U.S. Department of Energy's Carbon Sequestration Program. Int J Greenh Gas Control 2 (2008) 9-20.

[6] Freguia S, Rochelle G. Modeling of CO_2 capture by aqueous monoethanolamine. AICHE J 49(2003) 1676-86.

[7] Resnik K, Garber W, Hreha D, Yeh J, Pennline H. A parametric scan for regenerative ammonia-based scrubbing for the capture of CO_2. Proceedings of 23rd Annual International Pittsburgh Coal Conference 2006.

[8] Shackley S, Gough C. Carbon Capture and its Storage: An Integrated Assessment 2006.

[9] Energy, DOE/NETL's Carbon Capture R&D Program for Existing Coal-Fired Power Plants Energy 2009.

[10] Ebner A, Ritter J. State-of-the-art adsorption and membrane separation processes for carbon dioxide production from carbon dioxide emitting industries. Separ Sci Technol 44:6 (2009) 1273-421.

[11] Ho M, Allinson G, Wiley D. Reducing the cost of CO_2 capture from flue gases using pressure swing adsorption. Ind. Eng. Chem. Res 47:14 (2008) 4883-90.

[12] Tarka T, Ciferno J, Gray M, Fauth D. CO capture systems using amine enhanced solid sorbents. Presented at the Fifth Annual Conference on Carbon Capture & Sequestration, Alexandria, VA, USA. 30 (2006) 152.

[13] Li J, Kuppler R, Zhou H. Selective gas adsorption and separation in metal-organic frameworks. Chem. Soc. Rev. 38 (2009) 1477-504.

[14] Ruthven D. Principles of adsorption and adsorption processes. New York; Toronto: Wiley, 1984.

[15] Thomas W, Crittenden B. Adsorption technology and design. Oxford; Boston: Butterworth-Heinemann, 1998.

[16] Davini P. Flue gas treatment by activated carbon obtained from oil-fired fly ash. Carbon 40:11 (2002) 1973-9.
[17] Choi S, Drese J, Jones C. Adsorbent materials for carbon dioxide capture from large anthropogenic point sources. ChemSusChem 2:9 (2009) 796-854.
[18] Lozano D, Cazorla D, Linares A. Powdered Activated Carbons and Activated Carbon Fibers for Methane Storage: A Comparative Study. Energy Fuels 16:5 (2002) 1321- 8.
[19] Rodriguez F, Molina M. Activated carbons from lignocellulosic materials by chemical and/or physical activation: an overview. Carbon 30:7 (1992) 1111-8.
[20] Ahmadpour A, Do DD. The preparation of active carbons from coal by chemical and physical activation. Carbon 34:4 (1996) 471-9.
[21] Chue K, Kim J, Yoo Y, Cho S, Yang R. Comparison of activated carbon and zeolite 13X for CO_2 recovery from flue gas by pressure swing adsorption. Ind. Eng. Chem. Res. 34:2 (1995) 591-8.
[22] Siriwardane R, Shen M-, Fisher E, Poston J, A. Adsorption of CO_2 on molecular sieves and activated carbon. Energy Fuels 15:2 (2001) 279–284.
[23] Do DD, Wang K. A new model for the description of adsorption kinetics in heterogeneous activated carbon. Carbon 36:10 (1998) 1539-54.
[24] Na B, Koo K, Eum H, Lee H, Song HK. CO_2 Recovery from Flue Gas by PSA Process using Activated Carbon. Korean J. Chem. Eng. 18:2 (2001) 220-7.
[25] Sircar S, Golden T. Isothermal and isobaric desorption of carbon dioxide by purge. Ind. Eng. Chem. Res. 34:8 (1995) 2881-8.
[26] Kikkinides E, Yang R, Cho S. Concentration and recovery of CO_2 from flue gas by pressure swing adsorption. Ind. Eng. Chem. Res. 32:11 (1993) 2714-20.
[27] Himeno S, Komatsu T, Fujita S. High-pressure adsorption equilibria of methane and carbon dioxide on several activated carbons. J Chem. Eng. Data 50:2 (2005) 369-76.
[28] Lal R. Sequestration of atmospheric CO_2 in global carbon pools. Energy Environ. Sci. 1 (2008) 86-100.
[29] Sayari A, Belmabkhout Y, Serna R. Flue gas treatment via CO_2 adsorption. Chem. Eng. J 171:3 (2011) 760-74.
[30] Walton K, Abney M, LeVan M. CO_2 adsorption in y and X zeolites modified by alkali metal cation exchange. Micropor. Mesopor. Mat. 91:1-3 (2006) 78-84.

[31] Barrer R, Gibbons R. Zeolitic carbon dioxide: Energetics and equilibria in relation to exchangeable cations in faujasite. Trans. Faraday Soc. 61 (1965) 948-61.

[32] Maurin G, Llewellyn P, Bell R. Adsorption mechanism of carbon dioxide in faujasites: Grand canonical Monte Carlo simulations and microcalorimetry measurements. J. Phys. Chem. B 109:33 (2005) 16084-91.

[33] Siriwardane R, Shen M, Fisher E, Losch J. Adsorption of CO_2 on zeolites at moderate temperatures. Energy Fuels 19:3 (2005) 1153-9.

[34] Harlick P, Tezel F. An experimental adsorbent screening study for CO_2 removal from N_2. Micropor. Mesopor. Mat. 76:1-3 (2004) 71-9.

[35] Hernández R, Díaz L, Aguilar G. Adsorption equilibria and kinetics of CO_2, CH_4 and N_2 in natural zeolites. Sep. Purif. Techno.l 15:2 (1999) 163-73.

[36] Cavenati S, Grande C, Rodrigues A. Adsorption Equilibrium of Methane, Carbon Dioxide, and Nitrogen on Zeolite 13X at High Pressures. J. Chem. Eng. Data 49:4 (2004) 1095-101.

[37] Díaz E, Muñoz E, Vega A, Ordóñez S. Enhancement of the CO_2 retention capacity of y zeolites by Na and Cs treatments: Effect of adsorption temperature and water treatment. Ind. Eng. Chem. Res. 47 (2008) 412-8.

[38] Gallei E, Stumpf G. Infrared spectroscopic studies of the adsorption of carbon dioxide and the coadsorption of carbon dioxide and water on CaY- and NiY-zeolites. J. Colloid Interf. Sci. 55:2 (1976) 415-20.

[39] Harlick P, Sayari A. Applications of pore-expanded mesoporous silicas. 3. Triamine silane grafting for enhanced CO_2 adsorption. Ind. Eng. Chem. Res. 45 (2006) 3248-55.

[40] Brandani F, Ruthven D. The effect of water on the adsorption of CO_2 and C_3H_8 on type X zeolites. Ind. Eng. Chem. Res. 43:26 (2004) 8339-44.

[41] Eddaoudi M, Moler D, Li H, Chen B, Reineke T, O'Keeffe M et al. Modular chemistry: Secondary building units as a basis for the design of highly porous and robust metal-organic carboxylate frameworks. Acc. Chem. Res. 34:4 (2001) 319-30.

[42] Férey G. Hybrid porous solids: Past, present, future. Chem. Soc. Rev. 37 (2008) 191-214.

[43] Férey G. Some suggested perspectives for multifunctional hybrid porous solids. Dalton Trans. (2009) 4400-15.

[44] Batten S, Robson R. Angew. Chem Int. Edit 37 (1998) 1460-94.

[45] Li J, Ma Y, McCarthy M, Sculley J, Yu J, Jeong H et al. Carbon dioxide capture related gas adsorption and separation in metal-organic frameworks. Coordin. Chem. Rev. 255:15 (2011) 1791-823.

[46] Klinowski J, Almeida F, Silva P, Rocha J. Microwave-Assisted Synthesis of Metal-Organic Frameworks. Dalton Trans. 40 (2011) 321-30.

[47] Jung D, Yang D, Kim J, Kim J, Ahn W. Facile synthesis of MOF-177 by a sonochemical method using 1-methyl-2-pyrrolidinone as a solvent. Dalton Trans. 39:11 (2010) 2883-7.

[48] Pichon A, James S. An array-based study of reactivity under solvent-free mechanochemical conditions-insights and trends. CrystEngComm 10 (2008) 1839-47

[49] Klinowski J, Almeida F, Silva P, Rocha J. Microwave-assisted synthesis of metalorganic frameworks. Dalton Trans. 40 (2011) 321-30.

[50] Biemmi E, Christian S, Stock N, Bein T. High-throughput screening of synthesis parameters in the formation of the metal-organic frameworks MOF-5 and HKUST-1. Micropor. Mesopor. Mat. 117 (2009) 111-7.

[51] Ahnfeldt T, Guillou N, Gunzelmann D, Margiolaki I, Loiseau T, Férey G et al. $[Al_4(OH)_2(OCH_3)_4(H_2N\text{- }Bdc)_3]\cdot xH_2O$: A 12-connected porous metal-organic framework with an unprecedented aluminum-containing brick. Angew. Chem Int. Edit. 48:28 (2009) 5163-6.

[52] Horike S, Shimomura S, Kitagawa S. Soft porous crystals. Nature Chemistry 1 (2009) 695-704.

[53] Hamon L, Llewellyn PL, Devic T, Ghoufi A, Clet G, Guillerm V et al. Co-adsorption and separation of CO_2-CH_4 mixtures in the highly flexible MIL-53(Cr) MOF. J. Am. Chem. Soc. 131:47 (2009) 17490-9.

[54] Llewellyn P, Bourrelly S, Serre C, Filinchuk Y, Férey G. How hydration drastically improves adsorption selectivity for CO_2 over CH_4 in the flexible chromium terephthalate MIL-53. Angew. Chem Int. Edit. 45:46 (2006) 7751-4.

[55] Serre C, Mellot C, Surblé S, Audebrand N, Filinchuk Y, Férey G. Role of solvent host interactions that lead to very large swelling of hybrid frameworks. Science 315 (2007) 1828-31.

[56] Choi H, Suh M. Highly selective CO_2 capture in flexible 3d coordination polymer networks. Angew. Chem Int. Edit. 48:37 (2009) 6865-9.
[57] D'Alessandro D, Smit B, Long J. Carbon dioxide capture: Prospects for new materials. Angew. Chem Int. Edit. 49:35 (2010) 6058-82.
[58] Liang Z, Marshall M, Chaffee AL. CO_2 adsorption-based separation by metal organic framework (Cu-BTC) versus zeolite (13X). Energy Fuels 23:5 (2009) 2785-9.
[59] Yazaydin A, Benin A Faheem S, Jakubczak P, Low J, Richard R. Willis et al. Enhanced CO_2 adsorption in metal-organic frameworks via occupation of open-metal sites by coordinated water molecules. Chem. Mater. 21:8 (2009) 1425-30.
[60]Sumida K, David L, Rogow, Jarad A. Mason, Thomas M. McDonald, Eric D. Bloch, Zoey R. Herm, Tae-Hyun Bae, and Jeffrey R. Long. Carbon Doixide Capture in Metal-Organic Frameworks. Chem. Rev. 112:2 (2012) 724-781.
[61] Murray L, Dinca M, Yano J, Chavan S, Bordiga S, Brown C et al. Highly-selective and reversible O_2 binding in Cr_3(1,3,5-benzenetricarboxylate)$_2$. J. Am. Chem. Soc. 132:23 (2010) 7856-7.
[62] Xie L, Liu S, Gao C, Cao R, Cao J, Sun C, Su Z. Mixed-Valence Iron(II, III) Trimesates with Open Frameworks Modulated by Solvents. Inorg. Chem. 46:19 (2010) 7782-7788.
[63] Kramer M, Schwarz U, Kaskel S. Synthesis and properties of the metal-organic framework $Mo_3(BTC)_2$ (TUDMOF-1). J. Mater. Chem. 16 (2006) 2245-8.
[64] Dietzel P, Besikiotis V, Blom R. Application of metal-organic frameworks with coordinatively unsaturated metal sites in storage and separation of methane and carbon dioxide. J. Mater. Chem. 19 (2009) 7362-70.
[65] Caskey S, Wong A, Matzger A. Dramatic tuning of carbon dioxide uptake via metal substitution in a coordination polymer with cylindrical pores. J. Am. Chem. Soc. 130:33 (2008) 10870-1.
[66] Millward A, Yaghi O. Metal-organic frameworks with exceptionally high capacity for storage of carbon dioxide at room temperature. J. Am. Chem. Soc. 127:51 (2005) 17998-9.

[67] Demessence A, D'Alessandro D, Foo M, Long J. Strong CO_2 binding in a waterstable, triazolate-bridged metal-organic framework functionalized with ethylenediamine. J. Am. Chem. Soc. 131:25 (2009) 8784-6.

[68] Serre C, Bourrelly S, Vimont A, Ramsahye NA, Maurin G, Llewellyn P et al. An explanation for the very large breathing effect of a metal-organic framework during CO_2 adsorption. Adv. Mater. 19:17 (2007) 2246-51.

[69] Couck S, Denayer J, Baron G, Rémy T, Gascon J, Kapteijn F. An aminefunctionalized MIL-53 metal-organic framework with large separation power for CO_2 and CH_4. J. Am. Chem. Soc. 131:18 (2009) 6326-7.

[70] Arstad B, Fjellvåg H, Kongshaug K, Swang O, Blom R. Amine functionalised metal organic frameworks (MOFs) as adsorbents for carbon dioxide. Adsorption 14:6 (2008) 755-62.

[71] Eddaoudi M, Kim J, Rosi N, Vodak D, Wachter J, O'Keeffe M et al. Systematic design of pore size and functionality in isoreticular MOFs and their application in methane storage. Science 295 (2002) 469-72.

[72] Cavka J, Jakobsen S, Olsbye U, Guillou N, Lamberti C, Bordiga S et al. A new zirconium inorganic building brick forming metal organic frameworks with exceptional stability. J. Am. Chem. Soc. 130:42 (2008) 13850-1.

[73] Serre C, Millange F, Thouvenot C, Noguès M, Marsolier G, Louër D et al. Very large breathing effect in the first nanoporous chromium(III)-based solids: MIL-53 or $CrIII(OH)\cdot\{O_2C\text{-}C_6H_4\text{-}CO_2\}\cdot\{HO_2C\text{-}C_6H_4\text{-}CO_2H\}_x\cdot H_2O_y$. J. Am. Chem. Soc. 124 (2002) 13519-26.

[74] Lin X, Telepeni I, Blake A, Dailly A, Brown C, Simmons J, Zoppi M, Walker G, Thomas K, Mays T, Hubberstey P, Champness N, and Schr der M. High Capacity Hydrogen Adsorption in Cu(II) Tetracarboxylate Framework Materials: The Role of Pore Size, Ligand Functionalization, and Exposed Metal Sites. J. Am. Chem. Soc. 131:6 (2009) 2159-2171.

[75] Zhang Y-, Zhang W, Feng F, Zhang J, Chen X. A highly connected porous coordination polymer with unusual channel structure and sorption properties. Angew. Chem Int. Edit 48 (2009) 5287-90.

[76] Furukawa H, Ko N, Go Y, Aratani N, Choi S, Choi E et al. Ultrahigh porosity in metal-organic frameworks. Science 329 (2010) 424-8.

[77] Seo J, Chun H. Hysteretic gas sorption in a microporous metal-organic framework with nonintersecting 3d channels. Eur. J. Inorg. Chem. 33 (2009) 4946-9.

[78] Dietzel P, Johnsen R, Fjellvåg H, Bordiga S, Groppo E, Chavan S et al. Adsorption properties and structure of CO_2 adsorbed on open coordination sites of metal-organic framework Ni_2(dhtp) from gas adsorption, IR spectroscopy and X-ray diffraction. Chem. Commun. (2008) 5125-7.

[79] Stylianou K, Warren J, Chong S, Rabone J, Bacsa J, Bradshaw D et al. CO_2 selectivity of a 1D microporous adenine-based metal-organic framework synthesised in water. Chem. Commun. 47 (2011) 3389.

[80] Aprea P, Caputo D, Gargiulo N, Iucolano F, Pepe F. Modeling carbon dioxide adsorption on microporous substrates: Comparison between Cu-BTC metal-organic framework and 13X zeolitic molecular sieve. J. Chem. Eng. Data 55 (2010) 3655-61.

[81] Bloch ED, Britt D, Doonan CJ, Uribe-Romo FJ, Furukawa H, Long JR et al. Metal Insertion in a Microporous Metal-Organic Framework Lined with 2,2'-Bipyridine. J. Am. Chem. Soc. 132:41 (2010) 14382-84.

[82] Surblé S, Serre C, Mellot C, Millange F, Férey G. A new isoreticular class of metalorganic-frameworks with the MIL-88 topology. Chem. Commun. (2006) 284-6.

[83] Suh M, Cheon Y, Lee E. Reversible transformation of ZnII coordination geometry in a single crystal of porous metal-organic framework [Zn3(ntb) 2(EtOH)2]·4EtOH. Chem. Eur. J. 13 (2007) 4208-15.

[84] Zhao Z, Li Z, Lin Y. Adsorption and diffusion of carbon dioxide on metal-organic framework (MOF-5). Ind. Eng. Chem. Res. 48 (2009) 10015-20.

[85] An J, Geib S, Rosi N. High and selective CO_2 uptake in a cobalt adeninate metalorganic framework exhibiting pyrimidine- and amino-decorated pores. J. Am. Chem. Soc. 132:1 (2010) 38-9.

[86] Debatin F, Thomas A, Kelling A, Hedin N, Bacsik Z, Senkovska I, Kaskel S, Junginger M, Müller H, Schilde U, Jäger C, Friedrich A. and Holdt J. In Situ Synthesis of an Imidazolate-4-amide-5-imidate Ligand and Formation of a Microporous Zinc–Organic

Framework with H_2-and CO_2-Storage Ability. Angew. Chem Int. Edit 49 (2010) 1258–1262.

[87] Kim J, Yang S, Choi S, Sim J, Kim J, Ahn W. Control of catenation in CuTATB-n metal-organic frameworks by sonochemical synthesis and its effect on CO_2 adsorption. J. Mater. Chem. 21 (2011) 3070-76.

[88] Morris W, Leung B, Furukawa H, Yaghi O, He N, Hayashi H et al. A combined experimental-computational investigation of carbon dioxide capture in a series of isoreticular zeolitic imidazolate frameworks. J. Am. Chem. Soc. 132 (2010) 11006-8.

[89] Vaidhyanathan R, Iremonger S, Dawson K, Shimizu G. An amine-functionalized metal organic framework for preferential CO_2 adsorption at low pressures. Chem. Commun. (2009) 5230-32.

[90] Prasad T, Hong D, Suh M. High gas sorption and metal-ion exchange of microporous metal-organic frameworks with incorporated imide groups. Chem. Eur. J. 16 (2010) 14043-50.

[91] Chowdhury P, Bikkina C, Gumma S. Gas adsorption properties of the chromium based metal organic framework MIL-101. J. Phys. Chem. C 113:16 (2009) 6616-21.

[92] Chen S, Chen M, Takamizawa S, Wang P, Lv G, Sun W. Porous cobalt(ii)-imidazolate supramolecular isomeric frameworks with selective gas sorption property. Chem. Commun. 47 (2011) 4902-4.

[93] Miller S, Pearce G, Wright P, Bonino F, Chavan S, Bordiga S et al. Structural transformations and adsorption of fuel-related gases of a structurally responsive nickel phosphonate metal-organic framework, Ni-STA-12. J. Am. Chem. Soc. 130 (2008) 15967-81.

[94] Rallapalli P, Prasanth K, Patil D, Somani R, Jasra R, Bajaj H. Sorption studies of CO_2, CH_4, N_2, CO, O_2 and Ar on nanoporous aluminum terephthalate [MIL-53(Al)]. J. Porous Mat. 18:2 (2011) 205-10.

[95] Furukawa H, Ko N, Go Y, Aratani N, Choi S, Choi E et al. Ultrahigh porosity in metal-organic frameworks. Science 329 (2010) 424-8.

[96] Bourrelly S, Llewellyn P, Serre C, Millange F, Loiseau T, Férey G. Different adsorption behaviors of methane and carbon dioxide in the isotypic nanoporous metal terephthalates MIL-53 and MIL-47. J. Am. Chem. Soc. 127 (2005) 13519-21.

[97] Rowsell J, Yaghi O. Effects of functionalization, catenation, and variation of the metal oxide and organic linking units on the low-pressure hydrogen adsorption properties of metal-organic frameworks. J. Am. Chem. Soc. 128 (2006) 1304-15.

[98] Pachauri R, Reisinger A. IPCC Fourth Assessment Report. Intergovernmental Panel on Climate Change 2007.

[99] Herm Z, Swisher J, Smit B, Krishna R, Long J. Metal-organic frameworks as adsorbents for hydrogen purification and precombustion carbon dioxide capture J. Am. Chem. Soc. 133 (2011) 5664-7.

[100] Jung D, Yang D, Kim J, Kim J, Ahn W. Facile synthesis of MOF-177 by a sonochemical method using 1-methyl-2-pyrrolidinone as a solvent. Dalton Trans. 39 (2010) 2883-7.

[101] Carbon Capture and Storage, Full-Scale Demonstration Progress Update: www.iea.org/G8/docs/ccs_g8july09.pdf, OECD/IEA, 2009. .

[102] Llewellyn P Bourrelly S, Serre C, Vimont A, Daturi M, Hamon L, Weireld G, Chang J, Hong D, Hwang Y, Jhung S, and F rey G. High Uptakes of CO_2 and CH_4 in Mesoporous Metal-Organic Frameworks MIL-100 and MIL-101. Langmuir 24:14 (2008) 7245-50.

[103] Zhang Z, Huang S, Xian S, Xi H, and Li Z. Adsorption Equilibrium and Kinetics of CO_2 on Chromium Terephthalate MIL-101. Energy Fuels 25:2 (2011) 835-42.

[104] Yuan D, Zhao D, Sun D, Zhou H. An isoreticular series of metal-organic frameworks with dendritic hexacarboxylate ligands and exceptionally high gas-uptake capacity. Angew. Chem Int. Edit 49 (2010) 5357-61.

[105] Mu B, Schoenecker P, Walton K. Gas adsorption study on mesoporous metal organic framework UMCM-1. J. Phys. Chem. C 114:14 (2010) 6464-71.

[106] Volkringer C, Loiseau T, Haouas M, Taulelle F, Popov D, Burghammer M et al. Occurrence of uncommon infinite chains consisting of edge-sharing octahedra in a porous metal organic framework-type aluminum pyromellitate Al 4(OH) 8[C 10O $8H_2$](MIL-120): Synthesis, Structure, and Gas Sorption Properties. Chem. Mater. 21:24 (2009) 5783-91.

[107] Tan C, Yang S, Champness N, Lin X, Blake A, Lewis W et al. High capacity gas storage by a 4,8-connected metal-organic polyhedral framework. Chem. Commun. 47 (2011) 4487-9.

[108] Park Y, Sang B, Kim H, Kim K, Won B, Choi K et al. Crystal structure and guest uptake of a mesoporous metal-organic framework containing cages of 3.9 and 4.7 nm in diameter. Angew. Chem Int. Edit 46 (2007) 8230-3.
[109] Férey G, Serre C, Mellot C, Millange F, Surblé S, Dutour J et al. A hybrid solid with giant pores prepared by a combination of targeted chemistry, simulation, and powder diffraction. Angew. Chem Int. Edit 43 (2004) 6296-301.
[110] Moellmer J, Moeller A, Dreisbach F, Glaeser R, Staudt R. High pressure adsorption of hydrogen, nitrogen, carbon dioxide and methane on the metal-organic framework HKUST-1. Micropor. Mesopor. Mat. 138 (2011) 140-8.
[111] Hamon L, Jolimaître E, Pirngruber G. CO_2 and CH_4 separation by adsorption using Cu-BTC metal-organic framework. Ind. Eng. Chem. Res. 49 (2010) 7497-503.
[112] Surblé S, Millange F, Serre C, Düren T, Latroche M, Bourrelly S et al. Synthesis of MIL-102, a chromium carboxylate metal-organic framework, with gas sorption analysis. J. Am. Chem. Soc. 128 (2006) 14889-96.
[113] Park H, Suh M. Stepwise and hysteretic sorption of N_2, O_2, CO_2, and H_2 gases in a porous metal-organic framework [$Zn_2(BPnDC)_2(bpy)$]. Chem. Commun. 46 (2010) 610-2.
[114] Bastin L, Bárcia P, Hurtado E, Silva J, Rodrigues A, Chen B. A microporous metal-organic framework for separation of CO_2/N_2 and CO_2/CH_4 by fixed-bed adsorption. J. Phys. Chem. C 112 (2008) 1575-81.

Chapter 3: Review on Different Characterization Techniques

Several characterization techniques are used for the qualitative analysis of prepared catalyst. XRD, SEM, EDS, BET, TGA and GC-MS tests have used in order to check the properties of catalyst. The basic working conditions and the principles of the techniques are mentioned below.

3.1 X-ray powder diffraction (XRD)

A German scientist "Wilhelm Conrad Rontgen" discovered the X-rays in 1895. X-ray powder diffraction (XRD) is used for identification of phase of crystalline material and information on unit cell dimensions. X-rays are electromagnetic waves of shorter wavelength having energy between 200 eV to 1 MeV [1]. XRD uses the method of constructive interference of crystalline sample with monochromatic X-rays. The main operating principle of XRD is determined by Bragg‟s law. The radiation having wavelength similar to atomic spacing of crystal is scattered by atoms of crystalline solid and experience constructive interference. Consider Xrays strikes on a crystalline solid having inter planar distance „d‟. Some of the X-rays got scattered from the crystal atoms. If the dispersed waves affect productively, they stay in phase as the variation between the path lengths of the two waves is equivalent to an integer multiple of the wavelength. The variation in the path length of two waves experiencing interference is given by $2d\sin\theta$ and θ is the scattering angle. The Bragg's law describes the relation of θ with wavelength and interplaner spacing „d‟ for the constructive interference to be at its greatest by following equation

$$2d\mathrm{Sin}\theta = n\lambda$$

The material sample is finely pulverized and average bulk composition is defined using this technique. The high speed electrons are generated from filament, which strikes a metal plate (Cu) to give X-Rays. The generated x-rays are allowed to pass through a collimator which absorbs all X-rays except a narrow beam. Filters or crystal monochromators are

used for monochromatization of X-rays. Moreover the X-rays fall on sample and the scattered X-rays are recorded by a photographic film or counter methods. The result obtained from this technique is called diffractogram. The difractogram can be obtained in either intensity vs. transmittance or reflectivity format as shown in “Figure 3-1”. The apparatus used for analysis is “Bruker AXS Strahlenschutzbox (schmal) A25-A2”.

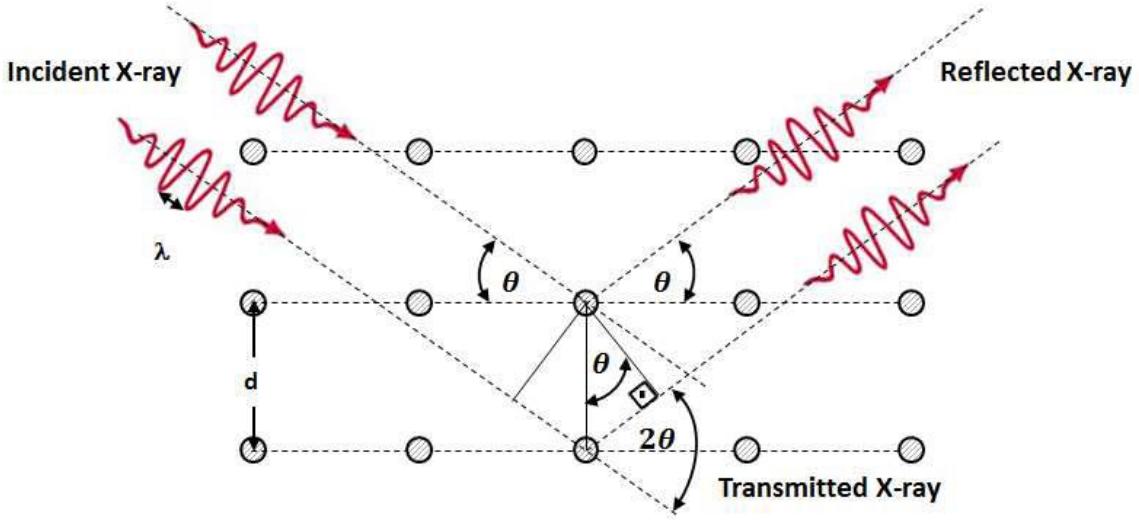

Figure 3-1: Bragg's Law figurative description

3.2 Scanning Electron Microscopy (SEM)

Scanning Electron Microscope is a technique that describes the structural properties of the material. There are two main component of SEM that is electronic console and electron column. Electronic console controls the knobs and switches are used to control the filament current, voltage, brightness and contrast. The function of electron column is generating electron beam with the help of vacuum pump, which is shown in “Figure 3-2”. Electromagnetic deflection coils are used to scan the sample image. The lower portion of the column is specimen chamber and second electron detector is present above the sample stage. Free electrons are produced from electron gun by thermionic emission from filament (tungsten) at temperature on 2700 K. the function of filament is to electrons generated from electron gun. Condenser lenses are used to converge the beam and pass through the focal point. The electrons column is used to find the aperture of sample image. These apertures reduce the extraneous electrons in the lenses. The size of

the beam regulates with the using of final lens. Detailed specimen of SEM is in following [2].

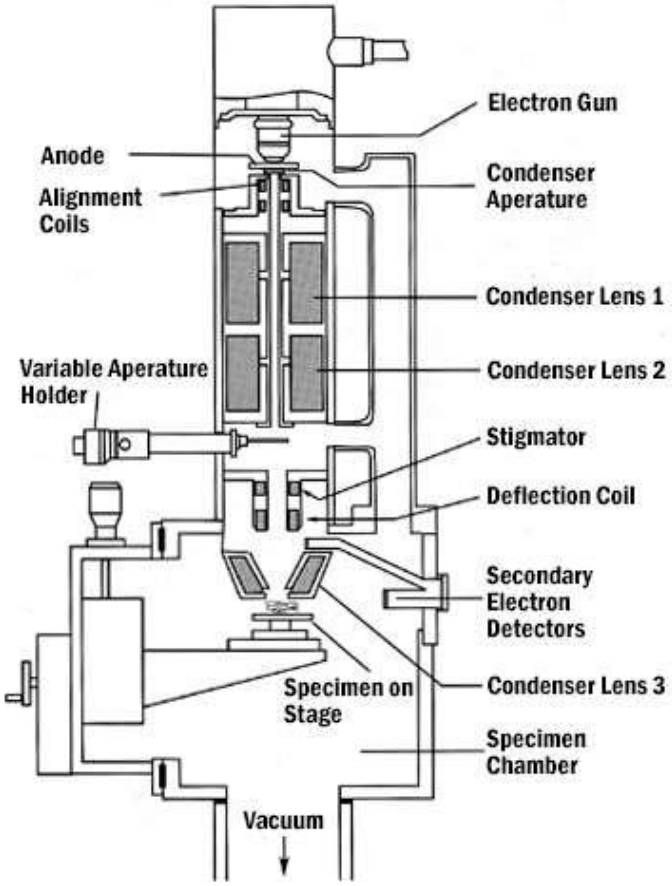

Figure 3-2: SEM instrument diagram

Objective lens contains the deflection coils and images are normally formed by scanning with the restoring of electron beam. Sample chamber contains the sample stage and controls are located at the lower portion of the column. The morphology analysis is controlled by electron beam. A high pressure is required for the detail and good images ranging about 5*10-5torr [3].

3.3 Brunauer-Emmett-Teller Analyses (BET)

BET is named after the first names of its inventors Brunauer-Emmett-Teller. This technique is used for the external surface area evaluation and pore measurements yielding important information about the effects of porosity and particle size properties [4]. The heterogeneous catalysts have individual or more group of pores whose size and volume are influenced by the method of preparation of catalyst.

The pores are differentiated in diverse classes reliant on their size.

- Micropores: Size < 2nm
- Mesopores: 2nm < Size < 50nm
- Macropores: Size > 50nm

Pores can further be divided in different categories depending upon their geometry. Pores can be cylindrical or slit shaped or more commonly irregular shaped. The irregular shaped pores can be bottleneck shaped or funnel shaped. Apart from that the pores can be divided into various categories depending upon their connectivity. Some pores are connected with each other to form a porous network whereas some pores are „closed" which means they have no access from any sides. Some pores are „through" which means they can be accessed from two or more sides where some pores are termed as „open pores" because they can be accessed from only one side. These attributes of pores can greatly affect the catalytic behavior of the porous solid.

Nitrogen Adsorption at 77K is the best extensively used technique for surface area analysis and characterization of porous texture. This analysis method uses the nitrogen multilayer physical adsorption studied against change of pressure. First step is the determination of adsorption isotherm; nitrogen adsorbed volume against its relative pressure. The adsorption isotherm depends upon the porous texture of the solid.

3.3.1 TYPE I (Microporous Solids)

There is strong contact among pore walls and the adsorbate because of which adsorption takes place at very low relative pressure. First the pores are filled at low relative pressures without capillary condensation. Once the pores got filled the adsorption is continued at external surface as in case of mesoporous solid.

3.3.2 TYPE II (Macroporous Solids)

At low pressure adsorption takes place due to formation of monolayer whereas at higher relative pressures multilayer adsorption takes pace. The monolayer and multilayer formation processes always overlaps.

3.3.3 TYPE III

In the Type III isotherm, the interactions between the adsorbate-adsorbent are relatively weak hence the molecules that are adsorbed are gathered around the sites on the surface of a macroporous or nonporous solid that are most favorable. As opposed to the

isotherm of Type II, there is a finite amount that remains adsorbed at the saturation pressure (i.e., at $p/p^o=1$).

3.3.4 TYPE IV (Meso porous Solid)

At low relative pressures monolayer formation takes place. At higher relative pressures multilayer formation occurs until a condensation pressure is achieved which gives a sharp rise in adsorbed volume.

3.3.5 TYPE V

At low p/p^o range, the isotherm shape of Type V is very comparable to that of Type III and this can be ascribed to the adsorbate-adsorbent interactions that are relatively weak. At p/p^o range which is higher, the clustering of the molecules is followed by pore filling.

3.3.6 TYPE VI (Ultra micro porous Solids)

The relative pressure at which adsorption occurs depends on the adsorbate-surface interaction. If the solid is energetically uniform the whole process takes place at a well-defined pressure. Whereas if the surface have energetically non uniform groups, a stepped isotherm is achieved.

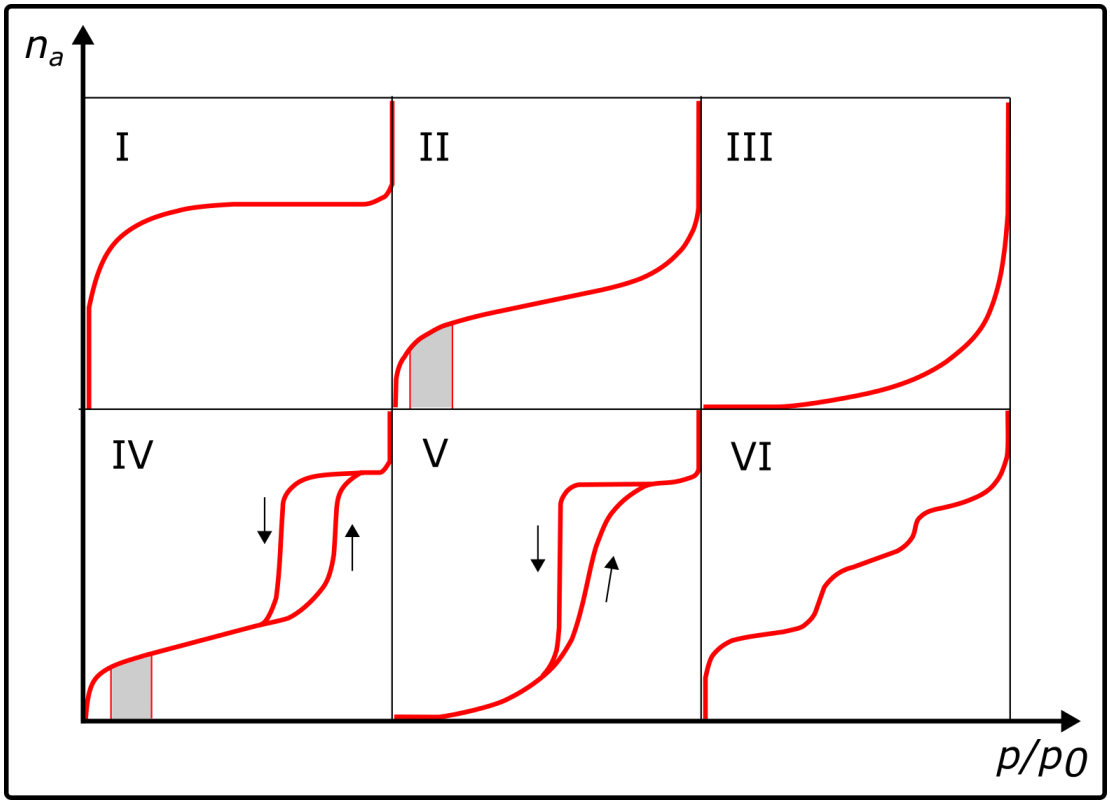

Figure 3-3: Different types of adsorption isotherms

3.4 Thermo-gravimetric analysis (TGA)

Thermal analysis is a technique used to study the changes in weight of a substance when subjected to the temperature change. When any material is subjected to heating under controlled environment it undergoes several changes due to reduction, oxidation, or decomposition. Such weight changes can be used to study the thermal stability and kinetics of any sample under temperature. The basic apparatus used for thermal analysis is mentioned in “Figure 3-4”.

Thermo-gravimetric analysis also termed as thermal gravimetric analysis is a kind of thermal analysis. It is defined by International Confederation for Thermal Analysis and Calorimetric (ICTAC) as a method in which the variation in the mass of a sample is observed as it is subjected to a temperature controlled program. In this technique we observe the variations in physical or chemical properties of sample by with constant heating rate, or as a function of time (through constant temperature or constant mass loss). There are three types of thermal gravimetric analysis used as given below

3.4.1 Dynamic TGA

Weight change is examined while temperature rise is linear with time.

3.4.2 Static TGA

Weight change is recorded against time while providing constant temperature.

3.4.3 Quasistatic TGA

A series of temperature increase is provided and sample weight remains constant for each series.

The dynamic thermal gravimetric analysis is performed in this study. The constant rise in temperature is provided and the weight changes are studied.

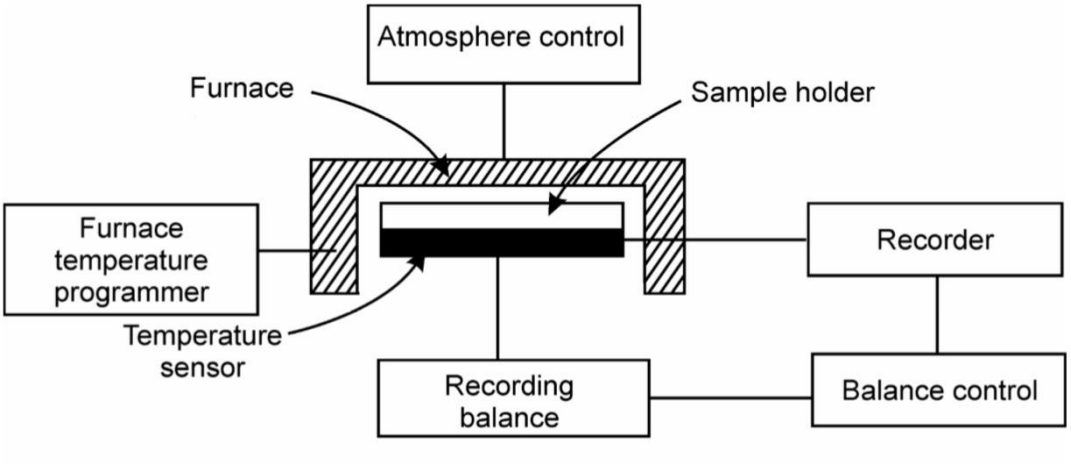

Figure 3-4: TGA Apparatus block diagram

3.5 Energy Dispersive X-ray Spectrometry (EDS)

EDS are attached with the scanning electron microscopy and solid sample are bombarded with the electron of focused beam to analyze the chemical composition. All the elements can be analyses from atomic number 4 (Be) to 92 (U). X-ray microanalysis can be done when high energy electron is bombarded with the sample in an electron microscopy. To separate the x-ray with the energy level so we use energy dispersive spectrometer. The basic diagram of apparatus is given in following figure.

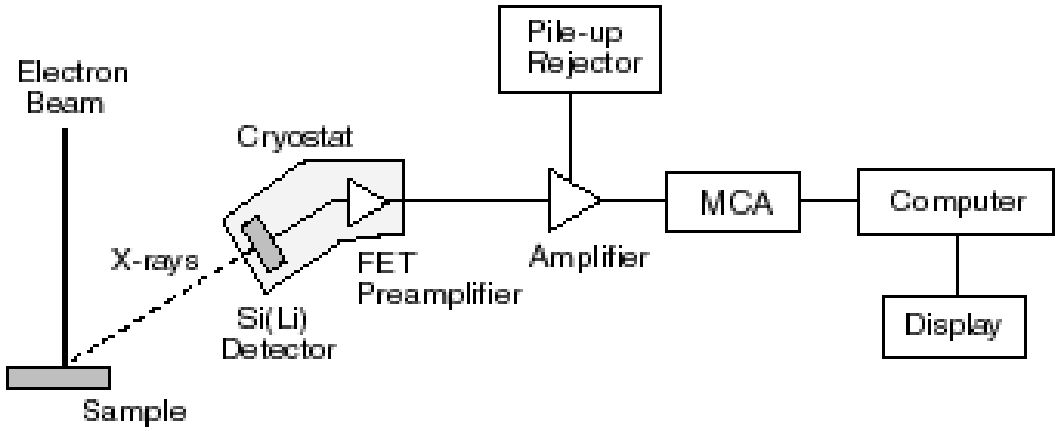

Figure 3-5: Energy Dispersive X-ray Spectroscopy

3.6 Single-Crystal X-ray Diffraction

Single-crystal X-ray Diffraction is an analytical technique in which detailed information is provided about the internal lattice of a substance that is crystalline. The

information provided includes bond-angles, bond-lengths, unit cell dimensions, and details of site-ordering. The refinement of the single-crystal is also directly related to SCXRD, in which the generated data from X-ray analysis is refined and interpreted so that the crystal structure is obtained.

There are three elements which are basic to an X-ray diffractometers, a sample holder, an X-ray tube, and an X-ray detector. A cathode ray tube is used to generate X-rays. The heating of a filament produces electrons which are accelerated towards a target by applying a voltage These X-rays are made parallel to each other and focused onto the sample. When the Bragg Equation is satisfied by the geometry of the incident X-rays impacting the sample, constructive interference occurs. This X-ray signal is recorded and processed by a detector which converts the signal to a count rate. This count rate is then sent to an output device such as a computer monitor or a printer which displays the result.

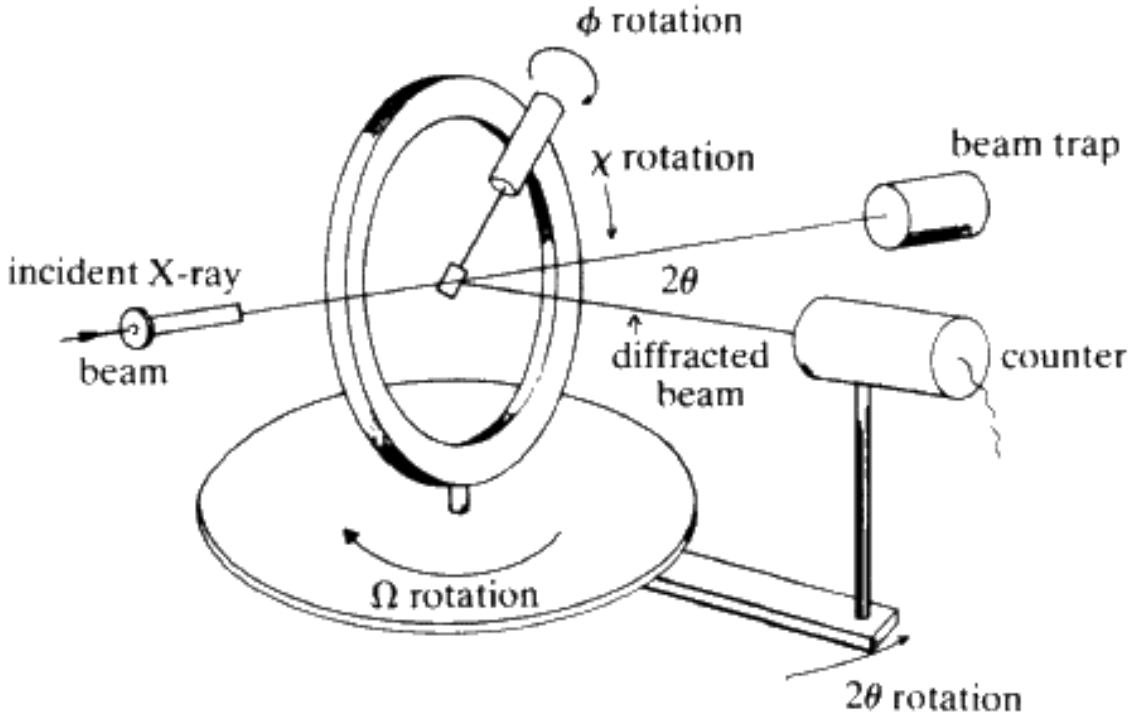

Figure 3-6: Single-crystal X-ray Diffractometer

3.7 Summary

For the testing of catalyst several characterization techniques like XRD, SEM, BET and TGA are used for the prepared catalyst. Scanning electron microscopy is a technique which can be used to find out the structural properties of the crystal. X-ray diffraction (XRD) is the technique to find out the phase of an unknown crystalline material and also

the information about the crystal shape and size. EDS was used for the elemental analysis and TGA gives the information about the thermal degradation of the material.

References

[1] C. Suryanarayana, M. G. Norton, X-ray Diffraction: A Practical Approach, Plenum, New York, 1998.

[2] Brandon Cheney, Introduction to Scanning Electron Microscopy

[3] S. Lowell, J. E. Shields, M. A. Thomas, M. Thommes, Characterization of Porous Solids and Powders: Surface Area, Pore Size and Density, Kluwer Acadamic Publishers, London, 2009.

[4] P. Gabbott, Principles and Applications of Thermal Analysis, Blackwell Publications, UK, 2011.

Chapter 4: Methodology

For the synthesis of MOFs, a so called “modular synthesis” method is employed in which a mixture of appropriate ligands and the metal precursors are combined in a solvent under mild conditions. This allows the MOF to be synthesized with a crystalline porous network. When the MOF is synthesized, it contains the solvent used during synthesis trapped in the pores which needs to be removed. This solvent is removed either by applying heat, vacuum or exchange with molecules that are volatile in nature. This removal of the solvent from MOF is known as the activation of MOF which results in a large surface area and pore volume of the MOF. Many other synthesis approaches have been developed for MOF which include sonication synthesis [1], microwave synthesis, solvothermal synthesis, solid start synthesis [2] and mechanochemical synthesis [3].

4.1 Materials and Methods

Copper Nitrate ($Cu(NO_3)_2$), terephthalic acid (BDC) , 2-aminoterephthalic acid (H_2ABDC), N,N-dimethylformamide (DMF) and methanol were all purchased from Sigma-Aldrich. For the synthesis of MOFs, all the chemicals were used as purchased, without any further purification.

4.1.1 Synthesis of Cu-BDC MOF

For the synthesis of Cu-BDC MOF, the procedure published by Carson et al. [4] was followed in which equimolar quantities of terephthalic acid (BDC, 0.724 g) and copper nitrate ($Cu(NO_3)_2$, 1.053 g) were dissolved in 87 ml of DMF used as a solvent. When the reactants were mixed and dissolved, a blue solution was obtained which was placed in a 120 ml closed glass bottle. The glass bottle with the blue solution was placed in an oven which was set at 110℃ for 36 hrs. After 36 hrs, when the solution was removed from the oven, blue precipitated crystals were visible in the bottom of the bottle which were recovered through centrifugation. For the recovery of MOF crystals, the centrifuge was run at 4500 rpm for 20 mins which separated the MOF from the solution. After recovery, the MOF crystals were washed several times using DMF. Once washed, the MOF crystals were then dried at a temperature of 180℃ to remove any DMF molecules present in the MOF.

4.1.2 Synthesis of Cu-ABDC MOF

The Cu-ABDC MOF was prepared using the solvothermal method for MOF synthesis which is the most common and widely used method for synthesizing MOFs. For the synthesis of Cu-ABDC MOF, H_2ABDC (1 g) and copper nitrate (2.07 g) were dissolved in 60ml of DMF. [5] The reagents for the synthesis were stirred at room temperature for 10 min and then transferred to an autoclave. The autoclave was heated in an oven at 110℃ for 24 hrs under autogenous pressure. Upon completion of the solvothermal reaction, light-green colored crystals were obtained which were recovered through centrifugation at 4000 rpm for 25 min, washed in DMF and then rinsed multiple times in methanol. The crystals obtained were then dried in at 60℃.

4.1.3 Activation of MOFs

When the MOFs were synthesized and dried, they still might contain some of the solvent molecules trapped in the pores. Before the characterization and testing of the MOF, it was activated by heating the MOF samples in a vacuum oven. The samples were heated at 160℃ under vacuum conditions for a period of 12 hrs. This helped to remove the trapped solvent molecules from the pores.

4.2 Characterization of MOFs

Several characterization techniques were used to qualitatively analyze the MOFs prepared. The characterization techniques used included SEM, EDS, XRD, SCXRD and TGA.

4.2.1 Scanning Electron Microscopy (SEM)

For the Scanning Electron Microscopy (SEM) of the MOF samples, a TESCAN SEM VEGA3 microscope was used. The samples were gold-coated before taking the SEM images in order to prevent the charging of the sample. The HV of the microscope was set to 20kV and images of the MOF crystals were taken at different resolutions.

4.2.2 Energy Dispersive X-ray Spectroscopy (EDS)

The EDS of the MOFs was also determined by using the TESCAN SEM VEGA3 microscope. An image was taken and different points were selected at which the software determined the elemental composition of the MOF samples.

4.2.3 Powder X-ray Diffraction

A Bruker Advanced X-ray diffraction system (40 kV, 30 mA) was used for the collection of Powder X-ray Diffraction (PXRD) patterns of the MOF samples. The operating 2θ range of the diffractometer was from 5 to 45° with a step size of 0.02°. For the Cu-BDC MOF, the PXRD patterns were compared with the reported MOF. [4] As for the PXRD pattern of Cu-ABDC MOF, it was compared with the simulated patterns obtained from single crystal data using the Mercury program.

4.2.4 Single Crystal XRD

For the single crystal XRD studies, the prepared sample was sent to UK where the tests were conducted in the lab of Cardiff University. Single-crystal structure analyses of the MOF were performed on an Oxford Diffraction Gemini CCD diffractometer which was operating in the ω scan mode.

4.2.5 Thermo-gravimetric Analysis

The thermal stability of the MOFs was analyzed on a DTG-60H Thermo Gravimetric Analyzer (TGA). The environment used during analysis was of N_2 for both the MOFs.

For Cu-BDC MOF, a 10 mg sample was used for the test and it was heated from 20 to 700°C at a heating rate of 10°Cmin^{-1}. For the Cu-ABDC MOF, a heating rate of 10°C min^{-1} from 20 to 500°C was used and the weight of sample was 3.57 mg. During the thermal stability test of the MOFs, N_2 gas was supplied at a flow-rate of 50 ml min^{-1}.

4.3 N_2 adsorption study

The N_2 adsorption studies of the MOF were conducted on a Quantachrome Nova 2200e and the Quantachrome NovaWin application was used for the calculation of surface area and pore volumes of the MOF. Before conducting the N_2 adsorption analysis, the sample was degassed at 160°C under vacuum for 12 hours. The N_2 adsorption isotherms were obtained at -196°C at a relative pressure of P/P^o= 0.005-0.9 for the surface area and pore volume analysis of the MOF.

4.4 CO_2 adsorption study

For the CO_2 adsorption studies of the MOF, Quantachrome Isorb-HP100 volumetric type sorption analyzer was used which evaluated the adsorption capacity by monitoring pseudo equilibrium adsorption uptakes. Prior to the CO_2 adsorption analysis

of the MOF, the sample was degassed at a temperature of 120℃ for 12 hours and then back filled with helium gas. During the CO_2 adsorption analysis, the Adsorbate Equation of State used was the Helmholtz. The sample was tested for adsorption at 0℃ and 25℃ at absolute pressures from 0 to 20 bar.

4.5 Summary

This study focused on the synthesis of two MOFs, Cu-BDC and Cu-ABDC. Both the MOFs were synthesized using the conventional method for MOF synthesis i.e. solvothermal reaction. Once the MOFs were prepared, they were characterized using different characterization techniques like SEM, EDX, XRD and TGA. The adsorption studies of both the MOFs were also carried out to identify their capabilities to adsorb CO_2 at different conditions of pressures and temperature.

References

[1] Jung D, Yang D, Kim J, Kim J, Ahn W. Facile synthesis of MOF-177 by a sonochemical method using 1-methyl-2-pyrrolidinone as a solvent. - Dalton Trans. 39:11 (2010) 2883-87.

[2] Klinowski J, Almeida F, Silva P, Rocha J. Microwave-assisted synthesis of metalorganic frameworks. Dalton Trans. 40 (2011) 321-30.

[3] Pichon A, James S. An array-based study of reactivity under solvent-free mechanochemical conditions-insights and trends. CrystEngComm 10 (2008) 1839-47.

[4] C. G. Carson et al., “Synthesis and structure characterization of copper terephthalate metal-organic frameworks,” Eur. J. Inorg. Chem. 16 (2009) 2338–2343.

[5] Ying Yang, Rijia Lin, Lei Ge, Lei Hou, Paul Bernhardt, Thomas E. Rufford, Shaobin Wang, Victor Rudolph, Yaoyu Wang and Zhonghua Zhu. Synthesis and characterization of three amino-functionalized metal–organic frameworks based on the 2-aminoterephthalic ligand. Dalton Trans. 44 (2015) 8190-97.

Chapter 5: Results and Discussion

5.1 Characterization Results

5.1.1 Scanning Electron Microscopy (SEM)

SEM is a technique of characterization of material which shows us the structure of the material and hence gives us information about the structural properties of the crystals in the material. Figure 5-1 shows the SEM images of Cu-BDC MOF taken at different resolutions. The images are taken at X1000 (Figure 5-1(a)), X2700 (Figure 5-1(b)) and X5000 (Figure 5-1(c)). From the images it is clearly visible that the prepared crystal of Cu-BDC MOF are somewhat regular and in the shape of independent cuboid crystals. It can also be noted that the Cu-BDC MOF shows good crystallinity.

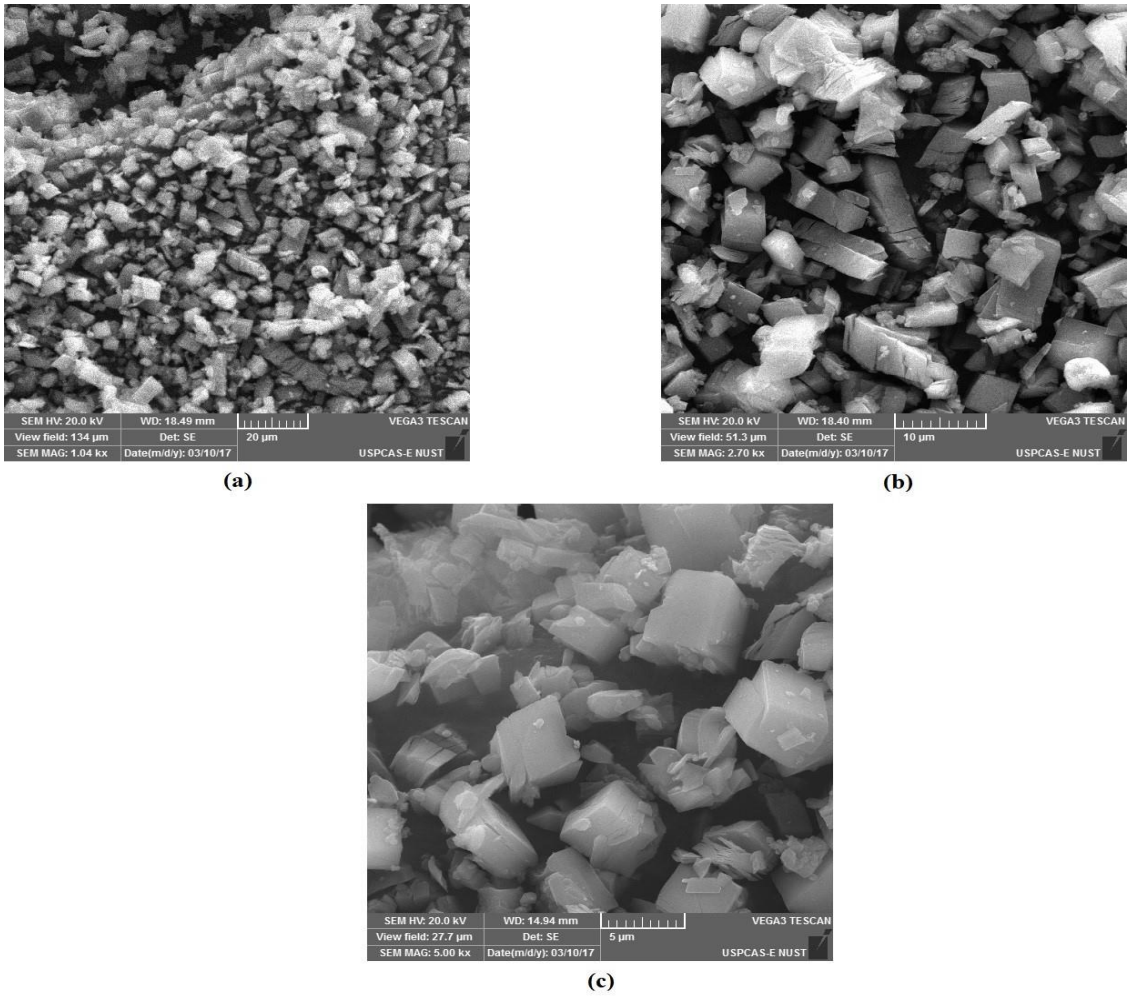

Figure 5-1: SEM images of Cu-BDC MOF

The SEM images of the Cu-ABDC MOF are shown in Figure 5-2. The first two images, Figure 5-2(a) and (b) are of a single crystal being focused but at different resolutions, Figure 5-2 (a) being at a resolution of X5000 and Figure 5-2 (b) being at X26000. It can be clearly seen that small and thin sheet like crystals are attached to the Cu-ABDC MOF crystal. The next three SEM images i.e. Figure 5-2 (c), (d) and (e) are of another area in the MOF showing irregular shaped crystals and it can be seen that there also exist thin sheet like structures in the MOF. Upon maximum magnification of X48000 in Figure 5-2 (e), we can see that small crystals are cluttered together.

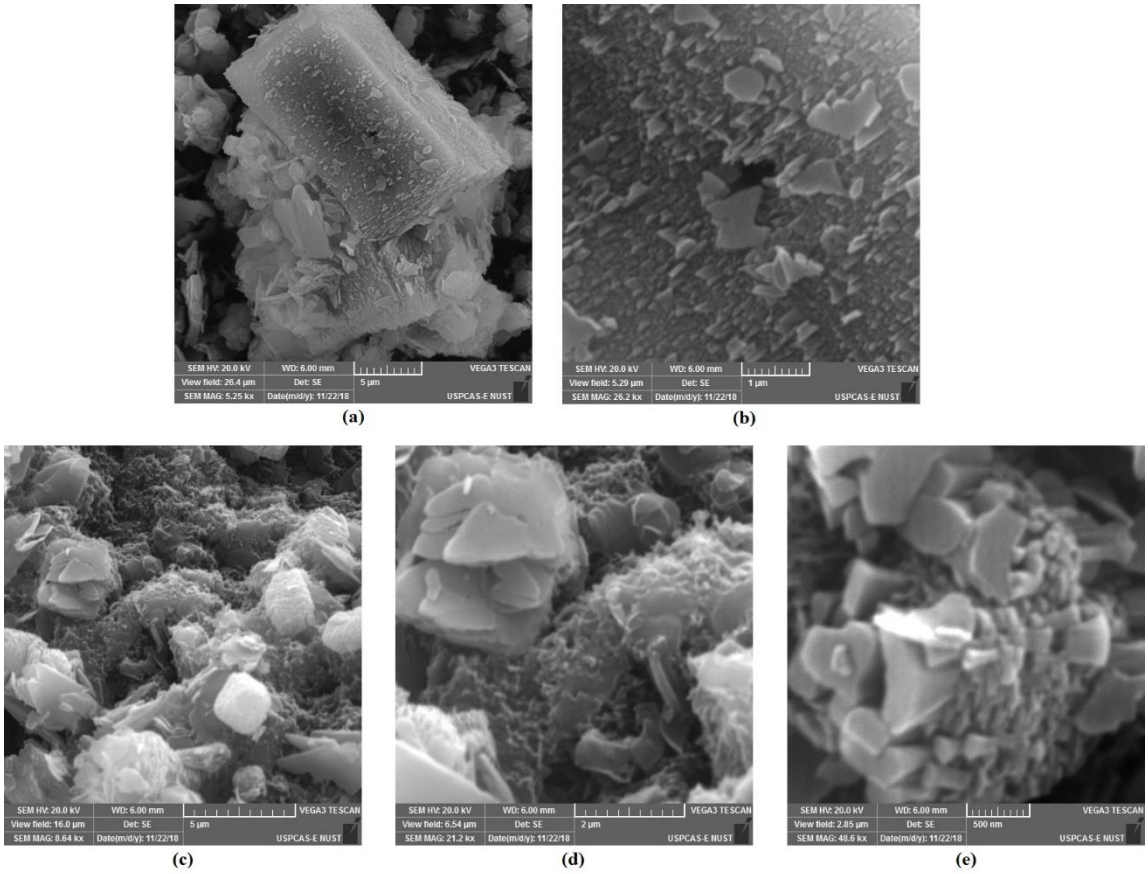

Figure 5-2: SEM images of Cu-ABDC MOF

Comparing the SEM images of both Cu-BDC MOF and Cu-ABDC MOF with each other, it can be noted that the crystals of Cu-BDC MOF are regular and show good crystallinity but those of Cu-ABDC MOF are irregularly shaped and are a mixture of different shaped crystals. It can also be observed that the crystals of Cu-ABDC MOF (Figure 5-2) are of much smaller size than that of Cu-BDC MOF (Figure 5-1).

5.1.2 Energy-dispersive X-ray Spectroscopy (EDS)

The EDS data of the synthesized MOFs during this study, Cu-BDC MOF and Cu-ABDC MOF, is given in Table 5-1. From the elemental composition of the MOFs, it can be confidently stated that the MOFs prepared are without any impurity because there is no foreign element present in the MOF.

Table 5-1: Elemental composition of MOFs from EDS

Element/Sample	Cu-BDC MOF	Cu-ABDC MOF
C wt%	51.93	55.17
O wt%	35.25	32.31
Cu wt%	12.82	5.03
N wt%	-	7.49

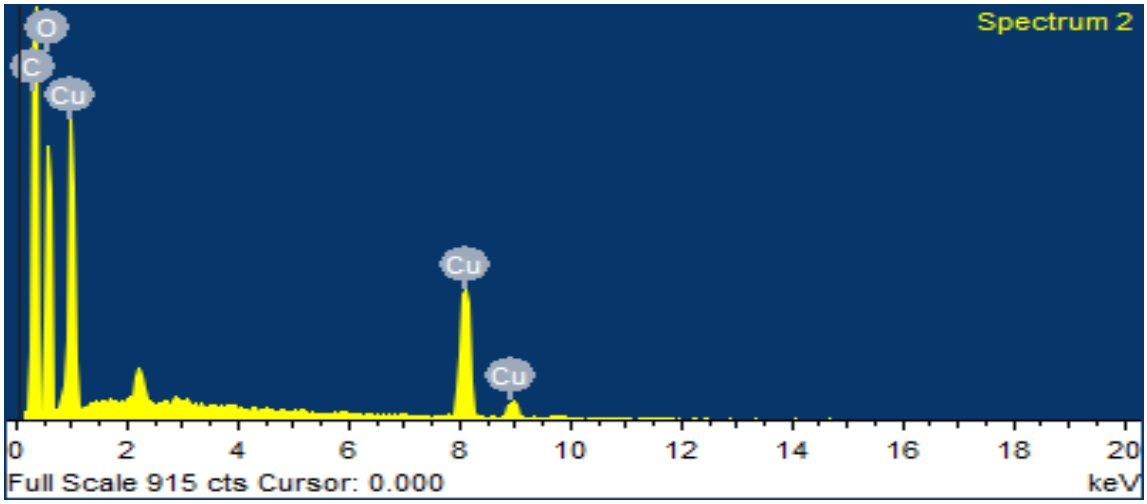

Figure 5-3: EDS data of Cu-BDC MOF

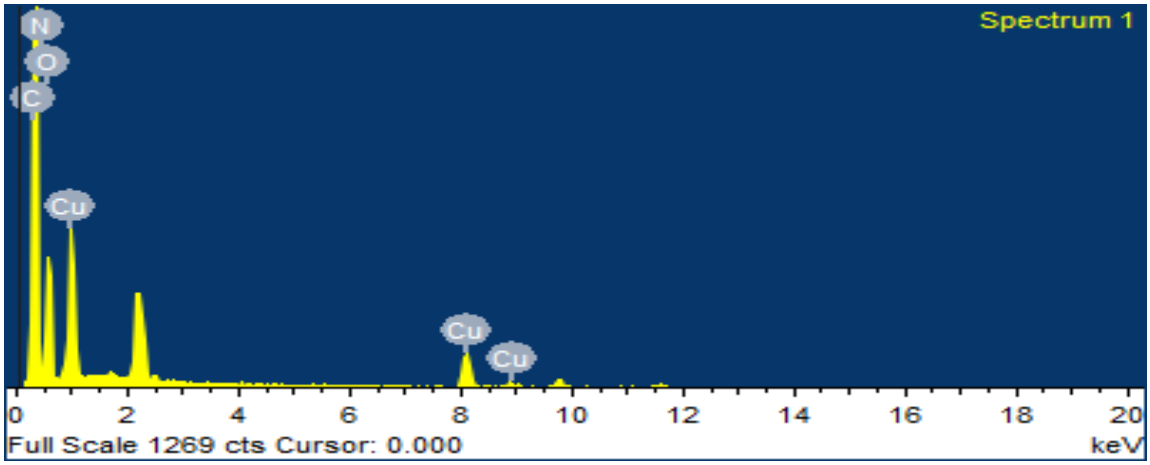

Figure 5-4: EDS data of Cu-ABDC MOF

5.1.3 X-ray diffraction (XRD)

X-ray diffraction (XRD) is a characterization technique which is used to determine the phase of a crystalline material that is unknown. It also gives the information about the size and shape of the crystal. Figure 5-5 shows the XRD pattern of the Cu-BDC MOF. In the XRD pattern, the peak at 2θ= 10.2º and 16.7º with miller indices (002) and (110) respectively corresponds to amorphous carbon (C70) with PDF # 48-1206. The peaks at angle 11.95º with miller index (002) and the one at angle 36.4º with miller index (111) are of Copper in the form of Copper Acetate (PDF # 27-1126) and Cuprite (PDF # 05-0667) respectively. Lastly the peak at 24.7º with miller index (110) is Mesotartaric acid hydrate with PDF # 40-0609.

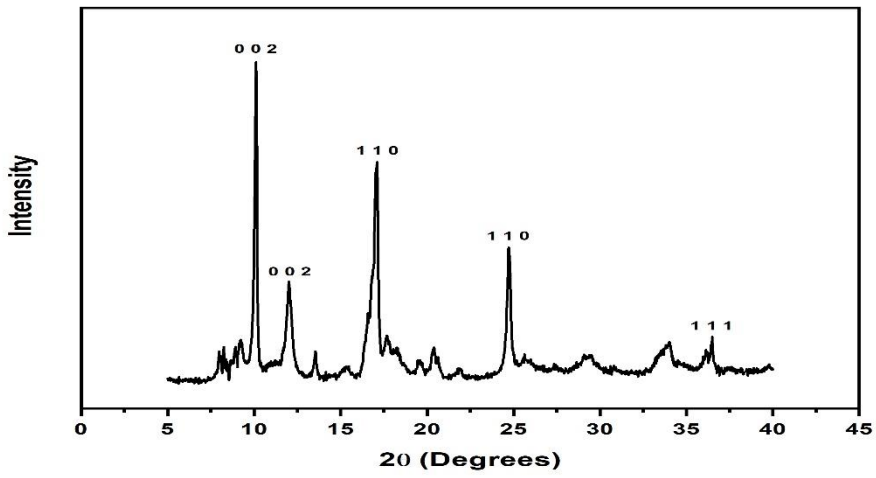

Figure 5-5: XRD pattern of Cu-BDC MOF

Figure 5-6 shows the PXRD patterns of the prepared Cu-ABDC MOF sample and PXRD pattern of the model Cu-ABDC structure which was predicted from the calculations of the SXRD. From the figure it can be clearly seen that both the patterns are highly similar which indicates that the prepared MOF sample is of high degree of purity. The peaks at 2θ 10° and 42.5° indicates the presence of carbon (PDF card # 48-1206) in the MOF, and the peaks at 2θ 11.9° confirms the presence of copper (PDF card # 27-1126). The peaks at 2θ 20.5° and 26.8° confirms the presence of Nitrogen (PDF Card # 06-0500 and 35-0845 respectively) in the MOF

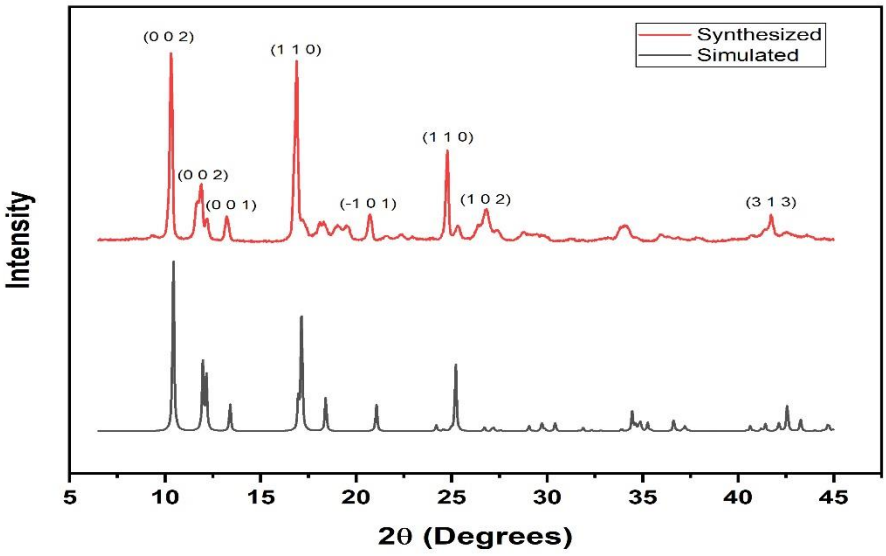

Figure 5-6: XRD patterns of Cu-ABDC MOF, simulated (black) and synthesized (red)

5.1.4 Thermo-gravimetric Analysis (TGA)

Thermal gravimetric analysis of both the MOF samples was done under nitrogen gas atmosphere. The weight loss (TGA) curve of the Cu-BDC MOF sample is shown in Figure 5-7. From the figure it is evident that there is an initial weight loss in the sample. This initial 10% weight loss which occurs at a temperature of 200°C and ends at 260°C is attributed to the loss of solvent which might be trapped in the pores of the MOF. At temperature above 260°C, there is no weight loss until 340°C which shows the stability of MOF up to a temperature of 340°C. When the temperature starts to rise above 340°C, pyrolysis starts and the structure of the MOF starts to breakdown and as is visible from

the figure, a very rapid weight loss occurs. The complete structure of the MOF breaks down at 380℃ leaving behind residue.

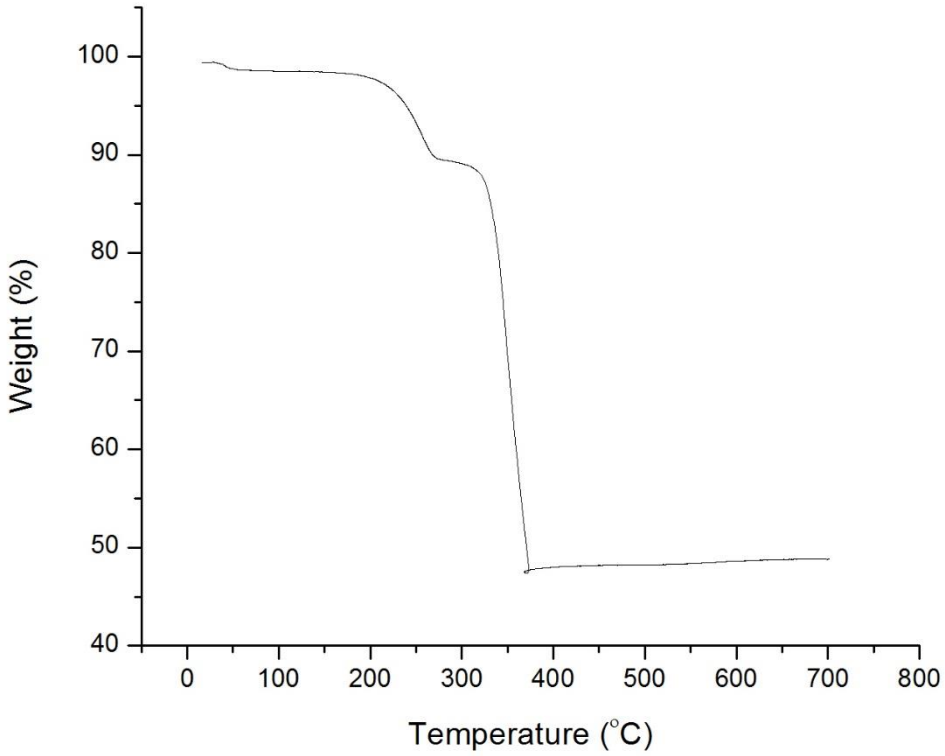

Figure 5-7: Weight loss (TGA) curve of Cu-BDC MOF

The weight loss (TGA) curve of Cu-ABDC MOF is shown in Figure 5-8. The initial weight loss (about 8%) of the Cu-ABDC MOF sample at 160 to 220°C indicates the degradation of DMF adsorbed at the surface of the MOF. At 255°C temperature, the decomposition of carboxylate ligand starts and afterwards a rapid degradation can be noted. At temperature above 368°C, no further weight loss can be seen which indicates that the structure of the MOF has completely been destroyed and residual Copper oxide is left behind.

Comparing the weight loss (TGA) curves of both the MOFs, we can confidently say that Cu-BDC MOF is thermally more stable than the Cu-ABDC MOF.

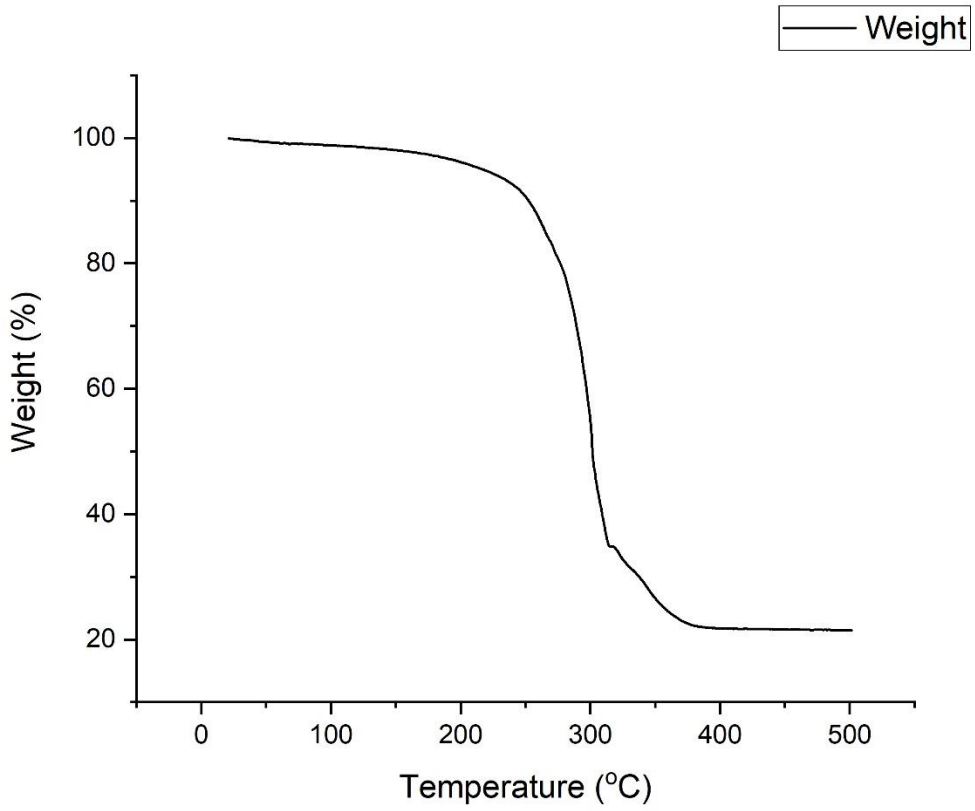

Figure 5-8: Weight loss (TGA) curve of Cu-ABDC MOF

5.1.5 Single Crystal XRD of Cu-ABDC MOF

The Single Crystal X-ray Diffraction reveals that the Cu-atom and the ABDC ligand are occupying the center of symmetry in the MOF. The metallic cluster is of a bimetallic nature where a Cu-atom is attached to another Cu-atom and 4 O-atoms from the carboxylate ligands and one from the O-bound DMF forming a cluster. As can be seen from Figure 5-9, the carboxylate ligands form a bridge in connecting a bimetallic cluster with another cluster hence forming a 3-dimensional framework. The amino group in the MOF is situated on two sites of the ABDC ligand and also on the non-bridging O-atom.

As is evident from the figure, the DMF solvent molecule which completes the coordination sphere of the metal ion can easily be used to generate Open Metal Sites (OMSs) in the MOF framework by the DMF molecule removal using solvent-exchange and evacuation method. This can aid in increasing the adsorption capacity of the MOF.

Table 5-2: Crystallographic Data of Cu-ABDC MOF

Frameworks	**Cu-ABDC**
Formula	C11H12CuN2O5
Space Group	I 2/m (12)
T, K	Room Temp. (283-303)
a, Å	7.9458 (7)
b, Å	14.9664 (8)
c, Å	11.1033 (10)
Volume, Å^3	1243.71
α	90
β	109.624 (10)
γ	90
Z	4
R-factor (%)	4.93

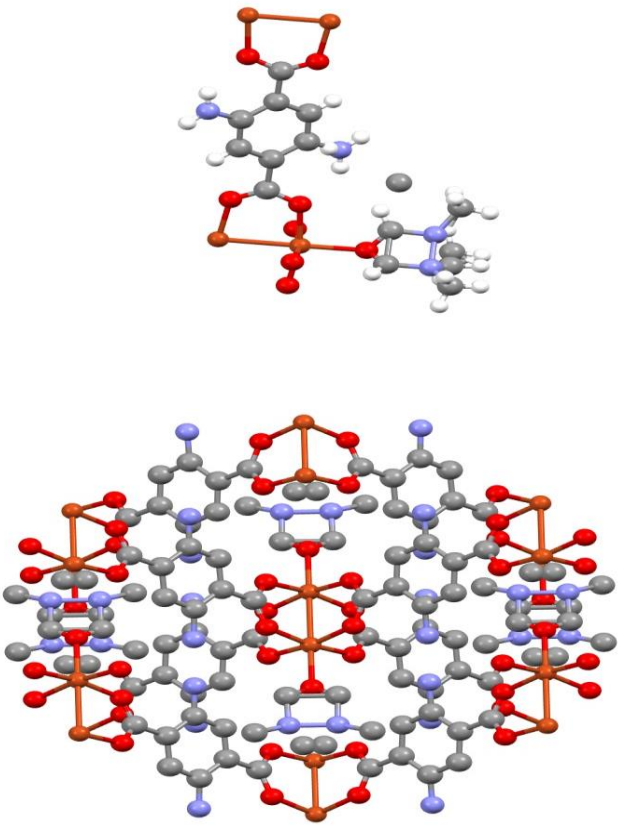

Figure 5-9: Structural description of Cu-ABDC MOF (N atoms marked in blue)

5.2 CO_2 adsorption study

Figure 5-9 shows the CO_2 adsorption capacities of the Cu-ABDC MOF which were measured at 10 °C and 25 °C. The pressures at these temperatures were from 0 to 20 bars. Three consecutive adsorption-desorption cycles were conducted on the sample at each condition. Before analysis, the sample was degassed at 120°C for 12 hours and the heating rate was set at 5°C min¬-1. The CO_2 adsorption capacity of the MOF at 25°C and 20 bar pressure measured was 5.85 $mmolg^{-1}$ and 5.75 $mmolg^{-1}$ at 10°C and 15 bar pressure.

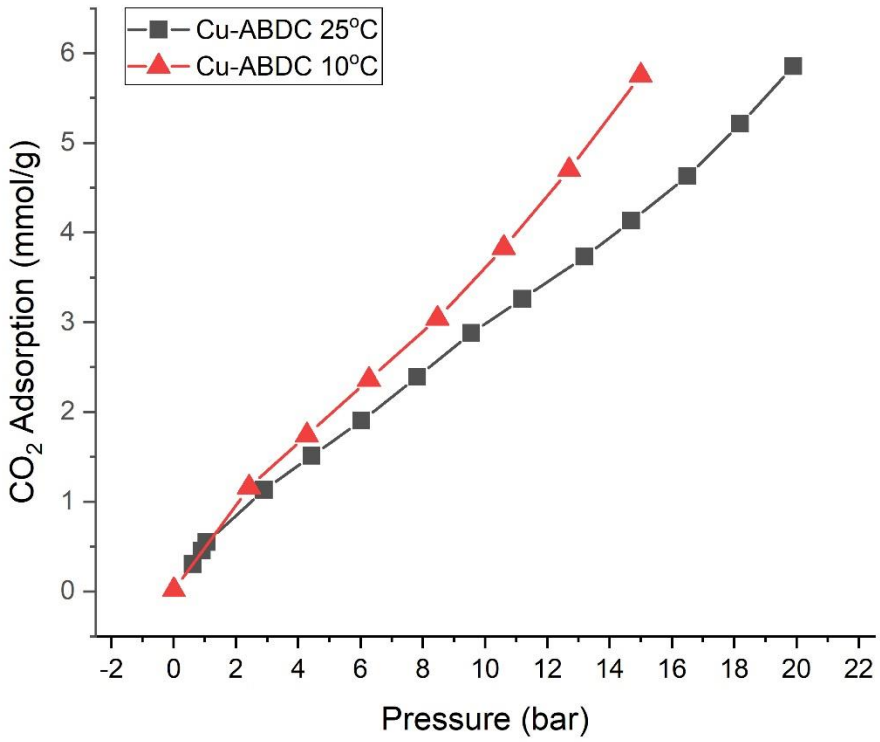

Figure 5-10: CO_2 adsorption of Cu-ABDC MOF at 25°C (black) and 10°C (red)

Although the MOF exhibits a good adsorption capacity of 5.85 and 5.75 $mmolg^{-1}$ at 25°C and 10°C respectively, but it should be noted that these high adsorption capacities are attained at high pressures of 15 bar and 20 bar. At low pressure of 1 bar, the MOF adsorbs 0.546 $mmolg^{-1}$ at 25°C and 0.46 $mmolg^{-1}$ at 10°C. Literature states that some other amine functionalized MOFs (Mg based, Co based and Sr based) also have CO_2 adsorption capacities ranging in the values stated here. [1] Among these MOFs, the Sr based MOF

have adsorption capacity which closely resembles with the adsorption capacity reported here.

The Cu-O bond in the Cu-ABDC MOF has a high ionic character but still its adsorption capacity is not as high. This can be due to the presence of the DMF solvent ligands in the framework of MOF. Theoretically, a higher adsorption capacity can be obtained from this MOF by removing the DMF ligands from the structure.

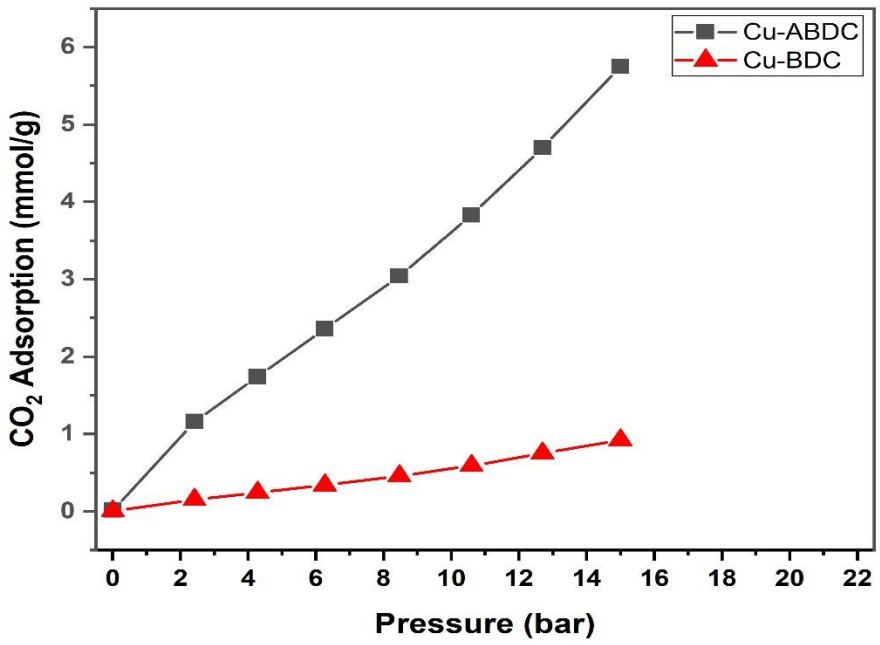

Figure 5-11: CO_2 adsorption of Cu-ABDC MOF (black) and Cu-BDC MOF (red) at 10°C

Figure 5-10 shows the comparison of the CO_2 adsorption capacities of the Cu-BDC and Cu-ABDC MOFs at a temperature of 10°C. It can be clearly observed that the adsorption of Cu-ABDC is much higher than that of Cu-BDC MOF. The main reason for this difference in adsorption capacities is the availability of Lewis Base Sites (LBSs) in the Cu-ABDC MOF which increases its affinity towards the CO_2 which is acidic in nature.

The comparison of sorption capacities and parameters of the reported Cu-BDC MOF [2] and the Cu-ABDC MOF is summaries in table 3.

Table 5-3: Comparison of sorption parameters of Cu-ABDC and Cu-BDC MOF with literature

MOF	Temp.	Pressure	CO_2 adsorption capacity ($mmolg^{-1}$)	Ref
Cu-BDC	-15℃	1 bar	0.78	[2]
	25℃	20 bar	1.15	[2]
Cu-BDC	10℃	15 bar	0.922	This Study
Cu-ABDC	10℃	1 bar	0.46	This Study
	25℃	20 bar	5.85	This Study

5.3 Surface area and porosity of Cu-ABDC MOF

The N_2 adsorption isotherm of Cu-ABDC MOF is presented in Figure 5-11. This N_2 adsorption of the MOF was measured at -196°C. The BET surface area calculated from the N_2 adsorption is 8.15 m^2/g. From the figure it is evident that there is a low adsorption of N_2 at low relative pressure but as the relative pressure increases from p/p°=0.6, a sharp increase in the adsorption can be noted. There also occurs a hysteresis at the desorption branch between p/p°=0.89-0.5. This hysteresis may indicate the presence of mesopores in the MOF. The cumulative adsorption pore volume of the MOF calculated by the BJH method is 0.01847cm^3/g. The S_{EXT}, external surface area, of the MOF calculated by the t-plot analysis is 8.152 m^2/g.

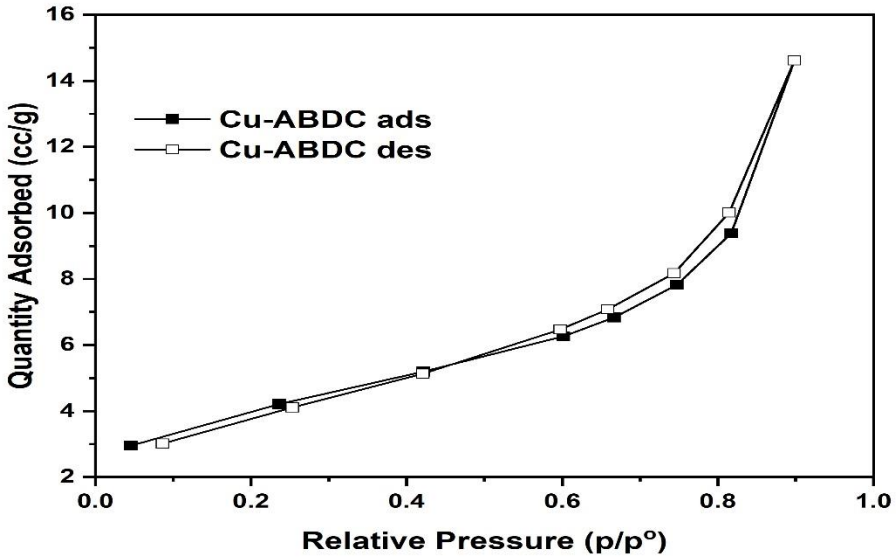

Figure 5-12: N_2 adsorption isotherm of Cu-ABDC MOF

5.4 Summary

In this chapter, the characterization results and the CO_2 adsorption studies for both the Cu-BDC MOF and Cu-ABDC MOF are presented. The Cu-BDC MOF shows regular crystallinity as compared to the Cu-ABDC MOF which have a mixture of crystal shapes. The EDS studies of both the MOFs are in accordance with the chemicals used for their synthesis. The TGA of the MOFs reveal the thermal stabilities of both the MOFs. The Cu-BDC MOF is more thermally stable than the Cu-ABDC MOF meaning that Cu-BDC MOF can withstand higher temperature without structural breakdown. The SCXRD studies of the Cu-ABDC MOF are also presented in this chapter showing the crystal lattice and indicating the nitrogen molecules in the structure which can help in the higher CO_2 adsorption capacity. This was then confirmed by the CO_2 adsorption studies carried out in the sorption analyzer and compared with the capacities reported for Cu-BDC MOF in literature. The N_2 adsorption isotherms of the Cu-ABDC MOF were also conducted for finding the surface area of the MOF which was $8.152 m^2/g$.

5.5 Conclusion and Recommendations

In this study, a new Cu based amine functionalized MOF is prepared using 2-aminoterephthalic ligand. The Cu-ABDC MOF exhibits a good thermal stability. The Cu-ABDC MOF showed capacity to be used in CO_2 adsorption and separation. The high CO_2 adsorption capacity of the Cu-ABDC MOF is attributed to the $–NH_2$ group present in the structure of the MOF which acts as LBS and hence enhance the affinity of the MOF towards CO_2. In addition to this, the Cu-ABDC MOF also represents the possibility of OMSs creation in the framework by the removal of the DMF ligands. Moreover, the implementation of efficient activation processes are required so that the Cu-ABDC MOF exhibit higher gas exchange sites and subsequently increase the adsorption capacity without damaging the framework.

References

[1] Ying Yang, Rijia Lin, Lei Ge, Lei Hou, Paul Bernhardt, Thomas E. Rufford, Shaobin Wang, Victor Rudolph, Yaoyu Wang and Zhonghua Zhu. Synthesis and characterization of three amino-functionalized metal–organic frameworks based on the 2-aminoterephthalic ligand. Dalton Trans. 44 (2015) 8190-97.

[2] Zhifeng Xin, Junfeng Bai, Yongming Shen, and Yi Pan. Hierarchically Micro- and Mesoporous Coordination Polymer Nanostructures with High Adsorption Performance. Crystal Growth & Design, 10:6 (2010) 2451-54.

Acknowledgements

Most of all I am thankful to Almighty Allah who gave me the will and determination to accomplish task in this manner.

I owe my sincere gratitude to Dr. Zuhair S. Khan (Principal/Dean USPCAS-E), Dr.Naseem Iqbal (HoD, ESE) and USPCAS-E Administration for their inspiration, guidance and support.

Writing this thesis and accomplishing this task so appreciably is only due to the unrelenting support and critical comments of my supervisor Dr. Naseem Iqbal and other GEC members for guidance and profitable knowledge whenever i needed it.

I would also like to offer my gratitude to Mr. Amin Durrani, Mr. Haider Ejaz, Mr. Naveed Ahmed, Mr. Qamaruddin for their sincere support and technical assistance.

Lastly I would thank Aisha Asghar a lot for helping me carry out the Single Crystal XRD in UK, without her help my research work would have been incomplete.

Sincerely,
Junaid Khan

Second International Conference on
Energy Systems for Sustainable Development
February 21-23, 2018

Annex I

Synthesis and application of Cu based MOF as a CO_2 adsorbent

Junaid Khan[a,*]; and Naseem Iqbal[a]

[a] U.S.-Pakistan Center for Advanced Studies in Energy, National University of Sciences & Technology Islamabad, Pakistan
[*] Corresponding Author
E-mail: 15esejunaid@uspcase.nust.edu.pk
Tel: +923159850839

Abstract
In this paper, the main focus is on the CO_2 adsorption capacity of Copper based Metal-Organic Framework. To investigate the application of Copper based MOF in CO_2 adsorption, the motivating factor was its reversible solvent-exchange property. Copper based MOF was synthesized using solvothermal treatment of terephthalic acid with copper nitrate in DMF. The MOF was characterized by Powder X-ray Diffraction (XRD), Thermal Gravimetric Analysis (TGA) and Scanning Electron Microscopy (SEM). CO_2 adsorption capacity of the MOF was measured by a cyclic adsorption-desorption method with adsorption at 25°C and desorption at 200°C in TGA. The maximum CO_2 adsorption capacity attained was 0.55 $mmolg^{-1}$. This adsorption capacity can further be improved by changing synthesis method and amine modification of prepared MOF. Further adsorption studies will be conducted with sorption analyzer.
Keywords: *metal organic framework; Cu based MOF; CO_2 adsorbent; MOF application; material engineering*

A. Introduction

Today our civilization is facing major environmental concerns among which carbon dioxide (CO_2) emissions is one of the most serious one[1]. Combustion of oil, coal, and natural gas are the main producers of these emissions as they are the driving energy resources of our daily life, industrial development and economic growth[2]. The contribution of CO_2 is approximately 60% to the total global warming effect[3]. During the period between 1970 and 2004, the annual global emissions of CO_2 escalated by about 80%. This ever increasing concentration of CO_2 in the atmosphere has led to urgent calls for strategies to alleviate this problem.

Environmentalists and climate specialists today recognize the need for technologies that remove CO_2 from the atmosphere to mitigate changes to the global climate caused by over a century of expanding anthropogenic CO_2 emissions. The concept of carbon dioxide using sorbents was first introduced in 1999, and in the ensuing decade and a half, a wide array of approaches employing different sorption materials have been described. Currently, the large-scale separation of CO_2 by the liquid phase amine-based absorption process is in commercial operation throughout the world. This "wet-scrubbing" CO_2 capture utilizes alkanolamines, such as MEA (monoethanolamine), as the solvent, which has been used industrially over the past 50 years [4][5]. Liquid and solid sorbents based on alkali and alkaline earth metal oxides and hydroxides, sorbents based on supported amines, and tailored MOFs have been studied.

Metal–organic framework (MOF) is a new class of materials where polyfunctional, organic ligands are bonded with more than one metal atom to form an extended polymeric structure in either one-, two-, or three dimensions. These MOFs are often highly porous, crystalline, and impervious to structural collapse once evacuated[6]. By varying the ligand character, spacer length, functionality, metal atom, and synthesis conditions, it is possible to form of an extensive number of porous compounds each with different properties and applications[7]. This particular and tunable nature of MOFs has increased the investigation of these materials for a wide assortment of potential applications including, however not constrained to, conductivity[8], gas storage and release[9], ion-exchange[10], catalysis[11], sensing[12], energy conversion and light harvesting[13], drug delivery[14] and toxic substances removal from water and air[15].

Porous metal-organic frameworks (MOFs), which are emerging rapidly, are promising as the efficient and cost-effective materials for CO_2 capture and separation[16][17]. The lower regeneration energy cost of these porous MOFs for CO_2 capture by the implementing pressure swing adsorption (PSA), temperature swing adsorption, and vacuum swing adsorption makes them a better option as compared to the alkanolamine technology mentioned above.

Here, we report the synthesis of a copper based MOF, the organic ligand of which is terephthalic acid, and its application for CO_2 capture. The first metal terephthalate

complex, nickel terephthalate, was synthesized back in 1967 by Acheson and Galwey using terephthalic acid and metal salt[18]. After that Sherif synthesized other hydrated metal terephthalates (Fe, Ag, Co, Cr, Cu, La, Mn)[19]. The Cu(tpa) MOF, however like MOF-2, displays a particularly higher surface area, this makes it a good choice for sieving applications, gas adsorption and gas seperation.

B. Experimental

C. Synthesis of MOF

In order to synthesize the Cu based MOF, equimolar quantities of terephthalic acid (Aldrich, 0.724 g) and copper nitrate trihydrate (Aldrich, 1.053 g) were dissolved in 87 ml of DMF. The prepared solution was placed in a closed bottle in an oven. The temperature of the oven was set at 110 °C and the solution was heated for 36 h. Upon removal of solution from the oven, blue precipitated crystals could be seen which were recovered through centrifugation at 4500 rpm for 20 mins. Once the crystals were recovered, the crystals were washed using DMF. The obtained crystals were then dried at 180 °C in a vacuum oven.

D. Characterization

Powder X-ray diffraction (PXRD) patterns of the sample were collected on a D8 Advanced X-ray diffraction system from Bruker (40 kV, 30 mA). The 2θ operating range of the diffractometer was in the range from 3 to 40° with a step size of 0.02°. The patterns recorded were then compared with the patterns reported from single crystal data in the literature.

Thermal stability of the Cu based MOF was measured in N_2 environment with a heating rate of 10°C min^{-1} from 20 to 700°C on a DTG-60H Thermo Gravimetric Analyzer (TGA). 10mg sample of the MOF was used for thermal stability test and the flow-rate of N_2 gas was 10 ml min^{-1}.

Scanning Electron Microscopy (SEM) images of the sample were also obtained on a TESCAN SEM VEGA3 microscope. The sample was gold-coated before the acquiring of images and the images were taken at SEM HV of 20 kV. The EDS analysis of the sample was also conducted to determine the atomic weights of the elements in the sample.

E. Results and Discussion

"Fig. 1" shows the SEM images of the synthesized Cu(tpa) particles, in which a large number of regular and independent crystal cuboids were observed. This indicates good crystallinity and high yield of the Cu(tpa) MOF. Upon higher magnification of the MOF (inset of "Fig. 1"), the cuboids could be clearly seen each with a diameter of about 3µm.

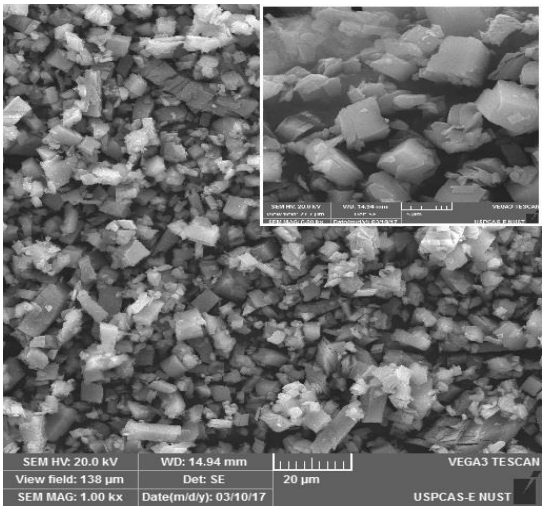

Fig 1 SEM images of Cu(tpa) MOF with low resolution (main image) and high resolution (inset)

The thermogravimetric profile of the MOF is shown in "Fig. 2". The profile clearly shows that a weight-loss step started at 200 °C and ended at 260 °C. This initial weight loss, which is about 10%, corresponds to the loss of solvent that might be trapped in the pores of the MOF. No significant change in weight of the MOF above 260 °C indicates the stability of the MOF until pyrolysis starts at 340 °C, breaking the structure of MOF and leaving behind just carbon.

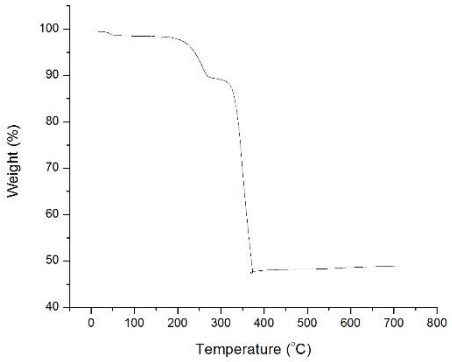

Fig 2 TGA curve of Cu(tpa) MOF

X-ray powder diffraction experiments were carried out to verify the crystals formed during the synthesis of Cu based MOF. "Fig. 3" depicts the peaks attained by XRD which exactly matches the peaks from the literature[20]. During the search match it was further verified that the peak at Θ=10.10° is of Cu(BDC) | Copper 1,4-Benzenedicarboxylate, which is the required MOF.

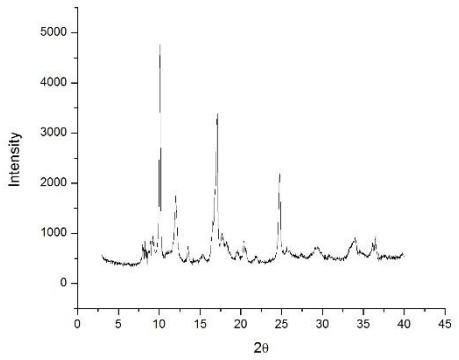

Fig. 3 The X-ray diffraction patterns of Cu(tpa) MOF

"Fig. 4" depicts the elemental peaks obtained during the EDS analysis of the MOF sample. A portion of sample was selected for elemental analysis and its spectrum was obtained indicating the elements present. The representative peaks of each element (inset of "Fig. 4") can be seen, confirming the presence of the structural elements of the MOF. "Table 1" shows the weight and atomic percentages of each element which are in accordance with the structure of the MOF and its chemical formula i.e. $C_8H_4CuO_4$.

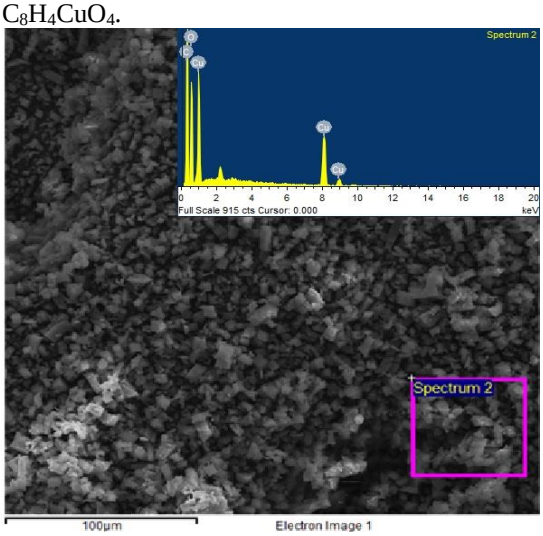

Fig. 4: EDS of the MOF

Table 1 Percentages of elements in MOF determined through EDS

Element	Percentage	
	Weight %	***Atomic %***
Carbon	51.93	64.26
Oxygen	35.25	32.74
Copper	12.82	3.00

The CO_2 adsorption capacity of the MOF was also conducted on a DTG-60H Thermo Gravimetric Analyzer (TGA). A 10 mg sample of the MOF was tested to determine its CO_2 adsorption capacity. Initially the sample was heated to 200°C in N_2 environment at a heating rate of 10°C min^{-1} and this temperature was held for 10 mins. This removed any solvent trapped in the pores of the MOF so that the pores can be available for CO_2 adsorption. In "Fig. 5" the initial drop in the weight of MOF from 10.30 mg to 9.95 mg shows that there was some solvent in the MOF which was removed by heating it. The sample was then cooled to 16°C at a cooling rate of 50°C min^{-1} and CO_2 was passed through it at a flow rate of 10ml min^{-1} at room pressure. CO_2 was passed through the sample overnight so that the maximum capacity of the MOF could be determined. With the passage of time, the weight of the MOF started to increase indicating that CO_2 is being adsorbed. A total of 0.24 mg of CO_2 was adsorbed by the sample overnight and the total adsorption capacity of the MOF was calculated to be 0.55 mmol g^{-1}. Keeping in view other MOFs, this is an acceptable value for CO_2 adsorption as the values for different MOFs range from 0.1 mmol g^{-1} to 4.00 mmol g^{-1}[17].

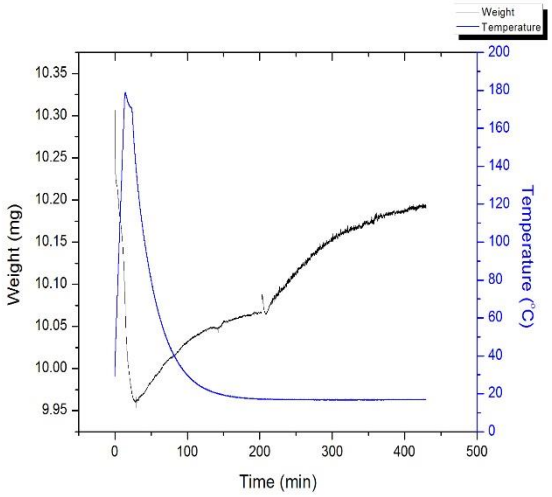

Fig. 5 CO_2 adsorption analysis of Cu(tpa) using Thermogravimetric Analyzer (TGA)

F. Conclusions

The results presented here clearly shows that the Cu based MOF, Cu(tpa), has a good potential for being used as a CO_2 adsorbent. The porous nature and reversible solvent-exchange property of this MOF also adds up in making it a good choice. Although the adsorption capacity is relatively less as compared to other MOFs reported, but the nature of Cu(tpa) provides a platform to improve its adsorption capacity. This improvement can achieved by modifying the structure of the MOF through varying conditions during the synthesis. Another approach can be by modifying the MOF through incorporating amines into the MOF structure which can provide additional sites for CO_2 adsorption hence enhancing the overall CO_2 adsorption capacity.

Currently the adsorption analysis was conducted using TGA but to know the CO_2 adsorption at different conditions, a sorption analyzer will be used in further studies. This will allow us know how the MOF behaves during CO_2 adsorption at different conditions of pressure and temperature.

ACKNOWLEDGMENT

We thank the U.S.-Pakistan Center for Advanced Studies in Energy, NUST Islamabad for their assistance in helping us carry out different test and analyses during our work. Thanks to the staff at Advanced Energy Materials & Systems laboratory at USPCAS-E, NUST for use of Powder X-ray diffraction system (PXRD), Thermogravimetric Analyzer (TGA) and Scanning Electron Microscopy (SEM).

REFERENCES

1. IPCC, *Climate Change 2007 Synthesis Report*. 2007.
2. R. Quadrelli and S. Peterson, "The energy-climate challenge: Recent trends in CO2 emissions from fuel combustion," *Energy Policy*, vol. 35, no. 11, pp. 5938–5952, 2007.
3. M. K. Debe, "Electrocatalyst approaches and challenges for automotive fuel cells," *Nature*, vol. 486, no. 7401, pp. 43–51, 2012.
4. Z. Z. Jiang, Z. B. Wang, Y. Y. Chu, D. M. Gu, and G. P. Yin, "Carbon riveted microcapsule Pt/MWCNTs-TiO2 catalyst prepared by in situ carbonized glucose with ultrahigh stability for proton exchange membrane fuel cell," *Energy Environ. Sci.*, vol. 4, no. 7, pp. 2558–2566, 2011.
5. Y. Zhao *et al.*, "Metal organic frameworks for energy storage and conversion," *Energy Storage Mater.*, vol. 2, pp. 35–62, 2016.
6. G. Férey, C. Mellot-Draznieks, C. Serre, and F. Millange, "Crystallized frameworks with giant pores: Are there limits to the possible?," *Acc. Chem. Res.*, vol. 38, no. 4, pp. 217–225, 2005.
7. D. Maspoch *et al.*, "A nanoporous molecular magnet with reversible solvent-induced mechanical and magnetic properties.," *Nat. Mater.*, vol. 2, no. 3, pp. 190–195, 2003.
8. L. Sun, M. G. Campbell, and M. Dincə, "Electrically Conductive Porous Metal-Organic Frameworks," Angew. Chemie - Int. Ed., vol. 55, no. 11, pp. 3566–3579, 2016.
9. J.-R. Li, R. J. Kuppler, and H.-C. Zhou, "Selective gas adsorption and separation in metal–organic frameworks," Chem. Soc. Rev., vol. 38, no. 5, p. 1477, 2009.
10. X. Zhao, X. Bu, T. Wu, S.-T. Zheng, L. Wang, and P. Feng, "Selective anion exchange with nanogated isoreticular positive metal-organic frameworks," Nat. Commun., vol. 4, no. May, pp. 1–9, 2013.
11. J. Lee, O. K. Farha, J. Roberts, K. A. Scheidt, S. T. Nguyen, and J. T. Hupp, "Metal–organic framework materials as catalysts," Chem. Soc. Rev., vol. 38, no. 5, p. 1450, 2009.
12. L. E. Kreno, K. Leong, O. K. Farha, M. Allendorf, D. Van Richard P., and J. T. Hupp, "2-40 Metal-Organic Framework Materials as Chemical Sensors.," Chem. Rev. (Washington, DC, United States), vol. 112, pp. 1105–1125, 2012.
13. M. C. So, G. P. Wiederrecht, J. E. Mondloch, J. T. Hupp, and O. K. Farha, "Metal–organic framework materials for light-harvesting and energy transfer," Chem. Commun., vol. 51, no. 17, pp. 3501–3510, 2015.
14. P. Horcajada, C. Serre, M. Vallet-Regí, M. Sebban, F. Taulelle, and G. Férey, "Metal-organic frameworks as efficient materials for drug delivery," Angew. Chemie - Int. Ed., vol. 45, no. 36, pp. 5974–5978, 2006.
15. J. B. Decoste and G. W. Peterson, "Metal − Organic Frameworks for Air Puri fi cation of Toxic Chemicals," 2014.
16. D. M. D'Alessandro, B. Smit, and J. R. Long, "Carbon dioxide capture: Prospects for new materials," Angew. Chemie - Int. Ed., vol. 49, no. 35, pp. 6058–6082, 2010.
17. K. Sumida et al., "Carbon dioxide capture in metal-organic frameworks," Chem. Rev., vol. 112, no. 2, pp. 724–781, 2012.
18. R. J. Acheson and A. K. Galwey, "The thermal decomposition of nickel terephthalate and nickel salts of other carboxylic acids," J. Chem. Soc. A Inorganic, Phys. Theor., no. 1174, pp. 1174–1178, 1967.
19. F. G. Sherif, "Heavy Metal Terephthalates," Ind. Eng. Chem. Prod. Res. Dev., vol. 9, no. 3, pp. 408–412, 1970.
20. C. G. Carson *et al.*, "Synthesis and structure characterization of copper terephthalate metal-organic frameworks," *Eur. J. Inorg. Chem.*, no. 16, pp. 2338–2343, 2009.

Annex II

Ethylendiamine (EDA) loading on MOF-5 for enhanced carbon dioxide capture applications

Aisha Asghar[1] Naseem Iqbal[1] Tayyaba Noor[2] Junaid Khan[1]

1 United States Pakistan Centre for Advanced studies in energy, National University of Sciences and Technology, Pakistan.
2. School of Chemical and Mechanical Engineering, National University of Sciences and Technology, Pakistan.

Abstract. Reducing carbon dioxide levels in atmosphere presents greatest challenge in controlling global climate change. Each stage of Carbon Capture and Storage (CCS) strategy requires specialized materials. Metal–organic framework, being highly porous and crystalline materials are captivating vast scientific attention for exploring their potential in gas adsorption applications. This research work presents an attempt to synthesis post amine modified MOF materials for enhanced carbon dioxide capture applications. Thermogravimetic studies reveal that EDA MOF-5 is far more thermally stable than MOF-5; moreover synthesis can be performed successfully with recycled solvent (DMF). Carbon dioxide adsorption studies represents better carbon dioxide capture tendency for MOF-5 and EDA MOF-5 i.e., 5 mmol/g and 3.9 mmol/g respectively at 0°C.

1. Introduction

Among various greenhouse gases listed under Kyoto Protocol; carbon dioxide is labeled as major contributor in global warning. Carbon dioxide absorbs and emits radiant energy within the thermal infrared range, thus raising global temperatures. CO_2 has the highest positive radiative forces of all the human-influenced climate drivers compared by the IPCC. After a pulse of CO_2 is emitted into the atmosphere, 40% will reside in the atmosphere for 100 years and 20% will remain for 1000 years, while the final 10% will take 10,000 years to turn over [1]. This literally means that these tiny heat trappers, we release today from our industries, vehicles and power plants are going to become part of the climate our next generations will inherit.

Metal−organic frameworks (MOFs) are advanced class of crystalline solid nanomaterials reinforced by metal coordination sites coupled with organic molecules [2−4]. Resulting organic/inorganic hybrid 3-D networks formed contains well-defined porosity, high surface area, and tunable chemical functionalities having versatile applications in catalysis [5, 6], Separations [7], and gas storage [8]. Owing to gas storage ability, a lot of research work has been done to capture carbon dioxide gas. Nevertheless, mostly MOFs adsorb carbon dioxide by weak physiosorption interactions so adsorption at low gas pressure and N_2/CO_2 selectivity is very low [9].

Amine sites being acidic in nature have affinity towards carbon dioxide and are known to be highly effective for CO_2 adsorption and to be amenable to use under dry or humid conditions. [10-13]. This

research work is an effort to incorporate ethylenediamine molecules within MOF-5 molecule using post-synthesis modification and study potential effects on its carbon dioxide gas adsorption capacity.

2. Experimental Section

All the chemicals were purchased from Sigma Aldrich and Merck. The reactions that require heating were conducted in 23 ml Parr bombs in oven. To test purity of reagents PXRD data for reagents was collected and verified prior to the synthesis.

2.1. Synthesis: MOF-5 synthesis

Synthesis Equimolar quantities (1:1) of Zn $(NO_3)_2.6H_2O$ 189.36 mg (1 mmol) and 166 mg of terepthalic acid (1 mmol) were dissolved in 10 ml DMF in a 50 ml beaker. Dissolved contents were ultra-sonicated at 100°C for 2 hours than solution was transferred to 23 ml Teflon vials. Parr bombs were sealed and heated in oven at 100˚C for 6 hours to yield white crystals. The reaction mixture was than decanted (and saved for recycling); crystals obtained were washed thrice with DMF than with THF thrice. Crystals were dried overnight at room temperature. Sample was activated in vacuum oven at 130°C for 6 hours before further analysis.

2.2. EDA MOF-5 synthesis

Prepared MOF-5 crystals were modified using ethylenediamine. 500 mg of MOF-5 was added to 15 % ethylenediamine solution in methanol. Contents were allowed to react under reflux with vigorous stirring for 6 hours. The product obtained was filtered and then washed with DI water and ethanol to remove any unreached ethylenediamine from sample. Sample was dried overnight at room temperature to collect a pale colored crystals of EDA-MOF-5.Crystals were activated in vacuum oven at 130°C for 6 hours before further analysis. Reaction scheme for EDA MOF-5 is given in Figure 1.

2.3. Solvent recovery and recycling

All reagents used in these MOFs synthesis are cheap only Dimethylformamide is expensive, so solvent recycling was also tested in this study. For Batch I fresh DMF was used with regent. Recycled solvent after crystal collection was filtered using 0.45 micron syringe filter and utilized for Batch II MOFs synthesis. Obtained batch II crystals were characterized using PXRD to compare these with Batch I MOFs.

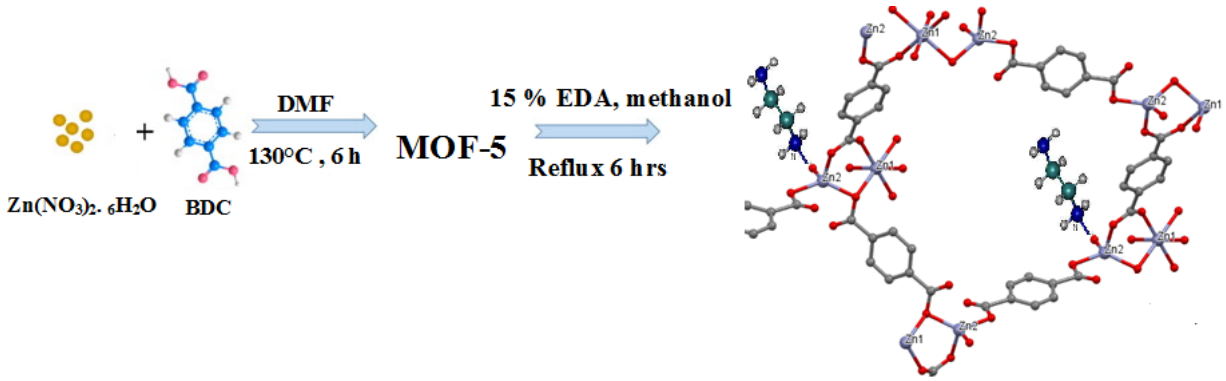

Figure 1. Reaction Scheme for EDA MOF-5 synthesis

3. Characterization

PXRD for synthesized MOF samples was collected at room temperature on an X'Pertpro panalytical Chiller 59 diffractometer using Copper Kα radiation. Activated samples were mounted onto zero-background silicon for PXRD analysis. Morphology of crystals was studied using scanning electron microscopy. TGA was performed using a Perkin Elmer Pyris 1 thermo-gravimetric analyzer. The samples were heated from 25°C to 700°C under a flow of air (20 ml min−1), using a heating rate of 5°C min−1. SHIMADZU IR Affinitt-1S spectrometer was used to obtain IR data. Elemental analysis

for EDA MOF-5 samples was performed to confirm presence of amine in prepared material, using FlashSmart NC ORG elemental analyzer with Thermal conductivity detector.

4. Results

To check the synthesis of MOF-5 and EDA MOF, powder X-ray diffraction (XRD) studies were carried out. PXRD patterns of MOF-5 and EDA MOF-5 prepared in this study are shown in Figure 2. Both synthesized materials, with and without addition of EDA, show sharp diffraction peaks indicating a well-formed crystalline structure. Peak positions match very well with the previously reported data for MOF-5, indicating successful synthesis of the MOF-5 [10]. Presence of some new peaks in EDA MOF-5 at 2θ~12.21° and 2θ~14.48° are indicative of slight difference in MOF-5 and EDA MOF-5 MOF crystalline structure.

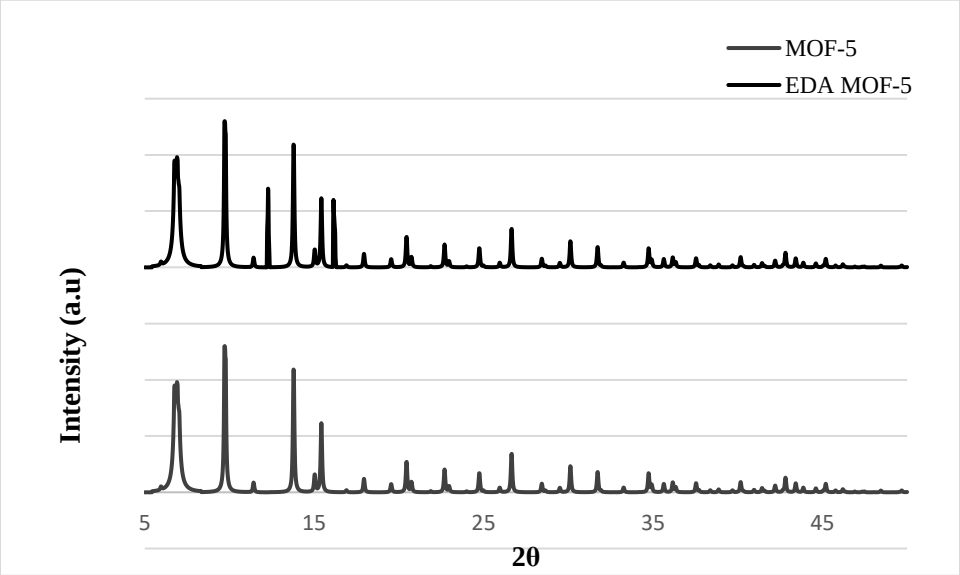

Figure2. PXRD pattern for MOF-5 and EDA MOF-5

Fourier transform infrared spectra (FTIR) collected for prepared materials confirm the presence of representative functional groups indicative of MOF-5 formation (Figure. 3). Two sharp peaks were obtained at 1589 cm^{-1} and 1375 cm^{-1} in MOF-5 sample is representative of symmetric and asymmetric stretching of C-O bonded to Zn, respectively [11]. . Various small peaks in the range of 1200 to 910 cm^{-1} represents to the in-plane bending of the C-H group present in the benzene ring of the linker [10-11]. Some small peaks in the region of 910 to 645 cm^{-1} show out of plane bending of C-H group of terepthalic acid [12]. The broad peak at 3410 cm^{-1} in MOF-5 represents adsorbed O-H groups. In addition to MOF-5 typical peaks, EDA MOF-5 sample illustrates some new peaks. It shows characteristic peak for amine-containing functional groups at 1090 cm^{-1} indicative of C-N stretching. [13] Presence of very low-intensity peaks in the region between 1275-1469 cm -1 can be attributed to the C-N anti symmetric stretching coupled with the NH_2 and NH out-of-plane modes [13] Typical peaks at 2845 and 2845 cm-1 are ascribed to stretching vibration of C-H bonds introduced by ethylenediamine molecules [14].

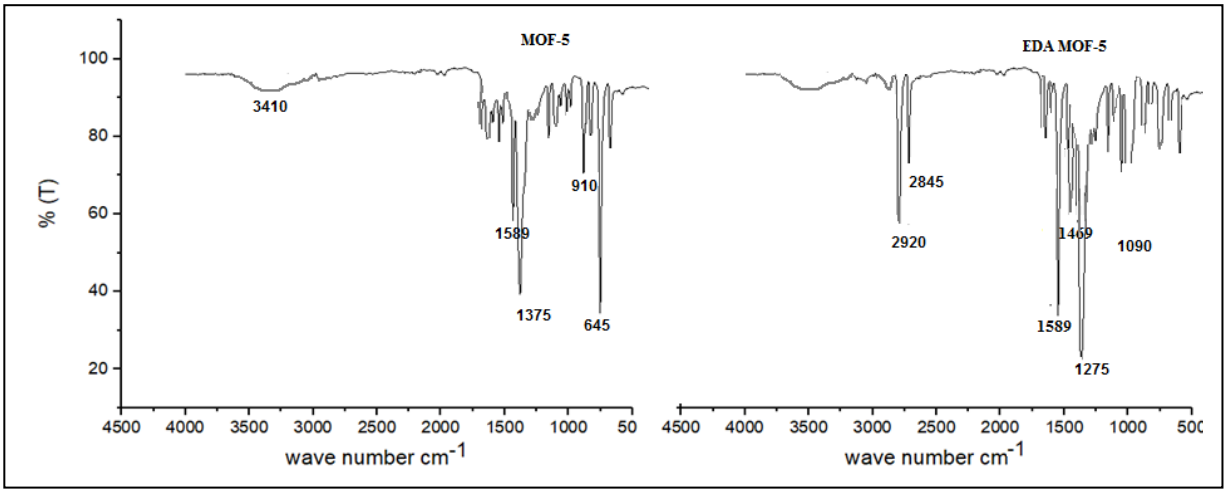

Figure 3. FTIR pattern for MOF-5 and EDA MOF-5

Thermogravimetic analysis (TGA) was performed to study thermal behaviors of prepared MOF materials (Figure. 4). For both MOFs there is no significant weight loss observed below 170°C, indicating there was no surface adsorbed moisture, THF and solvent molecules in prepared materials. Initial weight loss in both samples from 170°C to 320°C (approx 12 %) represents degradation of surface adsorbed DMF molecules. For MOF-5 decomposition of carboxylic linker started at 381°C, while in EDA MOF-5 linker degradation initiated at a bit higher temperature, i.e. 445°C than onwards there is rapid degradation in both materials. There is two-step degradation in EDA MOF-5, an extra step at 300 °C is indicative of EDA degradation, incorporated in structure. No further weight loss was observed as the temperature continued to rise leaving behind residual zinc oxide above 503°C for MOF-5 and 517°C for EDA MOF-5.

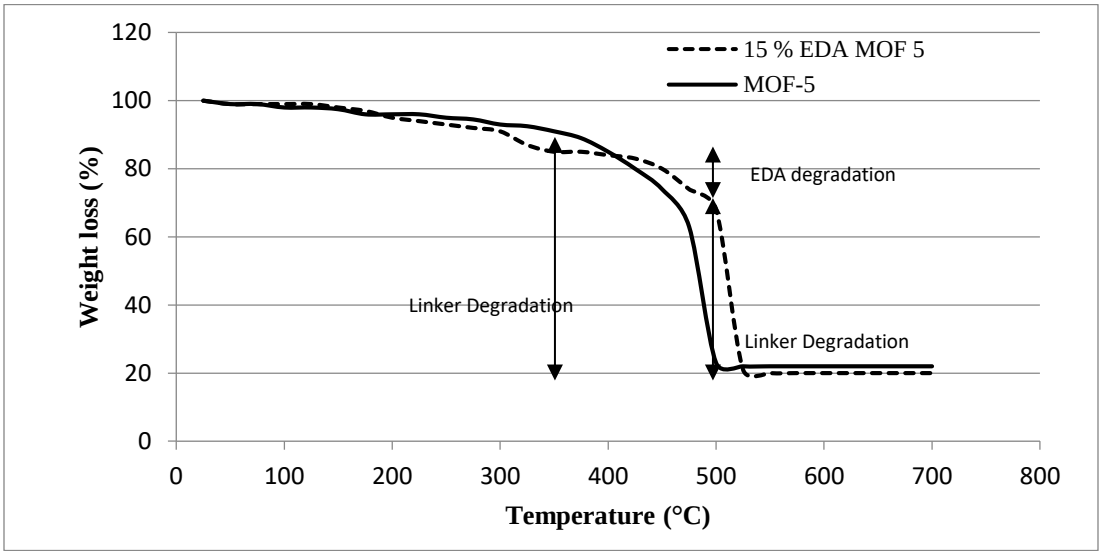

Figure 4. TGA graph for MOF-5 and EDA MOF-5

Scanning electron microscopy images of prepared MOF 5 sample are illustrates in Figure 5. It is observed that prepared MOF-5 has cubic crystals, supported by literature [4].

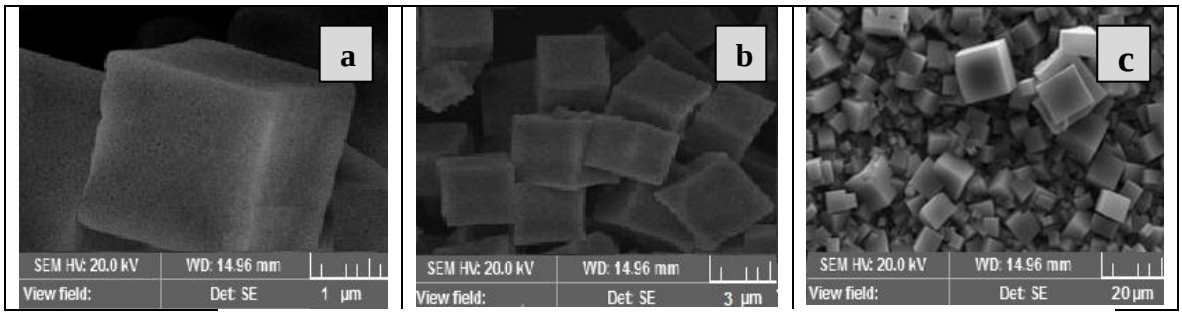

Figure 5. SEM images for MOF- 5 at (a) 1µm (b) 3 µm and (c) 20µm

Elemental analysis results (Table.1) shows elemental composition for EDA MOF-5. Results clearly indicate significant amount of nitrogen (6.76 - 6.83) representing presence of ethylenediamine in the sample.

Table 1. Elemental analysis for EDA MOF-5 Sample

Elemental Analysis for EDA MOF-5

% Carbon	% Hydrogen	% Nitrogen
45.01- 45.07	4.85 - 4.77	6.76 - 6.83

4.1 Solvent recovery and recycling

The absence of any alien peaks in Batch II MOF material PXRD results is indicative of the high purity MOF-5 and EDA MOF-5 production using recycled DMF. Solvent recovery and re-utilization is a clear indicator for cost advantage for this MOF synthesis.

5. CO_2 adsorption capacities of MOF-5 and EDA MOF-5

The CO_2 adsorption capacity for both MOF materials was evaluated by monitoring pseudo equilibrium adsorption uptakes using Quantarchrome Isorb-HP100 volumetric type sorption analyzer. Initially samples were degassed 130°C for 12 hours using a heating rate of 5°C min^{-1}. 200 mg of each sample was used for three consecutive adsorption-desorption cycles at 0°C and 25°C with adsorbate pressure ranging between 1 to 14 bar. The CO_2 capacities calculated at 0 °C and 14 bar pressure were 3.9 and 5 mmol/g for MOF-5 and EDA MOF-5, respectively. This trend found consistent with adsorption capacities calculated at 25°C (Figure.6).

Despite of showing very high carbon dioxide capturing tendency in the first cycle for both adsorbents tested here, MOF-5 revealed a significant loss in the adsorption capacity over successive operations compared to EDA MOF-5 (Figure.7). Literature states that carbon dioxide adsorption capacity for silica/PEI decreases by a value of 0.70 mmol/g after four consecutive adsorption-desorption cycles, from 2.35 to 1.64 mmol/g. An observed substantial adsorption capacity detoriation of amine-grafted amine-impregnated or metal organic framework materials have been attributed to the loss of physically adsorbed amines or amine detoriation by urea [15]. On the contrary, silica based surface-grafted amine based sorbents shows enhanced stability under dry conditions, illustrating relatively high values of CO_2 uptake with same number of adsorption cycles tested, with only a negligible adsorption decrease. Here we observed that initial CO_2 uptake for MOF 5 was higher for initial adsorption cycles at both 0° C and 25 °C, however, adsorption capacity declined considerably under successive cycles. Here adsorption capacity calculated at 25°C for MOF-5 lowered by about 22% after three cycles, from 0.93 to 0.70 mmol/g. This decrease in adsorption capacity over successive cycles was more prominent at higher temperature compared to lower temperature (0°C) adsorption. This significant adsorption capacity decline can either be attributed to material stability or desorption treatment [16]. Previous

researches, represent that moderate desorption conditions contribute towards regenerability of the Mn-BDC significantly [13, 14]. Very Mild desorption conditions were used in this study. i.e., He gas purging for 30 min at 36 °C. This fact implies that MOF-5 demands more energy input for its regeneration than applied in this work, possibly making a CO_2 capture process with this adsorbent significantly more energy-intensive. In contrast, EDA MOF-5 indicated complete regenerability under the moderate desorption conditions used here, showing negligible CO_2 adsorption capacities decline over successive test cycles. These observations suggest that newly synthesized robust EDA MOF-5 material is more stable adsorbent compared to the parent MOF-5.

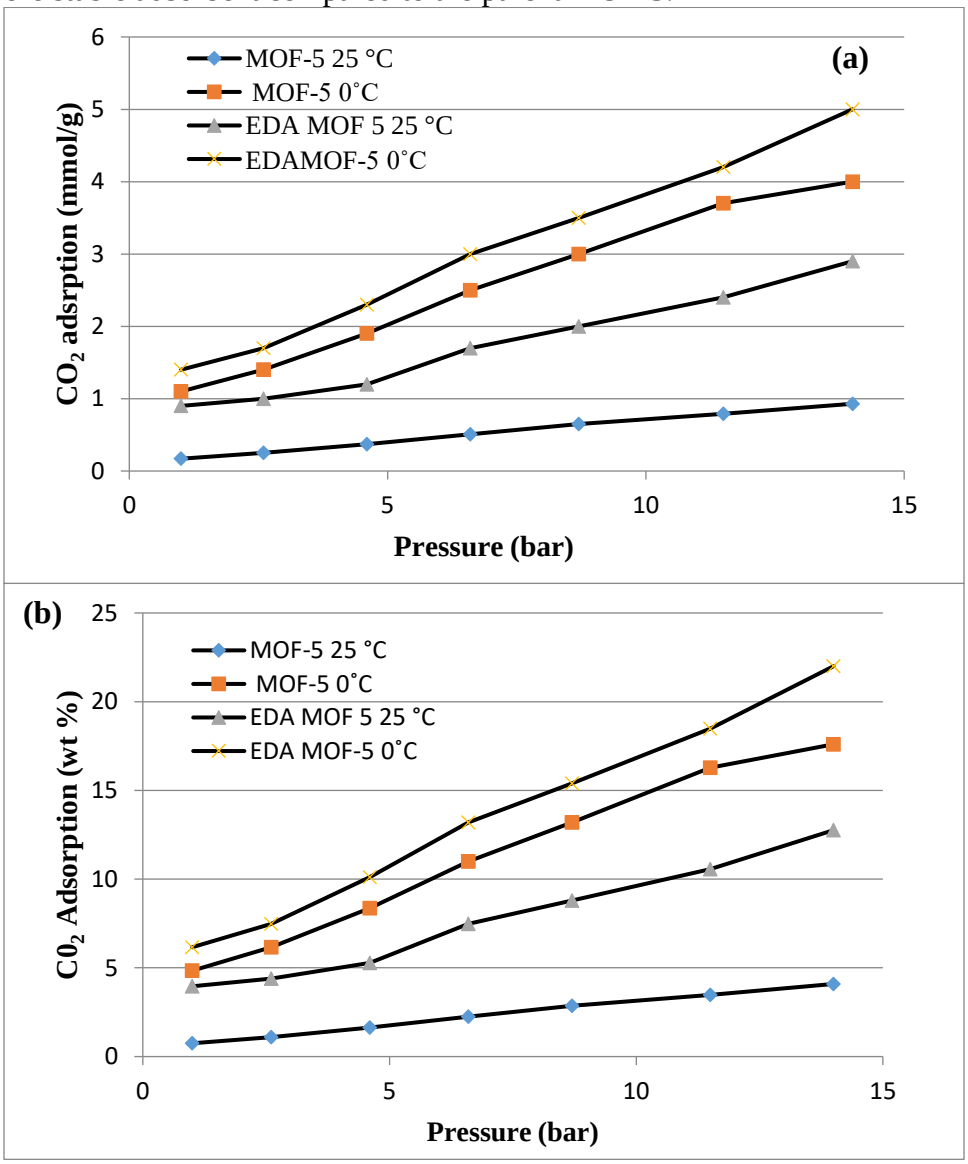

Figure 6. CO_2 adsorption results mmol/g (a) and wt% (b) for MOF-5 and EDA MOF-5

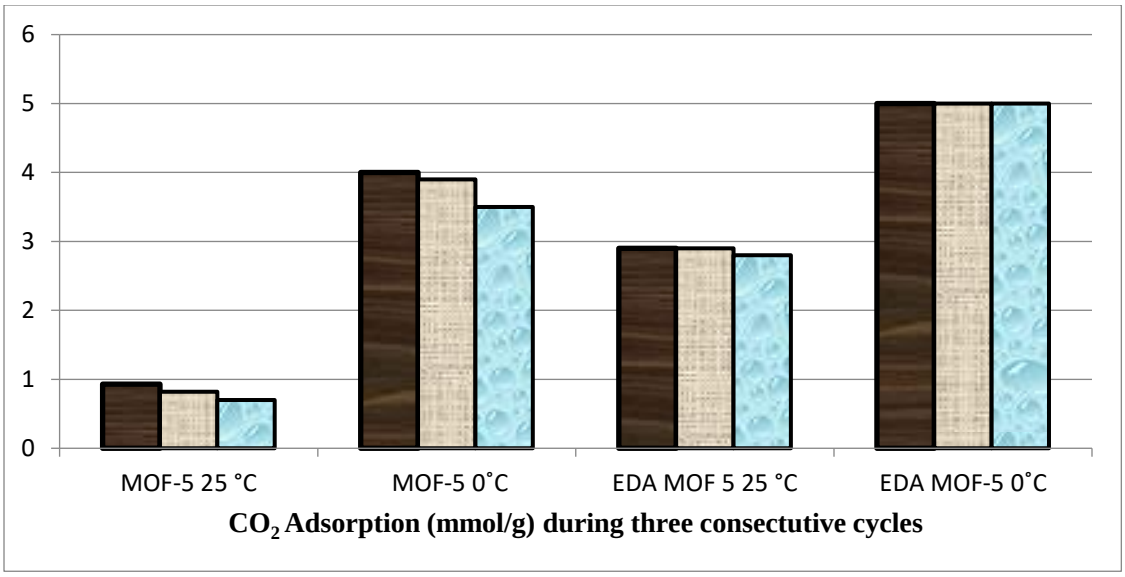

Figure 7. CO_2 adsorption mmol/g for
MOF-5 and EDA MOF-5 MOF at 0°C and 25°C

6. Conclusion

In summary, we report that or MOF-5 production, ultrasonication at 100°C for 2 hours prior to solvothermal reaction; can significantly reduce synthesis time from 24 hours to 6 hours. Characterization results confirmed good quality MOF-5 crystals synthesis with this method. Synthesis cost can further be reduced for both MOFs synthesis using recycled solvent (DMF). This work demonstrates simple modification of MOF-5, with ethylenediamine to substantially improve its thermal stability and CO_2 adsorption properties. Thermogravimetic studies reveal that EDA MOF-5 prepared is more thermally stable than MOF-5; moreover carbon dioxide adsorption studies for these samples reveal better carbon dioxide capture tendency i.e., 5 mmol/g and 3.9 mmol/g respectively at 0°C. The modified MOF, EDA MOF-5, indicate enhanced stability/regenerability, being cycled three times with identical adsorption capacities. Future studies are needed to address EDA MOF-5 long-term adsorption cycle studies, stability to contaminants and oxidation.

7. References

[1] Farha O and Hupp J 2010 *Acc. Chem. Res.* **43** pp 1166−1175.
[2] Meek S, Greathouse J and Allendorf M 2011 *Adv. Mater.* **23** pp 249−267.
[3] Ferey G 2008 *Chem. Soc. Rev.* **37** pp 191−214.
[4] Yaghi O, Keffee O, Ockwig N, Chae H, Eddaoudi M and Kim J 2003 *Nature*. **423** pp 705−714.
[5] Lee J, Farha O, Roberts J, Scheidt K, Nguyen S and Hupp J 2009 *Chem. Soc. Rev.* **38** pp 1450−1459.
[6] Ma L and Lin W 2010 *SpringerVerlag* **293** p 175.
[7] Tran U, Le K and Phan N 2011 *ACS, Catal*. **1** pp 120−127.
[8] Miralda C, Macias E, Zhu M, Ratnasamy P and Carreon M 2012 *ACS. Catal*. **2** pp 180−183.
[9] Bae Y and Snurr R 2011 *Angew. Chem. Int.* **50** pp 11586−11596.
[10] Alessandro D, Smit B, Long J 2010 *Chem. Int.* **49** pp 6058−6082.
[11] Coates J 2000. : *Encyclopedia of Analytical Chemistry, Meyers, R.A. John Wiley and Sons Ltd., New York.* **3** pp 10815-10837.
[12] Sabouni R, Kazemian H and Rohani H 2010 *Chem. Eng. J.* **165** pp 966-973.

[13] Stevens J, Huang A, Peng H, Chiang W, Khabashesku V, Margrave L 2003 *Nano. Lett.* **3** pp 331.
[14] Jia-lin Y, Gui-jiao C, Jun C, Wei Y, Bang-hu X, Ming-bo Y 2012 *New. Carbon. Mater.* **27** 370.
[15] Eddaoudi M, Kim J, Rosi N, Vodak D, Wachter J, Keeffe M and Yaghi O 2002 *Science.* **295** pp 469-472.
[16] Rosi N, Eckert J, Eddaoudi M, Vodak D, Kim J, Keeffe M and Yaghi O 2003 *Science.* **300** pp 1127-1129.

Acknowledgments
Authors are really grateful to Higher Education Commission, Pakistan for providing financial support to carry out some part of this research work at Cardiff University, UK.

Annex III

Effect of Amino Functionalization on Cu-BDC MOF for CO_2 Capture Capacity

Junaid Khan[a], Naseem Iqbal[a*], Aisha Asghar[a] and Tayyaba Noor[b]

[a] U.S.-Pakistan Center for Advanced Studies in Energy (USPCAS-E), National University of Sciences & Technology (NUST), H-12, Islamabad, Pakistan

[b] School of Chemical & Materials Engineering (SCME), National University of Sciences & Technology (NUST), H-12, Islamabad, Pakistan

[*] Corresponding Author

E-mail: naseem@uspcase.nust.edu.pk

Tel: +92-51-90855281

Abstract

The CO_2 concentration in the atmosphere is constantly rising mainly through industrial and power plant discharges this has led to urgent calls for strategies to reduce CO_2. Metal organic frameworks (MOFs), also known as coordination polymers, represent an interesting type of solid crystalline materials that can be straight forwardly self-assembled through the coordination of metal ions/clusters with organic linkers. These unique advantages enable MOFs to be used as a highly versatile and tunable platform for exploring multifunctional MOF materials. Amine groups being basic in nature have excellent affinity towards acidic CO_2 group. Amine functionalized metal organic framework materials have promising tendencies as dry adsorbents for post-combustion CO_2 capture, owing to their enhanced CO_2 capture capacity. This research work is focused on the synthesis of a new amino functionalized Cu based MOF using 2-aminoterephthalic as a linker. The structure was confirmed by Single Crystal XRD studies. The Single Crystal XRD studies reveal that an amine functionalized MOF is prepared which has free $–NH_2$ group aiding in the CO_2 adsorption. The CO_2 adsorption study tells us that the MOF exhibits a better CO_2 capture tendency of 5.85 $mmolg^{-1}$ at 25°C as compare to Cu-BDC MOF.

Keywords: *metal organic framework; Cu-BDC MOF; CO_2 adsorbent; MOF application; carbon capture; gas storage*

Introduction

The excessive global carbon emissions have become an environmental menace globally causing extreme climate change and environmental harm. [1] Currently, from burning fossil fuels the global CO_2 emissions have increased by about 2.7% in 2018 which was previously recorded at 1.6% increase in 2017. [2] This rapid increase in the global CO_2 concentrations requires extraordinary measures to come up with new methods to control these emissions. The implementation of Carbon Capture and Sequestration (CCS) can prove to be one of the promising strategies in reducing CO_2 concentration. [3, 4] An old and most commonly practiced approach to capture CO_2 is through amine scrubbing where the CO_2 is adsorbed by chemical adsorption between CO_2 molecule and amine groups. [5] Although this method is widely used but it has certain limitation which include chemical instability on heating, high regeneration energy input, and corrosion.

Scientists all around the globe have worked tirelessly to come up with new materials to capture CO_2 and they have been able to identify MOFs as potential materials to adsorb CO_2 from fossil fuel combustion processes. [6][7][8] A wide number of studies have shown different techniques which enable MOF structures to be optimized for increased CO_2 selectivity from mixture of gases. These techniques include variation and control in the pore size and shape of MOF, incorporation of open metal cation sites, functionalization of ligands and functionalization of MOFs with basic and polar functional groups. [9]

It has been reported in different studies that in order to increase the selectivity and capacity of CO_2, a widely used strategy is to incorporate polar functional groups into the MOF structure. [10][11][12][13][14] These polar functional groups include nitrogen-containing basic groups such as alkylamines, heterocycles and aromatic amines. This strategy of MOF synthesis and modification allows the polar nitrogen-containing groups of MOFs to act as Lewis Base Sites (LBSs). The property of these LBSs is to facilitate in the CO_2 adsorption because they introduce an acid-base interaction which occurs between the CO_2 (acting as an acid) and the active centers that are basic in nature. [15][16] Therefore, many studies have shown that MOFs can be functionalized with amino ligands either during the synthesis or after it so that these LBSs can be incorporated into the framework. [16]

Another approach which is common to enhance the selectivity and affinity of MOFs towards CO_2 is to build open metal sites (OMSs) in the framework of MOF. [17][18][19] OMSs in MOFs are typically created by desolvation of the MOFs. In this method the solvent molecules like DMF, H_2O etc. which are coordinated at the metal centers are knocked out of the MOF molecule at high temperature and/or under vacuum conditions. [16] When the OMSs are created, they act as binding sites which are dense in charge and hence their interaction with CO_2 is very strong during selective gas adsorption. In this way they play a vital role in separation of CO_2.

Here in this paper we report the preparation, characterization and enhanced CO_2 adsorption capacity of a new amino-functionalized Cu based MOF with open metal sites.

Experimental

Synthesis of MOF

During the synthesis of MOF, reagent grade copper nitrate ($Cu(NO_3)_2$); 2-aminoterephthalic acid (H_2ABDC); N, N-dimethylformamide (DMF) and methanol from Sigma-Aldrich were used without any further purification.

The MOF was prepared through the solvothermal method using H_2ABDC (1 g) and copper nitrate (2.67 g) in DMF (60ml). The reagents for the synthesis were stirred at room temperature for 10 min and then transferred to an autoclave. The autoclave was heated in an oven at 110^oC for 24 hrs under autogenous pressure. Upon completion of the solvothermal reaction, light-green colored crystals were recovered through centrifugation at 4000 rpm for 25 min, washed in DMF and then rinsed multiple times in methanol. The crystals obtained were then dried in a vacuum oven at 60^oC.

Characterization

A Bruker Advanced X-ray diffraction system (40 kV, 30 mA) was used for the collection of Powder X-ray Diffraction (PXRD) patterns of the sample. The operating 2θ range of the diffractometer was from 5 to 45° with a step size of 0.02°. The recorded patterns were then compared with the simulated patterns from single crystal data using the Mercury program.

The thermal stability of Cu-ABDC MOF was measured on a DTG-60H Thermo Gravimetric Analyzer (TGA) in N_2 environment with a heating rate of 10°C min^{-1} from 20 to 500°C. A 3.57 mg sample of Cu-ABDC MOF was used for the test and the N_2 gas was supplied at a flow-rate of 50 ml min^{-1}.

Single-crystal structure analyses of the MOF were performed on an Oxford Diffraction Gemini CCD diffractometer which was operating in the ω scan mode. The crystallographic data of the MOF are given in Table 1.

Scanning Electron Microscopy (SEM) images of the MOF sample were obtained on a TESCAN SEM VEGA3 microscope. Prior to the imagery, the sample was gold-coated and the HV was set to 20kV. In order to identify the atomic weight percentage of the elements in the MOF, EDS analysis was conducted.

For the CO_2 adsorption studies of the MOF, Quantachrome Isorb-HP100 volumetric type sorption analyzer was used which evaluated the adsorption capacity by monitoring pseudo equilibrium adsorption uptakes. Prior to the CO_2 adsorption analysis of the MOF, the sample was degassed at a temperature of 120°C for 12 hours and then back filled with helium gas. During the CO_2 adsorption analysis, the Adsorbate Equation of State used was the Helmholtz. The sample was tested for adsorption at 0°C and 25°C at absolute pressures from 0 to 20 bar.

The N_2 adsorption studies of the MOF were conducted on a Quantachrome Nova 2200e and the Quantachrome NovaWin application was used for the calculation of surface area and pore volumes of the MOF. Before conducting the N_2 adsorption analysis, the sample was degassed at 160°C under vacuum for 12 hours. The N_2 adsorption isotherms were obtained at -196°C at a relative pressure of P/P°= 0.005-0.9 for the surface area and pore volume analysis of the MOF.

Results and Discussion

Structural description of Cu-ABDC MOF

The Single Crystal X-ray Diffraction reveals that the Cu-atom and the ABDC ligand are occupying the center of symmetry in the MOF. The metallic cluster is of a bimetallic nature where a Cu-atom is attached to another Cu-atom and 4 O-atoms from the carboxylate ligands and one from the O-bound DMF forming a cluster. As

can be seen from Fig.1, the carboxylate ligands form a bridge in connecting a bimetallic cluster with another cluster hence forming a 3-dimensional framework. The amino group in the MOF is situated on two sites of the ABDC ligand and also on the non-bridging O-atom.

Table 4 Crystallographic Data of Cu-ABDC MOF

Frameworks	**Cu-ABDC**
Formula	$C_{11}H_{12}CuN_2O_5$
Space Group	I 2/m (12)
T, K	Room Temp. (283-303)
a, Å	7.9458 (7)
b, Å	14.9664 (8)
c, Å	11.1033 (10)
Volume, Å^3	1243.71
A	90
B	109.624 (10)
Γ	90
Z	4
R-factor (%)	4.93

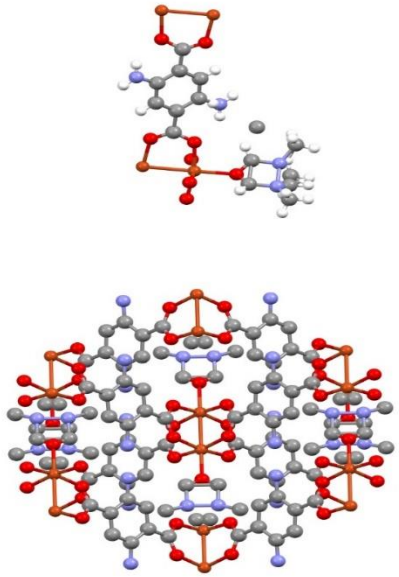

Fig. 1 Structural description of Cu-ABDC MOF (N atoms marked in blue)

As evident from the figure, the DMF solvent molecule which completes the coordination sphere of the metal ion can easily be used to generate OMSs in the MOF framework by the DMF molecule removal using solvent-exchange and evacuation method. This can aid in increasing the adsorption capacity of the MOF.

PXRD pattern of Cu-ABDC

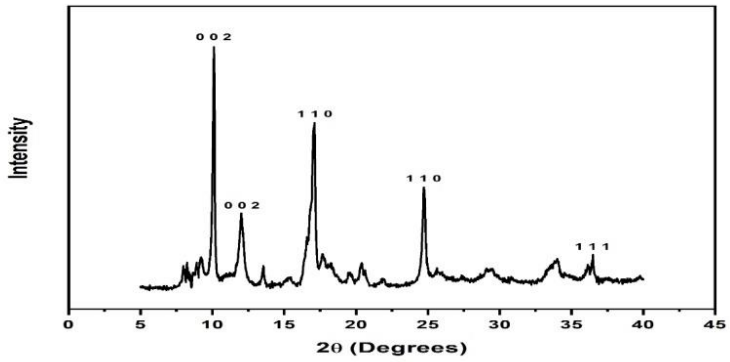

(a)

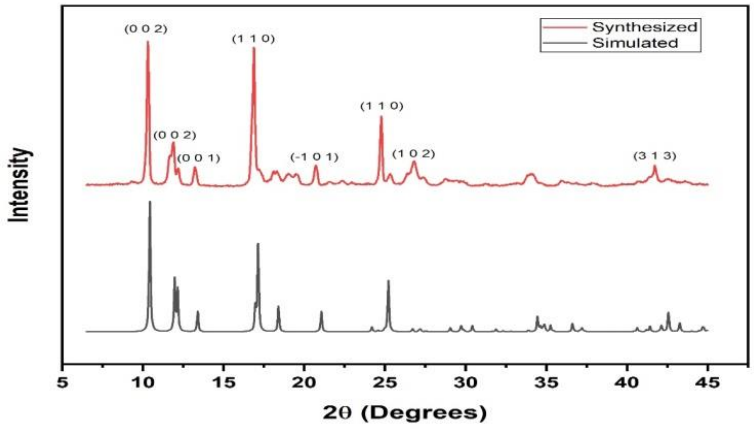

(b)

Fig. 2 XRD patterns of Cu-BDC MOF (a), Cu-ABDC MOF (b) simulated (black) and synthesis (red)

Fig. 2 shows the PXRD patterns of prepared Cu-ABDC MOF sample and PXRD pattern of the model Cu-ABDC structure which was predicted from the calculations of the SXRD.

From the figure it can be clearly seen that both the patterns are highly similar which indicates that the prepared MOF sample is of high degree of purity. The peaks at 2θ 10° and 42.5° indicates the presence of carbon (PDF card # 48-1206) in the MOF, and the peaks at 2θ 11.9° confirms the presence of copper (PDF card # 27-1126).

Fig. 2 also shows the PXRD of the simple Cu-BDC MOF with terephthalic acid as a ligand. The difference between the XRD of the Cu-BDC MOF and the Cu-ABDC MOF is at the peaks of 2θ 20.5° and 26.8°. These peaks in the Cu-ABDC confirms the presence of Nitrogen (PDF Card # 06-0500 and 35-0845 respectively) in the MOF.

Thermal stability of Cu-ABDC

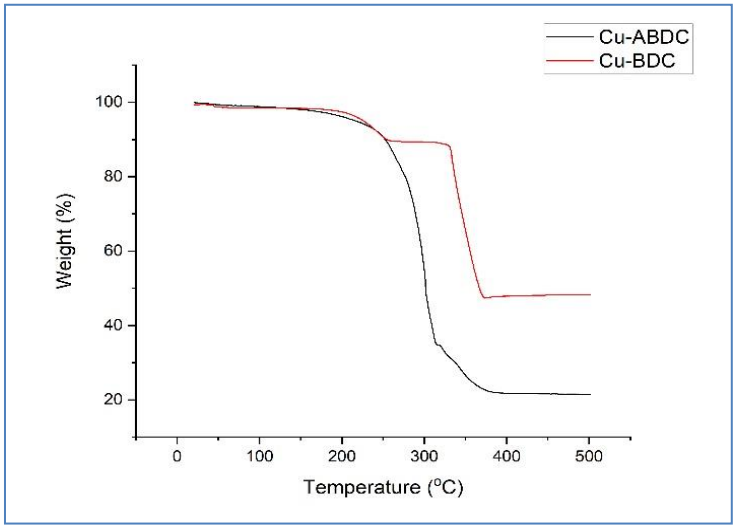

Fig. 3 Weight loss (TGA) curve of Cu-ABDC (black) and Cu-BDC (red) MOF

In order to determine and study the thermal behavior of the MOF, TGA analysis were performed (Fig. 3). The initial weight loss (about 8%) of the Cu-ABDC MOF sample at 160 to 220°C indicates the degradation of DMF adsorbed at the surface of the MOF. At 255°C temperature, the decomposition of carboxylate ligand starts and afterwards a rapid degradation can be noted. At temperature above 368°C, no further weight loss can be seen which indicates that the structure of the MOF has completely been destroyed and residual Copper oxide is left behind.

Fig. 3 also shows the TGA of Cu-BDC MOF and it is evident from the graphs that the Cu-BDC MOF is more stable than the Cu-ABDC MOF. In the Cu-BDC MOF, the initial 10% weight loss which occurs at a temperature of 200°C and ends at 260°C is attributed to the loss of solvent which might be trapped in the pores of the MOF. The actual structural breakdown of the MOF starts at relatively higher temperature of 340°C, which is much higher than the structural breakdown of Cu-ABDC MOF.

SEM and EDX of Cu-ABDC

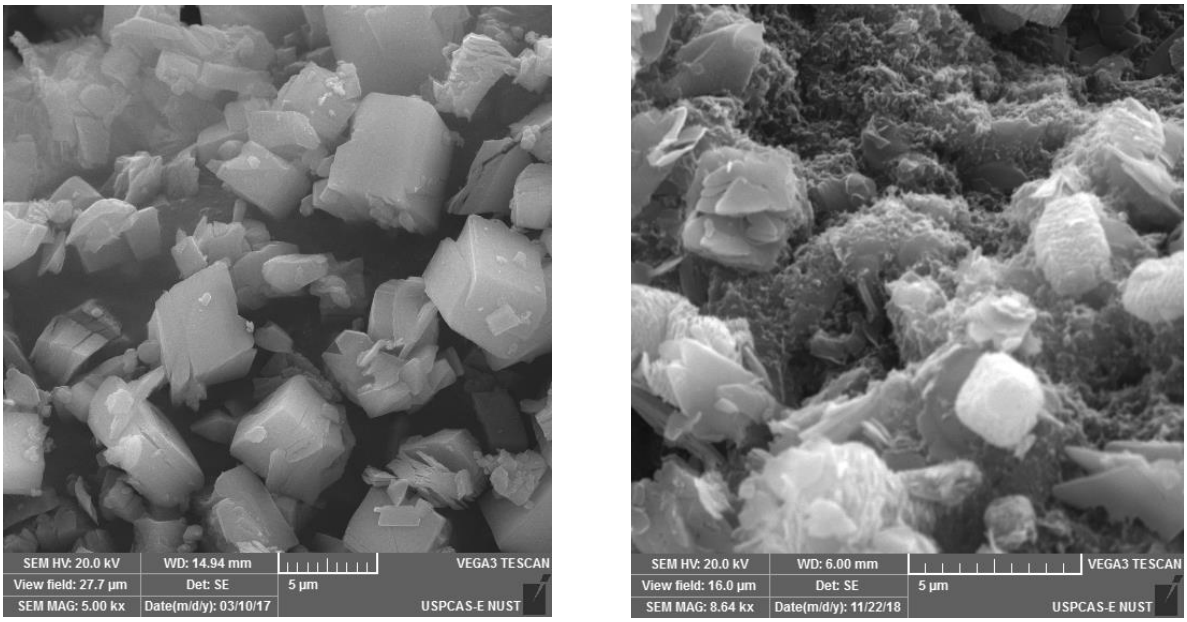

(a) (b)

Fig. 4 SEM images of the Cu-BDC (a) and the Cu-ABDC MOFs (b).

The SEM images revealed that crystals of the Cu-BDC MOFs are regular shaped cuboids while the crystals of the Cu-ABDC are a mixture of cuboids and thin sheet like structures. The MOF crystals of Cu-ABDC are of smaller size as compared to those of Cu-BDC MOF.

Table 5 Elemental Composition of Cu-BDC and Cu-ABDC MOF

Element/Sample	**Cu-BDC MOF**	**Cu-ABDC MOF**
C wt%	51.93	55.17
O wt%	35.25	32.31
N wt%	-	7.49
Cu wt%	12.82	5.03

The elemental composition in EDX analysis shows the chemical composition of both the MOFs is shown in table 2. The Cu-ABDC MOF due to its 2-aminoterephthalic acid ligand contains nitrogen which is clearly indicated in the results of the EDX analysis.

Surface area and porosity of Cu-ABDC MOF

The N_2 adsorption isotherm of Cu-ABDC MOF is presented in Fig. 5. This N_2 adsorption of the MOF was measured at -196°C. The BET surface area calculated from the N_2 adsorption is 8.15 m^2/g and the Langmuir surface area is 62.49 m^2/g. From the figure it is evident that there is a low adsorption of N_2 at low relative pressure but as the relative pressure increases from p/p°=0.6, a sharp increase in the adsorption can be noted. There also occurs a hysteresis at the desorption branch between p/p°=0.89-0.5. This hysteresis may indicate the presence of mesopores in the MOF. The cumulative adsorption pore volume of the MOF calculated by the BJH method is 0.01847cm^3/g. The S_{EXT}, external surface area, of the MOF calculated by the t-plot analysis is 8.152 m^2/g.

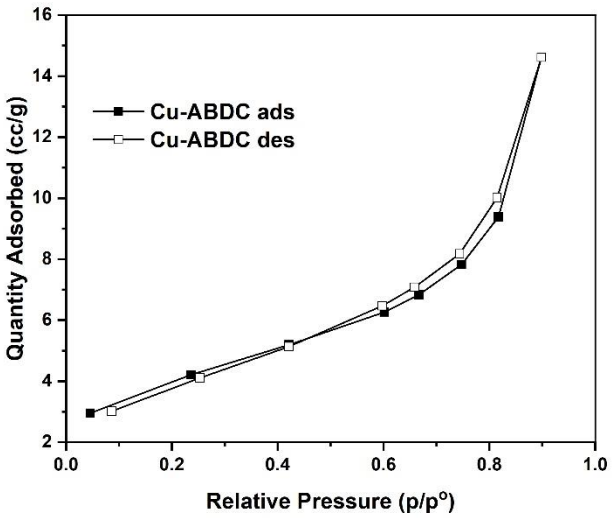

Fig. 5 N_2 adsorption isotherm of Cu-ABDC MOF

As compared to the Cu-BDC MOF, the N_2 adsorption of Cu-ABDC MOF is relatively low. This may be attributed to the presence of residual guest molecules which can decrease the adsorption capacity of the MOF. Moreover, the amino group in the Cu-ABDC MOF can cause the reduction of the surface area of the MOF as is indicated by other amine functionalized MOFs [20].

CO_2 adsorption capacities of Cu-ABDC

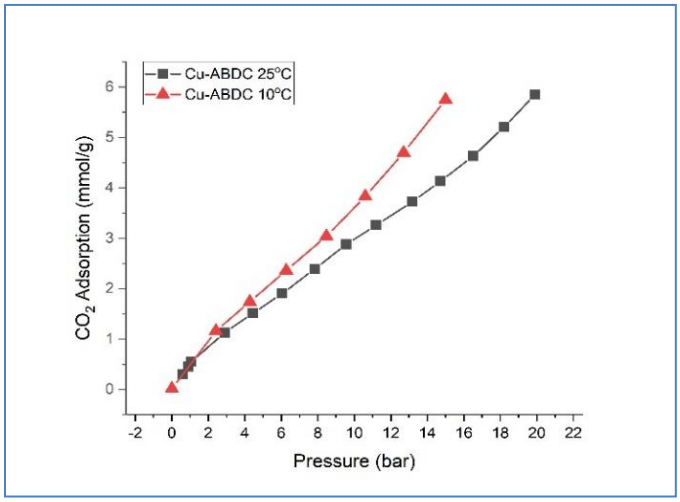

Fig. 6 CO_2 Adsorption of Cu-ABDC MOF at 10℃ and 25℃

Fig. 6 shows the CO_2 adsorption capacities of the Cu-ABDC MOF which were measured at 10 °C and 25 °C. The pressures at these temperatures were from 0 to 20 bars. Three consecutive adsorption-desorption cycles were conducted on the sample at each condition. Before analysis, the sample was degassed at 120°C for 12 hours and the heating rate was set at 5°C min^{-1}. The CO_2 adsorption capacity of the MOF at 25°C and 20 bar pressure measured was 5.85 $mmolg^{-1}$ and 5.75 $mmolg^{-1}$ at 10°C and 15 bar pressure.

Although the MOF exhibits a good adsorption capacity of 5.85 and 5.75 $mmolg^{-1}$ at 25°C and 10°C respectively, but it should be noted that these high adsorption capacities are attained at high pressures of 15 bar and 20 bar. At low pressure of 1 bar, the MOF adsorbs 0.546 $mmolg^{-1}$ at 25°C and 0.46 $mmolg^{-1}$ at 10°C. Literature states that some other amine functionalized MOFs (Mg, Co and Sr based MOFs) also have CO_2 adsorption capacities ranging in the same region [20]. Among these MOFs, the Sr based MOF have adsorption capacity which closely resembles with the values reported here.

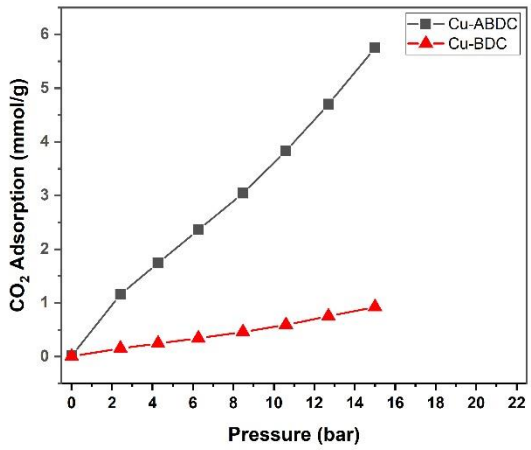

Fig. 7 CO_2 adsorption of Cu-ABDC MOF (black) and Cu-BDC MOF (red) at 10℃

The Cu-O bond in the Cu-ABDC MOF has a high ionic character but still its adsorption capacity is not as high. This can be due to the presence of the DMF solvent ligands in the framework of MOF. Theoretically, a higher adsorption capacity can be obtained from this MOF by removing the DMF ligands from the structure.

Fig.7 shows the comparison of the CO_2 adsorption capacities of the Cu-BDC and Cu-ABDC MOFs at a temperature of 10°C. It can be clearly observed that the adsorption of Cu-ABDC is much higher than that of Cu-BDC MOF. The main reason for this difference in adsorption capacities is the availability of LBSs in the Cu-ABDC MOF which increases its affinity towards the CO_2 which is acidic in nature.

The comparison of sorption capacities and parameters of the reported Cu-BDC MOF [21] and the Cu-ABDC MOF is summaries in table 3.

Table 6 Comparison of sorption parameters of Cu-ABDC and Cu-BDC MOF with literature

Element/Sample	Temperature	Pressure	CO_2 adsorption capacity	S_{BET} (m^2/g)	S_{EXT} (m^2/g)	Reference
Cu-BDC	-15°C	1 bar	0.78	241	0.47	[21]
	25°C	20 bar	1.15			[21]
Cu-BDC	10°C	15 bar	0.922			This Study
Cu-ABDC	10°C	1 bar	0.46	8.15	8.152	This Study
	25°C	20 bar	5.85			This Study

Cyclic CO_2 adsorption study

For the long-term application of a MOF, it is essential for the MOF to be durable during cyclic adsorption/desorption process. In order to determine the durability of the Cu-ABDC MOF, a cyclic adsorption/desorption study of the MOF was carried out. In this cyclic study, the CO_2 was adsorbed and desorbed by the MOF in five consecutive cycles. The cyclic study was conducted at a temperature of 25℃ and pressure of 20 bar. The adsorption capacity in terms of percent CO_2 uptake of the MOF during different cycles is shown in Fig. 8.

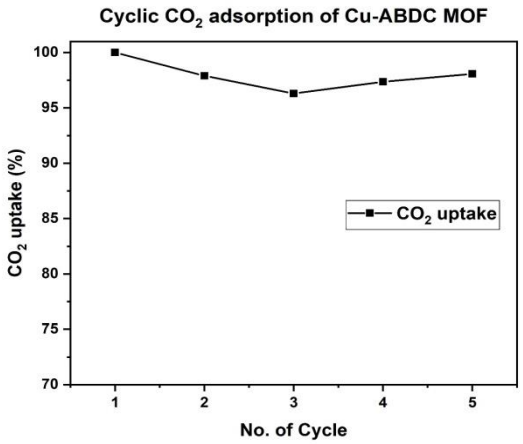

Fig. 8 Cyclic adsorption/regeneration run of Cu-ABDC MOF at 25℃ and 20 bar

The cyclic data of the Cu-ABDC MOF reveals that it is a fairly stable MOF. As it can be seen from the figure 8 that during the consecutive cycles, there is a very low drop in the CO_2 uptake of the MOF. After 5 cycles overall 2% decrease in CO_2 uptake took place. In last two cycles, an increase in the adsorption capacity as compared to initial cycles can be noted. This increase can be ascribed to the gradual expansion of mesopores in the MOF. With the expansion of mesopores, the MOF is able to increase CO_2 adsorption capacity.

Conclusions

In this study, a new Cu based amine functionalized MOF is prepared using 2-aminoterephthalic ligand. The Cu-ABDC MOF exhibits a good thermal stability. The Cu-ABDC MOF showed capacity to be used in CO_2 adsorption and separation. The high CO_2 adsorption capacity of the Cu-ABDC MOF is attributed to the $–NH_2$ group present in the structure of the MOF which acts as LBS and hence enhance the affinity of the MOF towards

CO_2. In addition to this, the Cu-ABDC MOF also represents the possibility of OMSs creation in the framework by the removal of the DMF ligands. Moreover, the implementation of efficient activation processes are required so that the Cu-ABDC MOF exhibit higher gas exchange sites and subsequently increase the adsorption capacity without damaging the framework.

Acknowledgments

The author would like to acknowledge US Pakistan for advance studies in energy (USPCASE) and School of chemical and material engineering (SCME) at NUST for providing the lab facilities. Financial support from HEC under NRPU project no (6013) is greatly acknowledged.

References

1. R. Quadrelli and S. Peterson, Energy Policy, 2007, 35, 5938–5952.
2. Le Quéré, C., Andrew, et al.: Global Carbon Budget 2018, Earth Syst. Sci. Data, 10, 2141-2194, https://doi.org/10.5194/essd-10-2141-2018, 2018.
3. K. Sumida, D. L. Rogow, J. A. Mason, T. M. McDonald, E. D. Bloch, Z. R. Herm, T. H. Bae and J. R. Long, Chem. Rev., 2012, 112, 724–781.
4. R. S. Haszeldine, Science, 2009, 325, 1644–1645.
5. G. T. Rochelle, Science, 2009, 325, 1652–1654.
6. T. R. Karl and K. E. Trenberth, Science, 2003, 302, 1719–1723.
7. H. L. Jiang and Q. Xu, Chem. Commun., 2011, 47, 3351–3370.
8. K. Sumida, D. L. Rogow, J. A. Mason, T. M. McDonald, E. D. Bloch, Z. R. Herm, T.-H. Bae and J. R. Long, Chem. Rev., 2011, 112, 724–781.
9. S. Couck, J. F. M. Denayer, G. V. Baron, T. Rémy, J. Gascon and F. Kapteijn, J. Am. Chem. Soc., 2009, 131, 6326–6327.
10. S. J. Garibay and S. M. Cohen, Chem. Commun., 2010, 46, 7700–7702.
11. A. Torrisi, C. Mellot-Draznieks and R. G. Bell, Crystal Growth & Design., 2010, 10, 2839–2841.

12. P. Serra-Crespo, E. V. Ramos-Fernandez, J. Gascon and F. Kapteijn, Chem. Mater., 2011, 23, 2565–2572.
13. X. Y. Chen, H. Vinh-Thang, D. Rodrigue and S. Kaliaguine, Ind. Eng. Chem. Res., 2012, 51, 6895–6906.
14. B. Yuan, D. Ma, X. Wang, Z. Li, Y. Li, H. Liu and D. He, Chem. Commun., 2012, 48, 1135–1137.
15. J.-R. Li, Y. Ma, M. C. McCarthy, J. Sculley, J. Yu, H.-K. Jeong, P. B. Balbuena and H.-C. Zhou, Coord. Chem. Rev., 2011, 255, 1791–1823.
16. Z. Zhang, Y. Zhao, Q. Gong, Z. Li and J. Li, Chem. Commun., 2013, 49, 653–661.
17. M. Dincă and J. R. Long, Angew. Chem., Int. Ed., 2008, 47, 6766–6779.
18. P. D. C. Dietzel, V. Besikiotis and R. Blom, J. Mater. Chem., 2009, 19, 7362–7370.
19. B. Chen, S. Xiang and G. Qian, Acc. Chem. Res., 2010, 43, 1115–1124.
20. Ying Yang, Rijia Lin, Lei Ge, Lei Hou, Paul Bernhardt, Thomas E. Rufford, Shaobin Wang, Victor Rudolph, Yaoyu Wang and Zhonghua Zhu, Dalton Trans., 2015,44, 8190-8197.
21. Zhifeng Xin, Junfeng Bai, Yongming Shen, and Yi Pan, Crystal Growth & Design, 2010, 10 (6), 2451-2454.